

The Pennsylvania State University

The Graduate School

**ASSESSING THE ROLE OF GAP AVOIDANCE MECHANISMS AND NUCLEOSOME
ASSEMBLY PATHWAYS AS GUARDIANS OF DNA REPLICATION FORK
STABILITY**

A Dissertation in

Biomedical Sciences

by

Tanay Thakar

© 2022 Tanay Thakar

Submitted in Partial Fulfillment
of the Requirements
for the Degree of

Doctor of Philosophy

August 2022

The dissertation of Tanay Thakar was reviewed and approved by the following:

George-Lucian Moldovan
Dissertation Advisor
Chair of Committee
Associate Professor,
Department of Biochemistry and Molecular Biology

James R. Broach
Distinguished Professor and Chair,
Department of Biochemistry and Molecular Biology

Lisa M. Shantz
Associate Professor,
Department of Cellular and Molecular Physiology

Hong-Gang Wang
Lois High Berstler Professor
Department of Pediatrics and Pharmacology

Zhonghua Gao
Associate Professor,
Department of Biochemistry and Molecular Biology

Ralph L. Keil
Chair of the Biomedical Sciences Graduate Program
Associate Professor,
Department of Biochemistry and Molecular Biology

ABSTRACT

A global response to DNA replication stress is replication fork reversal, which involves the slowing and reversal of replication forks accompanied by the annealing of nascent DNA strands to form pseudo-four-way junctions. Functionally, reversal is thought to enable replication forks to avert DNA damage while replication stress is resolved. However, despite the protective functions of fork reversal, the annealed nascent arms of reversed forks a novel substrate that resembles one-end of a double stranded break, potentially susceptible to resection by milieu of nucleases such as CTIP, MRE11, EXO1 and DNA2. To prevent the undue processing of reversed replication forks, an extensive range of fork protection mechanisms are put into place. The most prominent of these mechanisms involves the Breast Cancer Susceptibility Proteins BRCA1 and BRCA2. Upon fork reversal, BRCA1 and BRCA2 directly influence the activity of the downstream effector protein RAD51, putatively by enabling it to form stable nucleofilaments on reversed fork substrates, which restricts the activity of nucleases and prevents the resection of stalled replication forks. In BRCA1/2 deficient cells CTIP, MRE11, EXO1 and DNA2 cooperate to elicit the long-range resection of forks that have undergone stalling and reversal. This long-range resection of reversed forks is associated with endonucleolytic DNA double strand break (DSB) induction and consequent genomic instability, thereby establishing fork protection as an essential component of BRCA-mediated tumor suppression. Critically, fork degradation also underlies sensitivity of BRCA-deficient cells to chemotherapeutic agents. As a corollary to this, the restoration of fork protection is associated with acquired chemoresistance in BRCA-deficient cancers. Therefore, gaining a better understanding of the fundamental determinants of fork protection is essential to gaining a better understanding of the etiology and therapeutic response of BRCA-deficient cancers.

The first study reveals Proliferating Cell Nuclear Antigen (PCNA) K164-ubiquitination as a critical post-translational modification governing fork stability in a manner distinct from the BRCA-pathway. Through CRISPR/Cas9 mediated genome editing we create a homozygous PCNA-K164R mutation in human 293T and RPE-1 cells to render them completely devoid of PCNA ubiquitination. We show that PCNA-K164R cells are susceptible to DNA2-mediated fork degradation upon replication arrest by the ribonucleotide reductase inhibitor hydroxyurea (HU). We find that fork degradation in these cells is connected to their inability to mitigate replication associated gaps which interferes with Okazaki fragment (OF) synthesis and maturation, and consequently interferes with PCNA unloading from lagging strands. A direct result of this is the improper recycling of the PCNA-interacting histone chaperone CAF-1 which causes replication coupled nucleosome assembly defects, priming stalled forks for nucleolytic resection upon stalling and reversal. We further uncover a critical role for PCNA-ubiquitination in enabling the survival of BRCA-deficient cells upon treatment with PARP-inhibitors by suppressing single-stranded DNA (ssDNA) gaps, a novel therapeutic vulnerability in BRCA-deficient cancers.

In the subsequent study we reveal an unexpected central role for nucleosome assembly in determining BRCA-dependent fork protection. We find inactivation of CHAF1A (the p150 subunit of CAF-1), through the activation of a compensatory replication-independent nucleosome assembly pathway dependent on the histone chaperone HIRA, restores fork stability to BRCA-deficient cells. Critically, we reveal ASF1-dependent nucleosome assembly as a general mechanism ensuring fork stability which operates in epistasis with the BRCA-pathway. Lastly, we elucidate the importance of BRCA-mediated replication associated gap suppression in ensuring CAF-1-dependent nucleosome assembly, thereby ensuring fork protection. We show that BRCA-deficient cells accumulate both leading and lagging strand ssDNA gaps during replication stress. Lagging strand gaps elicit PCNA unloading defects due to incomplete OF

synthesis which result in a consequent CAF-1 recycling defect and impaired replication coupled nucleosome assembly. We therefore reveal CAF-1 as an essential effector of BRCA-mediated fork protection that operates through efficient replication associated gap suppression and PCNA unloading. These findings enable us to posit a model that unifies two major hallmarks of BRCA-deficiency in cancer, i.e., replication fork degradation and replication coupled ssDNA gap accumulation, into a sequential mechanism underlying genomic instability connected by PCNA-recycling and nucleosome assembly by CAF-1.

TABLE OF CONTENTS

LIST OF FIGURES	viii
ACKNOWLEDGEMENTS	x
Chapter 1 Literature Review: The Emerging Determinants of Replication Fork Stability	1
Introduction	1
The Classical FA/BRCA Fork Protection Pathway	2
Emerging Determinants of Replication Fork Stability	4
RAD51-dependent fork protectors	4
RAD51-independent fork protectors	6
Emerging insights into fork reversal pathways in fork degradation	11
The emerging role of chromatin dynamics in fork protection	15
Fork Protection and the Impact of Cellular Survival	18
Restoration of fork protection	18
Fork protection and cellular survival	20
Fork stability and PARPi sensitivity	23
Concluding Remarks	28
Chapter 2 Uncovering the Role of PCNA-Ubiquitination in Maintaining Replication Fork Integrity	31
Rationale	31
Results	32
Generation of PCNA-K164R mutant cells	32
Replication stress and increased fork speed in PCNA-K164R cells	35
PCNA-ubiquitination protects stalled forks from degradation	37
Impact of fork reversal enzymes on fork degradation in PCNA-K164R cells	40
Okazaki fragment ligation underlies fork protection	44
PCNA retention on chromatin drives fork degradation	45
Loss of PCNA-ubiquitination enhances the effects of BRCA-deficiency	48
Chapter 3 Lagging strand gap suppression connects BRCA-mediated fork protection to nucleosome assembly by ensuring PCNA-dependent CAF-1 recycling	51
Rationale	51
Results	52
CAF-1 inactivation rescues fork stability in BRCA-deficient cells	52
Loss of CAF-1 averts DNA damage and drives chemoresistance in BRCA deficient cells	56
Nucleosome assembly ensures replication fork protection	59
Restoration of fork stability upon CAF-1 inactivation in BRCA-deficient cells depends on compensatory nucleosome assembly pathways	62
BRCA-deficient cells exhibit CAF-1 recycling defects during replication stress	64
Lagging strand gaps cause CAF-1 recycling defects in BRCA-deficient cells	68

PCNA unloading ensures CAF-1 mediated fork protection in BRCA-proficient cells	73
Chapter 4 Discussion	78
Nucleosome assembly is a determinant of replication fork stability	78
Inadequate gap evasion during DNA replication contributes to lagging strand synthesis defects.....	80
PCNA-unloading and CAF-1 recycling connect gap evasion to replication fork stability	84
Future Directions	86
Chapter 5 Materials and Methods	90
Cell culture techniques.....	90
Protein techniques.....	91
Gene knockdowns.....	92
Comet assay	93
DNA fiber assay.....	93
S1 nuclease fiber spreading assay.....	94
Functional assays	95
Translesion synthesis SupF assay	95
Immunofluorescence.....	96
In situ analysis of protein interactions at replication forks (SIRF)	97
Cellular gene dependency analyses	98
TCGA dataset analyses	98
Quantification of gene expression by real-time quantitative PCR (RT-qPCR)	99
Micrococcal nuclease sensitivity assay.....	99
Appendix A Supplementary Information to Chapter 2.....	101
Appendix B Supplementary Information to Chapter 3	112
References.....	124

LIST OF FIGURES

Figure 1.1: Fork reversal factors and their impact on fork degradation.....	11
Figure 1.2: The impact of histone modifications and nucleosome remodeling on replication fork stability.....	16
Figure 1.3: Proposed mechanisms of PARPi-mediated cellular lethality in BRCA-deficient cells.....	25
Figure 2.1: Generation and characterization of PCNA-K164R cells.....	34
Figure 2.2: Endogenous replication stress in PCNA-K164R cells.....	36
Figure 2.3: Increased fork speed in PCNA-K164R cells.....	37
Figure 2.4: PCNA-K164R cells exhibit DNA2-mediated nascent DNA degradation.....	39
Figure 2.5: Factors involved in fork reversal are required for nascent strand degradation in PCNA-K164R cells.....	41
Figure 2.6: Defective Okazaki fragment maturation results in nascent strand degradation. ..	43
Figure 2.7: Abnormal retention of PCNA on chromatin drives replication fork degradation by altering nucleosome deposition.....	46
Figure 2.8: Genetic interaction between PCNA ubiquitination and the BRCA pathway.	49
Figure 2.9: Loss of PCNA-ubiquitination sensitizes BRCA-deficient cells to PARP inhibition.....	50
Figure 3.1: Loss of CAF-1 promotes fork stability in BRCA-deficient cells.....	53
Figure 3.2: CHAF1A loss restores fork stability to BRCA-deficient cells in a RAD51-independent manner.....	55
Figure 3.3: Loss of CAF-1 suppresses genomic instability in BRCA-deficient cells.....	57
Figure 3.4: CHAF1A inactivation drives chemoresistance in BRCA-deficient cells.....	59
Figure 3.5: Determinants of CHAF1A-mediated fork protection.....	60
Figure 3.6: Fork protection upon CAF-1 loss in BRCA-deficient cells requires the histone chaperone HIRA.....	63
Figure 3.7: CAF-1 unloading defects in BRCA-deficient cells.....	65

Figure 3.8: BRCA-deficient cells exhibit CAF-1 recycling defects.	66
Figure 3.9: Accumulation of lagging strand gaps in BRCA-deficient cells.....	69
Figure 3.10: Lagging strand gaps drive CHAF1A and HIRA accumulation at stalled forks.	71
Figure 3.11: BRCA-deficient cells display PCNA unloading defects dependent on Pol α -mediated repriming during replication stress.....	74
Figure 3.12: Restoring PCNA unloading rescues fork stability in BRCA-deficient cells.	75
Figure A1.1: Generating isogenic 293T PCNA-WT and PCNA-K164R cells.....	101
Figure A1.2: Fork degradation does not depend on ZRANB3 loss of function.	101
Figure A1.3: DNA2 degrades stalled replication forks in PCNA-K164R cells.....	102
Figure A1.4: Impact of PCNA modification by ubiquitin or SUMO on fork stability.	104
Figure A1.5: Impact of fork reversal on nascent strand degradation in PCNA-K164R cells.	106
Figure A1.6: Impact of Okazaki fragment maturation factors and TLS polymerases on replication fork protection.....	107
Figure A1.7: PCNA chromatin retention in ATAD5-depleted cells and consequences on fork stability.	109
Figure A1.8: Genetic interaction between PCNA ubiquitination and the BRCA pathways.....	111
Figure A2.1: Confirmation of gene knockdowns.....	112
Figure A2.2: Impact of CAF-1 loss in BRCA-deficient cells.....	113
Figure A2.3: Confirmation of gene knockdowns.....	114
Figure A2.4: Impact of nucleosome deposition by HIRA on BRCA-deficient cells.....	115
Figure A2.5: CHAF1A recycling in BRCA-deficient cells.	117
Figure A2.6: PRIMPOL independent lagging strand synthesis defects in BRCA-deficient cells.	118
Figure A2.7: Correcting PCNA unloading defects.	120
Figure A2.8: Schematic representations of the proposed models.	122

ACKNOWLEDGEMENTS

Firstly, I would like to thank my thesis adviser, George-Lucian Moldovan, for his mentorship and support through my graduate education. Under your guidance I gained the confidence to trust my scientific instinct and taught me that there was something to be learned from every experimental result. You supported me in exploring new ideas and made an invaluable contribution to my growth and confidence as a scientist.

I would also like to express my gratitude to present and past members of the Moldovan lab. I would like to specially thank Dr. Claudia Nicolae for teaching me the techniques I used almost every day in my work, her direct help in experiments during tight deadlines and her overall reassuring presence in the lab. I also want to acknowledge Kristen Clements and Michael O'Connor for taking time out of their own work for in-depth scientific discussions and being my friends from the first day I joined the lab.

I also wish to thank my thesis committee and faculty at the Biomedical Sciences Graduate Program – Dr. Keil, Dr. Broach, Dr. Shantz, Dr. Wang and Dr. Gao for their constant support and help in aiding my professional development. I am also eternally grateful to my Master's research mentor Dr. Qingshen Gao, for his mentorship, patience and commitment in getting me started in scientific academia.

Pursuing a PhD would have been an impossible undertaking without the support of my many friends in Hershey, for the camaraderie we shared in facing the challenges of graduate school and research and for contributing to some of the happiest memories I have to look back on.

Tejaswi (TJ), Tatsuya, Roberto, Praneet, Joaquin, Melat, Suriya, Cecilia, Kushal, and too many more to name, you made these years of my life irreplaceable. I am also grateful to my extended family in the U.S. and India for providing me with encouragement, advice, security, and a home away from home when I needed them most.

Lastly, I would like to dedicate this dissertation to my family- my father Anuraag Thakar, my mother Gauri Thakar, my brother Raghav Thakar and my cat Bobo. You were the pillars I leaned on the most during my time as a PhD student and through life. Your unconditional love and support, your belief in me and your sacrifices through our extended times apart, through times of loss, and times of change are what made this endeavor possible.

This work was funded by the National Institutes of Health R01ES026184 and R01GM134681 to G. L. Moldovan; R01CA244417 to C. M. Nicolae. The conclusions drawn in this dissertation reflect the views of authors alone and do not represent the views of the funding agency.

Chapter 1

Literature Review: The Emerging Determinants of Replication Fork Protection

Introduction

The genome is at its most vulnerable during DNA replication since this process seldom progresses completely unobstructed. Several factors of endogenous and exogenous origin can pose obstacles to the progression of replication forks resulting in replication stress. A global response upon encountering replication stress involves the remodeling of replication forks to enable the annealing of nascent DNA strands, a process known as replication fork reversal. Fork reversal, intrinsically coupled to an initial fork slowing response, is thought to safeguard fork integrity by granting tolerance to transient replication stress. Mechanistically, the protective effect of fork reversal is thought to manifest in distinct ways: 1) Fork regression, which accompanies fork reversal, allows for the template lesion to be brought back into a double-stranded DNA configuration permissive to excision repair; 2) The regressed complementary arms of nascent DNA can potentially allow for the bypass of template DNA obstructions by employing the nascent strand of the sister chromatid as a template; 3) Fork reversal allows forks under stress to assume a dormant configuration until the replication stress can be resolved, thereby protecting them from adverse outcomes of unrestrained progression such as fork breakage. However, in certain genetic backgrounds or under conditions of prolonged fork arrest, reversal can render forks susceptible to nucleolytic resection. Excessive nucleolytic resection (also known as degradation) of reversed forks is often associated with the accumulation of chromosomal abnormalities. Fork degradation is thus a prominent mechanism of genome instability. In

addition, fork degradation is considered a major predictor of chemosensitivity and cellular fitness. The best described mechanism ensuring protection against fork degradation involves the BRCA proteins (comprised of the breast cancer susceptibility factors BRCA1 and BRCA2) and components of the Fanconi anemia (FA) tumor suppressor pathway, which are known effectors of homologous recombination (HR) in metazoan cells. These mechanisms rely on stabilizing RAD51 nucleofilaments on the regressed nascent DNA of reversed replication forks. However, recent work has revealed a multitude of additional factors and pathways which directly affect fork protection by either influencing RAD51 nucleofilament formation or through completely distinct mechanisms. In this review, we examine the recent advances in the understanding of the classical fork protection pathways, as well as the emerging determinants of fork protection.

The Classical FA/BRCA Fork Protection Pathway

The role of RAD51 in orchestrating protection of stressed replication forks was first documented in *X. laevis* egg extracts. It was observed that upon inhibiting the chromatin binding of RAD51, the nuclease MRE11 drives the accumulation of internal ssDNA gaps in replicating DNA¹. Subsequently, a more general role for RAD51 in protecting nascent DNA was established in mammalian cells when it was revealed that loss of BRCA2, a known effector of the HR pathway, resulted in excessive MRE11-dependent resection of hydroxyurea (HU) – stalled replication forks². This resection of nascent DNA occurred due to the inability of these cells to form stable RAD51 nucleofilaments, thereby resulting in a diminished ability of RAD51 to protect stalled replication forks. Subsequent studies established the role of the other core HR effector BRCA1 as well as the FA pathway components FANCA and FANCD2 as serving critical functions in RAD51 stabilization on nascent DNA, hence protecting stalled forks from degradation³. These initial studies also established chromosomal instability as a direct

consequence of fork degradation^{2,3}, therefore identifying a major mechanism of genome instability and cancer predisposition associated with mutations in the BRCA and FA genes. In addition to this, the well appreciated role of BRCA1 and BRCA2 mutations in cancer predisposition has led to the BRCA pathway being most widely studied in the context of fork protection, with RAD51 as the primary effector. Indeed, perturbing RAD51 activity in WT cells through the ectopic expression of the BRC4 peptide (which sequesters RAD51 from chromatin) or of RADX (which competes with RAD51 for ssDNA) renders forks susceptible to degradation²⁻⁴. Similar effects were observed upon treatment with B02, a small molecule inhibitor of RAD51⁵.

A critical enabler of excessive fork degradation in cells lacking a functional FA/BRCA-pathway is fork reversal. However, the potential role of fork reversal in the resection of stalled forks was first established in the context of BRCA-proficient cells subjected to HU-mediated fork stalling. Specifically, cells subjected to prolonged HU treatment were found to exhibit fork degradation through an alternative pathway involving the nuclease DNA2 and the WRN helicase⁶. Importantly, this degradation was enhanced upon the depletion of RECQ1, a specialized helicase responsible for restarting reversed replication forks. Moreover, depletion of RAD51 rescued this degradation, in line with its previously established role in mediating fork slowing and reversal upon exposure to replication stress⁷. Subsequent work in BRCA-deficient systems showed that the SNF2 family translocases SMARCAL1, ZRANB3 and HLTF, which remodel replication forks into reversed fork substrates, are essential for the degradation of stalled forks^{5,8-10}. Intriguingly, studies in BRCA-deficient cells also shed light on the surprising dichotomous roles of RAD51 in both protecting stalled replication forks upon formation of stable nucleofilaments, as well as promoting their degradation by orchestrating fork reversal⁹. These opposing roles of RAD51 were further exemplified through gradients of RAD51 depletion using

titrated RNA interference in BRCA-proficient cells, where partial RAD51 depletion promoted fork degradation but complete depletion rescued fork stability⁴.

The study of fork reversal in BRCA2-deficient cells also provided valuable insights into the mechanisms underlying the pathological consequences of fork degradation. Specifically, in BRCA2-deficient cells, the degradation of reversed forks prompts a controlled induction of double strand breaks (DSBs) by MUS81, triggering a POLD3-mediated fork restart – highly reminiscent of the break induced replication (BIR) pathway of fork rescue¹⁰. Indeed, it was shown that RAD52 promotes MRE11-mediated degradation, setting the stage for fork cleavage, in line with its role in orchestrating BIR – dependent DNA synthesis, likely during mitosis^{11,12}. However, it is still unclear whether BIR contributes to chromosomal aberrations in cells lacking BRCA1 or FA pathway function.

Emerging Determinants of Fork Protection

RAD51-dependent fork protectors

Recent studies have revealed the existence of several previously unknown factors involved in the protection of stalled forks from degradation. Interestingly, these factors employ fork protection mechanisms often distinct from the FA/BRCA pathway. However, several of these mechanisms still rely on the fork protection activity of RAD51. A relatively well-studied enabler of RAD51-mediated fork protection is BOD1L which operates in the FA pathway of genome stability¹³. However, unlike the mechanism previously described for the FA pathway³, loss of BOD1L promotes fork degradation in a manner dependent on DNA2 rather than MRE11. Despite this, these observations remain in line with the role of excessive nuclease-mediated

resection as underlying genome instability in FA cells¹⁴. Further studies have revealed that the fork protection function of BOD1L occurs through its interaction with the histone methyltransferase SETD1A which triggers the histone chaperone function of FANCD2 to mediate RAD51 recruitment at stalled forks, in addition to inhibiting the pro-resection activity of CHD4¹⁵. These functions of BOD1L-SETD1A likely explain the role of FANCD2 in protecting against fork degradation in BRCA-deficient cells^{16,17}. Another recently described fork protection factor operating through RAD51 is WRNIP1¹⁸. Specifically, WRNIP1 was shown to mediate both replication fork restart as well as protection through its distinct ATPase activity and RAD51 stabilization functions, respectively. Interestingly, WRNIP1 depletion results in MRE11-dependent fork degradation and does not enhance fork degradation in BRCA2 depleted cells, suggesting a potential epistasis through RAD51 stabilization. Despite protecting against two different nucleolytic degradation pathways, both BOD1L and WRNIP1 interact with BRCA2, implying their potential roles as effectors in BRCA-mediated fork protection^{13,18}.

A unique player in the RAD51-mediated fork protection pathway is RAD52. Despite its role in promoting MRE11-mediated degradation in BRCA2-deficient cells⁹, recent studies revealed that inactivation of RAD52 itself, in an otherwise BRCA-proficient background, predisposes forks to MRE11-mediated degradation¹⁹. This fork protection function is unrelated to any RAD51-stabilizing activity of RAD52. Rather, RAD52 likely functions to safeguard RAD51 pools in cells upon induction of replication stress by counteracting the fork reversal function of SMARCAL1. Moreover, this function appears to operate independently of the RAD52-MUS81 pathway of fork rescue.

RAD51-independent fork protectors

The occurrence of fork degradation independently of defects in a RAD51-mediated fork protection mechanism was documented in HR-proficient cells subjected to prolonged HU-mediated fork stalling⁶. As mentioned in previous sections, prolonged stalling triggers fork degradation through the alternative DNA2-WRN-associated pathway. This degradation is further exacerbated by inactivating the helicase RECQ1, which functions in resolving reversed fork intermediates. Importantly, in later studies, using RADX depletion to ameliorate potential defects in RAD51 function failed to prevent fork degradation in this setting⁴. Functional evidence suggests that this DNA2-mediated degradation aids in the restart of stalled/reversed replication forks. Indeed, these findings appear to be in line with the previously described role of DNA2 in suppressing the prevalence of reversed forks in fission yeast, thereby presumably preventing fork collapse²⁰.

Interestingly, recent work has revealed novel players which operate specifically in protecting replication forks from undergoing degradation through the DNA2-WRN pathway. One such fork protection factor is ABRO1, a paralog of ABRAXAS, a BRCA1-interacting protein²¹. ABRO1-mediated fork protection occurs independently of RAD51-mediated protection. Interestingly, the inability of ABRO1-deficient cells to protect forks from the DNA2-WRN pathway of degradation correlates with pathological defects in genome maintenance, such as accumulation of mitotic defects and 53BP1 nuclear bodies.

We recently uncovered an unexpected role for PCNA ubiquitination in protecting stalled replication forks from degradation through the DNA2-WRN pathway²². In line with the apparent mutual exclusivity of DNA2-WRN dependent fork degradation pathways and defects in RAD51-

mediated fork protection, we found that suppression of fork degradation by PCNA ubiquitination does not involve RAD51 activity. Rather, defects in fork protection in cells unable to ubiquitinate PCNA at the K164 residue (PCNA-K164R cells) were associated with previously described defects in PCNA unloading from the lagging strand, caused by defective Okazaki fragment ligation²³ resulting from the inability to mitigate replication-associated gaps²². In accordance with previous literature^{24,25}, the inability to unload PCNA from the lagging strand coincided with a loss of CAF-1 function in replication-associated nucleosome assembly, presumably caused by its abnormal sequestration through aberrant PCNA interactions. Indeed, we found that independent inactivation of factors governing each step, including: PCNA ubiquitination, LIG1 (Okazaki fragment ligation), ATAD5 (PCNA unloading) and CAF-1, triggered DNA2-driven fork degradation. Similar to ABRO1, the BRCA-independent nature of the PCNA ubiquitination-dependent fork protection was confirmed by the finding that loss of PCNA ubiquitination further exacerbated fork degradation in BRCA2-depleted cells. Like ABRO1, the failure to protect forks upon loss of PCNA ubiquitination was associated with pathological consequences such as HU-induced DSBs and the accumulation of 53BP1 nuclear foci.

Recent work has revealed roles for AND1 and TIM1, members of the fork protection complex (FPC, composed of TIM1, TIPIN, CLASPIN and AND1) in protecting stalled forks from MRE11-mediated degradation. A role for TIM1 in fork protection was identified through the characterization of the PCNA-interacting genome surveillance protein SDE2 and its function in preventing fork degradation^{26,27}. Specifically, SDE2 was found to promote the association of TIM1 with replication forks, ensuring their protection from MRE11-mediated resection upon stalling. Similarly, AND1 was found to protect replication forks from MRE11-mediated degradation²⁸. Importantly, it was observed that ssDNA at digested fork substrates efficiently

recruited RAD51 upon AND1 ablation, suggesting that RAD51 mediates fork protection independently of AND1 - and by extension the FPC.

A unique fork integrity pathway depends on the Y-family polymerase POLK. Recent studies showed that inactivation of POLK results in MRE11-dependent degradation of stalled forks²⁹. Notably, the ability of POLK to protect stalled forks appears to be linked to its role in restarting stalled replication forks in a manner dependent on the FA pathway. Furthermore, in line with known roles of Y-family polymerases in binding to ubiquitinated PCNA in order to mediate DNA damage tolerance^{30,31}, the ubiquitin binding domain (UBD) of POLK is essential for fork restart. However, it remains unclear whether the interactions of POLK with ubiquitinated PCNA entirely account for its fork protection function since, as mentioned above, PCNA ubiquitination operates in a distinct fork stability pathway, which restricts degradation by DNA2-WRN²². Furthermore, whether the fork protection function of POLK depends on RAD51 stabilization, as seen with the FA/BRCA pathway, remains unclear. Aside from POLK, other Y-family polymerases have also shown to potentially help bolster fork integrity. Recent work revealed a dependence of FA mutant cells, which are hypersensitive to interstrand crosslink (ICL)-inducing agents, on POLI for fork protection and restart upon stalling³². Roles for POLN and POLK in promoting crosslink repair have also been reported^{33,34}, suggesting a possible general function of Y-family polymerases in mitigating ICL-induced replication stress.

Components of the non-homologous end joining (NHEJ) pathway of DSB repair have also been implicated in protecting the stability of stalled replication forks. Recent works have revealed a role for the NHEJ effector RIF1 in protection from the DNA2-WRN pathway of degradation^{35,36}. Notably, this fork protection function occurs independently of 53BP1, but instead depends on interactions of the C-terminal domain of RIF1 with protein phosphatase 1

(PP1). DNA2-mediated degradation in RIF1-deficient cells was found to promote genome instability and sensitivity to replication stress, owing to defects in replication fork restart. Interestingly, in these studies, both DNA2 and WRN were found to be hyperphosphorylated in the absence of RIF1. However, if this hyperphosphorylation alters the function of DNA2-WRN at replication forks is unclear.

Despite the well-documented role of the loss of 53BP1, a master regulator of NHEJ, in restoring HR in BRCA1 deficient cells, 53BP1 loss has not been previously reported to exhibit functions in fork protection^{37,38}. Interestingly, in addition to promoting BRCA1-RAD51 recruitment at DSBs, the 53BP1 interactor TPX2 was recently shown to function in protecting stalled replication forks³⁹. This activity of TPX2 occurs in a manner parallel to the BRCA1 fork protection pathway and through its interaction with Aurora A. However, unlike in BRCA1-deficient cells, loss of 53BP1 ameliorates fork stability in TPX2-deficient cells, revealing a previously unappreciated function of 53BP1 in fork protection. Moreover, recent work also revealed an unexpected role of 53BP1 in suppressing DNA2-mediated nascent strand degradation in BRCA-proficient cells⁴⁰. Interestingly, this role of 53BP1 in replication fork protection was found to not be universally conserved, but rather stochastically dependent on cellular context and the nature of 53BP1 inactivation. These findings potentially reconcile the previously contrasting observations regarding the role of 53BP1 in maintaining replication fork stability³⁶⁻³⁹.

Recently, the Ku complex was found to mediate fork protection in *Schizosaccharomyces pombe*⁴¹. It was shown that upon binding DNA ends of reversed replication forks, Ku suppresses extensive resection of these structures. Upon fork reversal, the removal of Ku by the MRN-Ctp1 complex acts as a rate-limiting step prior to long range resection by EXO1. Intriguingly, the nuclease activity of MRE11 was found to be dispensable for the removal of Ku. This is in

contrast to previous reports of Ctp1 homologs Sae2 (*S. cerevisiae*) and CtIP (human) functioning to trigger the endonuclease activity of MRE11 at protein-blocked 5' DNA ends^{42,43}. In light of the well-documented role of the MRE11 nuclease activity in resecting forks, these observations suggest a differential regulation of MRE11 at forks without RAD51 protection defects, or perhaps simply a differential regulation of MRE11 at stalled forks in fission yeast.

Despite its role in the initiation of fork resection, loss of CtIP was recently found to result in DNA2-mediated degradation of stalled forks⁴⁴. While this activity appears to depend on its nuclease activity, CtIP-mediated fork protection was found to operate in the same pathway as BOD1L. Furthermore, loss of CtIP showed synergy with loss of BRCA1 in fork degradation and compromised the survival of BRCA1-deficient cells. Epistasis of CtIP with BOD1L in fork protection implies a possible indirect role of CtIP in contributing to RAD51-mediated stabilization^{13,15}. Indeed, recent work characterizing loss-of-function CtIP mutations found in individuals with high breast cancer risk, revealed a function for CtIP in stabilizing RAD51 at replication forks, thereby protecting them from degradation⁴⁵. The study of these mutations revealed that the fork-protective activity of CtIP depends on its Sae2-like domain and works by antagonizing the anti-recombinase activity of FBH1. Similar to CtIP, the MRE11-interacting protein EXD2, was also revealed as a guardian of fork stability. Through its nuclease activity, EXD2 prevents the accumulation of reversed forks which may otherwise be degraded⁴⁶. Similar to CtIP, which contributes to the survival of BRCA1-deficient cells, EXD2 is also required for cellular fitness in both BRCA1 and BRCA2 deficient cells.

Emerging insights into fork reversal pathways in fork degradation

As alluded to in previous sections, fork reversal is an important prerequisite for nuclease-mediated degradation of replication forks. In BRCA-deficient cells, fork reversal underlying fork degradation is RAD51-dependent. Importantly, RAD51 paralogs, namely RAD51B, RAD51C, RAD51D, XRCC2 and XRCC3, have also been revealed to be critical modulators of RAD51-mediated fork reversal⁴⁷. Specifically, the complex comprised of RAD51B,C,D and XRCC2 was found to be essential for fork slowing and reversal, thereby priming them for degradation in BRCA-deficient settings.

RAD51-dependent fork reversal is typically catalyzed by the SNF2-family DNA translocases SMARCAL1, ZRANB3 and HLTf^{5,8-10}. Interestingly, despite having distinct fork substrate preferences^{48,49}, depletion of each of the individual fork remodelers SMARCAL1, HLTf and ZRANB3 results in a complete rescue of fork stability in BRCA-deficient cells⁵. This suggests that, at least in the context of BRCA deficiency, SMARCAL1, HLTf and ZRANB3 may act cooperatively to mediate fork reversal, with each translocase playing an essential role (Fig. 1.1A). Interestingly, in cells unable to ubiquitinate PCNA, we uncovered that fork degradation showed no dependence on HLTf, a partial dependence on ZRANB3 and a complete dependence on SMARCAL1²² (Fig. 1.1B). The partial dependence on ZRANB3 in this context is somewhat expected since PCNA polyubiquitination at the K164 residue enhances the interaction with PCNA and the fork slowing/reversal function of ZRANB3^{50,51}. It remains unclear whether the lack of dependence on HLTf for fork reversal in PCNA ubiquitination-deficient cells reflects the role of HLTf in directly ubiquitinating PCNA^{52,53}, which may contribute to fork slowing by ZRANB3. HLTf also possesses an intrinsic translocase activity dependent on its HIRAN domain and readily remodels replication forks *in vitro*, as well as in cells upon the induction of replication

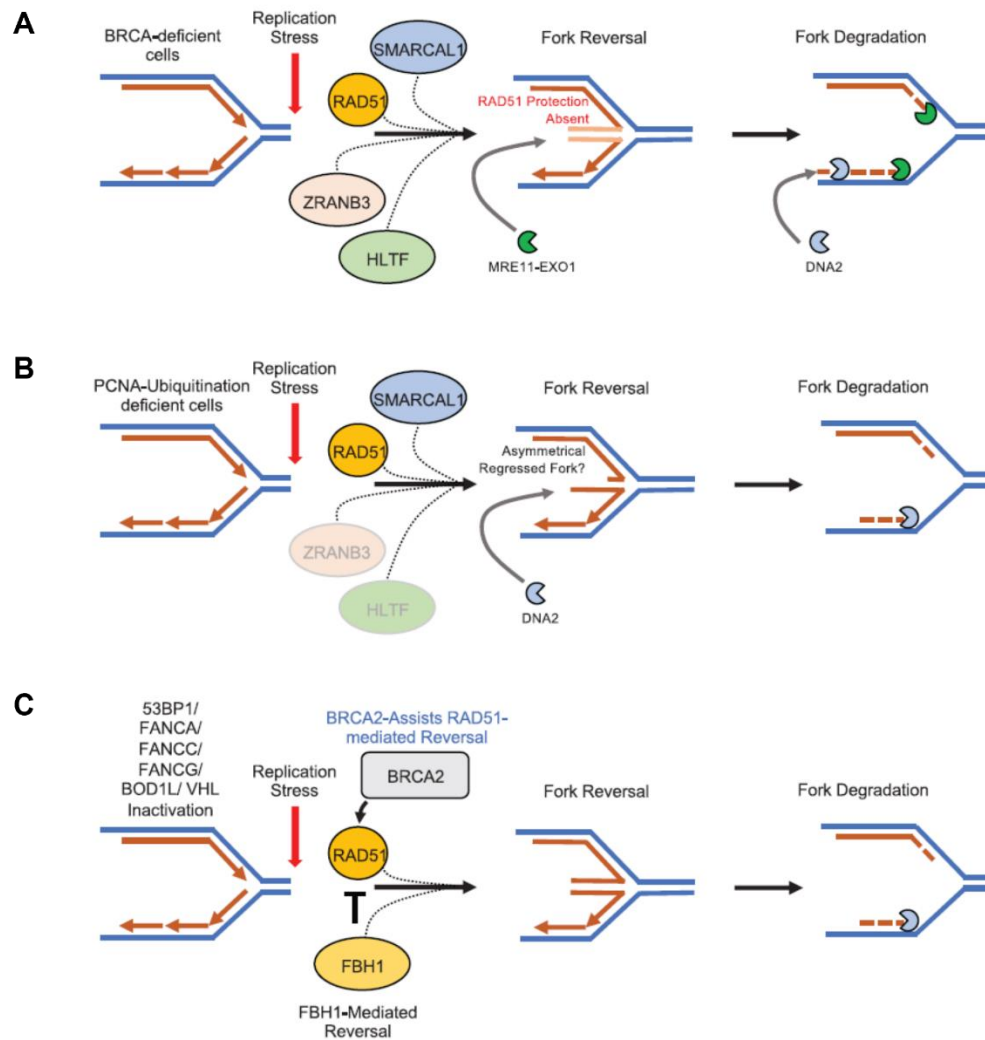


Figure 1.1: Fork reversal factors and their impact on fork degradation. Fork degradation in the context of BRCA-deficiency requires a coordinated function of the SNF2-family translocases SMARCAL1, ZRANB3 and HLTF, in addition to RAD51, in order to mediate fork reversal (**A**). Inactivation of either of these translocases is sufficient to rescue fork stability in BRCA-deficient cells. Fork degradation in the context of PCNA ubiquitination primarily involves the fork reversal activity of SMARCAL1, whereas ZRANB3 and HLTF show reduced roles (**B**). Fork reversal and subsequent degradation in the context of 53BP1, FANCA, FANCC, FANCG, BOD1L or VHL inactivation depends on the helicase FBH1 (**C**). Interestingly, in this context, BRCA2 aids in FBH1-mediated fork degradation by putatively bolstering RAD51 function against the RAD51-inhibitory effects of FBH1.

stress⁵⁴⁻⁵⁶. Overall, observations made in PCNA-ubiquitination deficient cells suggest that fork reversal may occur even without the coordinated activity of HLTf, ZRANB3 and SMARCAL1. Furthermore, each of these translocases have different fork substrate: SMARCAL1 shows a preference for leading strand-gaps, ZRANB3 for lagging strand gaps, and HLTf for unphosphorylated 3'-OH groups – potentially on leading strands or in the form of overhangs^{48,49,56,57}. Therefore, the selective activity of any of the translocases could potentially result in differences in the reversed fork structure. These differences may define the mechanism of fork degradation with regard to the nucleases involved (MRE11-EXO1 vs. DNA2) as well as dependence on RAD51 nucleofilament formation for fork protection. For example, the MRE11 nuclease is able to utilize its endonuclease activity and subsequently catalyze 3'-5' resection, enabling it to potentially act on both arms of reversed replication forks and prime the long range 5'-3' resection activity of EXO1^{58,59}. Therefore, it is possible that MRE11-mediated degradation is preferable in symmetrical reversed fork structures. In contrast, DNA2 is only able to catalyze 5'-3' resection and is also known to show activity against 5' ssDNA flaps arising during long-flap Okazaki fragment maturation⁶⁰⁻⁶². This raises the possibility of DNA2 requiring an asymmetrical reversed fork structure composed of an exposed 5' ssDNA end in order to act as the sole nuclease responsible for resection. We therefore propose that in PCNA ubiquitination-deficient cells, the selective activity of SMARCAL1 in recognizing leading strand gaps, in combination with the relative inactivity of ZRANB3, results in a preponderance of reversed fork structures revealing a 5' overhang. This 5' overhang may be subsequently degraded by DNA2 independently of the initial endonuclease and 3'-5' resection activity of MRE11 (Fig. 1.1B).

Recently, fork degradation mechanisms which operate by catalyzing fork reversal independently of the SNF2-family translocases were uncovered⁴⁰. Specifically, cells deficient of FANCA, FANCC, FANCG, BOD1L, VHL or 53BP1, showed fork degradation which depended

on RAD51 and the FBH1 helicase, previously found to catalyze fork reversal⁶³. Importantly, fork degradation in these contexts can occur independently of SMARCAL1, ZRANB3 and HLTF (Fig. 1.1C). Furthermore, upon SMARCAL1, ZRANB3 and HLTF abrogation, FBH1-mediated fork reversal and degradation in a 53BP1-deficient background was found to be dependent on BRCA2. BRCA2 was also required for fork reversal and subsequent degradation upon inhibition of RAD51 with the specific inhibitor B02. These findings reveal a previously uncharacterized role of BRCA2 in catalyzing fork reversal, likely in the same pathway as FBH1 (Fig. 1.1C). These observations are further complemented by the inability of BRCA-deficient cells to mediate efficient replication fork slowing upon exposure to low levels of replication stress⁶⁴. Conceptually, this could potentially underline the importance of BRCA2 in augmenting the function of RAD51 in restraining fork progression during replication stress. Additionally, the role of BRCA2 in mediating fork reversal could also offer a potential explanation for the dependence of BRCA-deficient cells on the concerted functions of SMARCAL1, ZRANB3 and HLTF in orchestrating fork reversal and subsequent degradation. Collectively, these findings reveal the existence of a number of fork remodeling pathways that directly influence the degradation of stalled replication forks.

While reversed forks appear to be the primary substrate for nucleolytic degradation, alternative fork substrates susceptible to nuclease activity have also been reported. The initial observation of MRE11-dependent post-replicative ssDNA gaps in RAD51-depleted *X. laevis* extracts, implies the existence of an entry point for MRE11 behind replication forks¹. Similar observations were later made in BRCA2-depleted *X. laevis* extracts⁸. Importantly, while fork reversal contributes to extensive fork degradation, MRE11-dependent post-replicative gap expansion could also contribute to nascent DNA loss. A recent study investigating the effect of HU-induced metabolic imbalances on replication forks showed that accumulation of reactive

oxygen species (ROS) triggers MRE11-dependent fork degradation as well gap accumulation⁶⁵. It was revealed that ROS specifically triggers ATM-dependent MRE11 phosphorylation, essential for the degradation of both stalled forks as well as post-replicative gap extension in progressing forks in HR-deficient cells. Since the absence of ROS precludes the apparent MRE11 activity at stalled forks, it is possible that the combined activity of MRE11 at reversed fork junctions as well as behind replication forks underlies HU-induced nascent DNA degradation. In this scenario, the absence of post-replicative gaps should preclude MRE11-dependent fork degradation. However, recent work identified separation-of-function BRCA2 mutants which rescued post-replicative gap formation but not fork protection⁶⁴. Overall, this suggests that while post-replicative gaps present a substrate for MRE11 activity, they may not be essential for the degradation of stalled forks, at least as measured by the DNA fiber assay. Nonetheless, it is possible that these gaps still play a role in enhancing nuclease-dependent fork instability. Further work will be needed to delineate their precise contribution.

The emerging role of chromatin dynamics in fork protection

The importance of nucleosome positioning and chromatin context during DSB resection is well documented^{66,67}. This raises the question of whether nucleosome dynamics and chromatin states also affect the susceptibility of stalled replication forks to nucleolytic degradation. The presence of nucleosomes in double stranded DNA directly counteracts long range nucleolytic resection⁶⁸. In recent work, we demonstrated that perturbing replication-associated nucleosome deposition by inactivating Chromatin assembly factor-1 (CAF-1), predisposes stalled forks to DNA2-dependent degradation (Fig. 1.2A)²². Indeed, previous research in yeast delineated the role of CAF-1 in establishing nucleosome periodicity, which closely correlates with Okazaki fragment length^{69,70}. Importantly, in the context of PCNA ubiquitination deficiency, where the

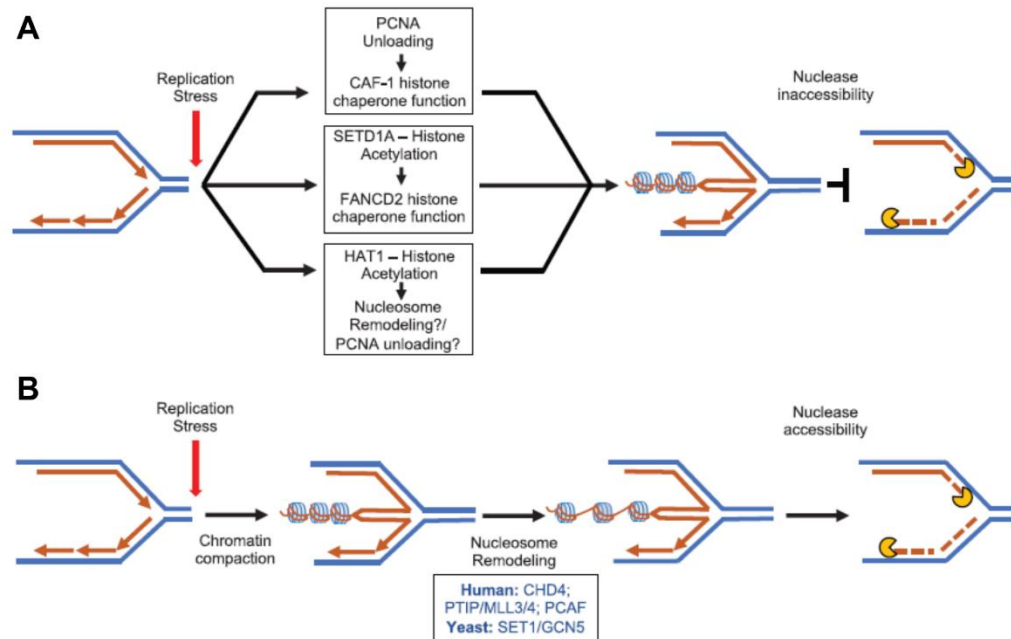


Figure 1.2: The impact of histone modifications and nucleosome remodeling on replication fork stability. The ability to mediate efficient histone chaperone activity by CAF-1 and FANCD2 is associated with replication fork protection. The chaperone activity of CAF-1 is enabled by efficient PCNA unloading from the lagging strand, which in turn depends on Okazaki fragment ligation and efficient lagging strand gap-filling by ubiquitinated PCNA. The fork protective histone chaperone activity of FANCD2 depends on the histone methyltransferase activity of SETD1A, which in turn restricts the activity of the CHD4, a member of the repressive NuRD complex. HAT1 promotes replication fork protection putatively through histone acetylation as well as ensuring timely PCNA unloading (A). Nucleosome remodeling may contribute to fork degradation by enhancing the activity of nucleases to reversed fork substrates. CHD4 enables the resection of stalled replication forks in cells deficient in BRCA2 and FANCD2, by promoting the activity of MRE11. The methyltransferase activity of the PTIP interacting histone methyltransferases MLL3/4 promote fork resection in BRCA-deficient cells by enabling the recruitment of MRE11. Similarly, the H4K8 acetyltransferase activity of PCAF promotes the recruitment of MRE11/EXO1 to stalled forks in BRCA-deficient cells. Finally, in yeast models, the methyltransferase and acetyltransferase activities of SET1 and GCN5 respectively are required for nucleosome remodeling events enabling the MRX complex to resect DNA at stalled replication forks (B).

inability to unload PCNA from lagging strands putatively sequesters CAF-1 away from active replication forks, the stability of reversed forks is compromised. This suggests a function of CAF-1 in stabilizing reversed replication forks. The role of nucleosomes in protecting reversed forks

was elucidated in further detail in RNF168-depleted systems, wherein histone H2A ubiquitination was found to be essential for fork progression, stability and restart⁷¹. Through psoralen-crosslinking coupled with EM under denaturing conditions, reversed forks were found to be increased in RNF168-depleted cells, and to contain ssDNA bubbles consistent with standard nucleosome periodicity. These observations indicate that nucleosomes can assemble on reversed forks and influence replication fork dynamics.

Chromatin remodelers were found to be important in determining the replication-coupled periodicity of nucleosomes⁷⁰ and influence DNA resection^{66,67}, suggesting their potential role in impacting fork stability. Interestingly, in yeast, the MRE11-RAD50-XRS2 (MRX) complex (equivalent to the MRN complex in metazoans), was shown to directly participate in chromatin remodeling to facilitate resection at stalled replication forks⁷². Specifically, MRX-associated remodeling depends directly on the activity of the yeast chromatin remodelers CHD1, ISW1 and the RSC complex, which in turn rely on the H3K4 methyltransferase and acetyltransferase activities of SET1 and GCN5 respectively, enabling increased chromatin accessibility (Fig. 1.2B). Similarly, in BRCA-deficient cells, the H3K4 and H4K8 methyltransferase activities of MLL3/4 and PCAF, respectively, promote the resection of stalled replication forks (Fig 1.2B)^{38,73}.

Interestingly, histone modifications which increase chromatin accessibility and subsequent remodeling do not exclusively work to facilitate fork resection, but rather, can also promote fork protection. For example, a dependence on the H3K4 methyltransferase SETD1A for fork protection was observed in mammalian cells¹⁵. Here, the requirement of H3K4 methylation was found to restrict the activity of CHD4, an ATPase component of the repressive NuRD complex, and promote the histone chaperone activity of FANCD2, thereby assisting in fork stability (Fig. 1.2A). Conversely, depletion of CHD4 was shown to restore fork protection in

BRCA2-deficient cells by suppressing the recruitment of MRE11 at HU-stalled forks (Fig. 1.2B)³⁸. Similarly, the loss of the histone acetyl transferase HAT1, primarily associated with increased chromatin accessibility, also renders stalled forks susceptible to degradation (Fig. 1.2A)⁷⁴. Another fork protection factor putatively dependent on chromatin accessibility is FANCI. Notably, loss of FANCI is associated with both fork degradation as well as abnormal chromatin compaction via H3K9-trimethylation (H3K9me3) at nascent DNA upon treatment with HU^{75,76}. However, it remains unclear whether excessive chromatin compaction at stressed nascent DNA in FANCI deficient cells directly underlies fork degradation, or simply reflects a protective mechanism against excessive fork resection. Recent work in fission yeast implies that *de novo* chromatin compaction at replication forks during replication stress may indeed confer protection against fork instability⁷⁷. Specifically, replication stress was shown to trigger H2BK33-deacetylation and H3K9me3 accumulation at replication forks. Importantly, H2BK33-deacetylation was found to prevent the untimely uncoupling of replisome components, thereby aiding fork restart and protecting against fork collapse.

Collectively, these observations underline the importance and the context-dependency of histone modifications in directly enabling the activities of chromatin remodelers and histone chaperones, thereby defining the nucleosomal landscape for the resection of stalled forks.

Fork Protection and the Impact on Cellular Survival

Restoration of fork protection

Recent studies identified an association between the restoration of fork stability and chemoresistance in BRCA-deficient cells, making fork stability an important component of the

etiology of BRCA-mutant cancers^{5,38}. As mentioned in earlier sections, a fundamental determinant of replication fork degradation is fork reversal mediated by the SNF2 family DNA2 translocases SMARCAL1, ZRANB3 and HLTF^{5,8-10}. Perturbing the activities of each of these fork remodelers restored not only fork protection but also resistance to cisplatin and PARP inhibitors (PARPi) in BRCA1-deficient cells⁵. However, the impact of abolishing fork reversal through translocase inactivation on genome stability in BRCA-deficient cells is less clear. While abolishing fork reversal by SMARCAL1 and ZRANB3 depletion rescued DSB formation and chromosomal aberrations in BRCA1/2-depleted cells treated with camptothecin (CPT)⁵, ZRANB3 loss in BRCA2-depleted cells was found to further exacerbate chromosomal abnormalities upon treatment with HU⁹. These divergent effects can be possibly explained by the differences in how HU and CPT create replication stress, thereby resulting in varied outcomes upon abolishing fork reversal in BRCA-deficient cells. Further work is needed to precisely reconcile these differences.

As mentioned in the previous section, loss of CHD4 restores both chemoresistance and fork protection in BRCA2-deficient cells^{38,78}. A possible explanation for this is the function of CHD4 as a chromatin remodeler, acting in a manner opposing SETD1A-mediated H3K4 methylation thereby facilitating resection¹⁵. However, previous work has suggested that the mechanism of chemoresistance upon CHD4 depletion in BRCA2-deficient cells is through the enhancement of RAD18-mediated PCNA ubiquitination⁷⁸. Since loss of PCNA ubiquitination enhances fork degradation in BRCA2-depleted cells²², it is plausible that PCNA ubiquitination triggered by CHD4 loss could bolster fork protection in BRCA2-deficient cells. However, loss of CHD4 in BRCA2-deficient cells may also contribute to chemoresistance independently of fork protection, by augmenting PCNA ubiquitination-dependent translesion synthesis (TLS). Similar to the loss of CHD4, inactivation of the NHEJ component PTIP and of the PTIP-interacting

H3K4 methyltransferases MLL3/4 also rescues fork stability and confers chemoresistance to BRCA2 deficient cells³⁸.

Restoration of RAD51 function was recently shown to rescue fork stability in cellular backgrounds which fail to form stable RAD51 nucleofilaments at stressed replication forks. Specifically, the loss of RADX, a competitor of RAD51 in binding to ssDNA, restores fork protection in cells deficient in components of the FA/BRCA pathway^{4,79}. Increasing RAD51 binding to DNA by perturbing RADX restores fork protection independently of restoring the function of upstream FA/BRCA pathway components. On similar lines, in recent work we uncovered that loss of E2F7, a transcriptional repressor of RAD51, restores RAD51 recruitment to chromatin, thereby promoting fork stability in BRCA2-deficient cells⁸⁰.

Through unbiased CRISPR knockout screens, we also established that loss of the acetyltransferase TIP60, previously described as a suppressor of 53BP1^{81,82}, confers resistance to the PARPi olaparib, and restores replication fork protection to BRCA2-deficient cells⁸³. Importantly, the olaparib resistance upon TIP60 depletion was dependent on the NHEJ effectors 53BP1 and REV7 and involved suppression of resection at olaparib-induced DSBs. However, it is unclear whether the restoration of fork stability in BRCA2-deficient cells upon TIP60-depletion also arises as a result of suppression of DNA resection, dependent on NHEJ components.

Fork protection and cellular survival

Restoration of fork protection is associated with acquired chemoresistance^{5,38}. However, much of recent work suggests that the restoration of fork protection may not always translate to

enhanced cell survival. Rather, this may depend on the context of the genetic background as well as the nature of replication stress encountered.

In the initial characterization of the function of BRCA2 in protecting stalled replication forks, it was found that HU-induced fork degradation did not directly translate into HU sensitivity². This is in contrast to the role of fork protection in restoring chemoresistance to both BRCA1 and BRCA2-deficient cells³⁸. Unlike the loss of BRCA2 function, loss of BRCA1 was found to confer sensitivity to HU⁸⁴. This fork protection function occurs independently of the BRCA1-PALB2 interaction (and therefore its interaction with BRCA2), but rather depends on the interaction of BRCA1 with BARD1^{84,85}. This mutual independence of BRCA1 and BRCA2 in their fork protection activities might, in part, explain the observed differential impact of fork degradation on cellular survival. Inactivation of fork reversal has only been documented to restore chemoresistance to BRCA1-deficient cells⁵, suggesting a differential impact of SMARCAL1, HLTF and ZRANB3 inactivation in the context of either BRCA1 or BRCA2 deficiency on DNA damage accumulation and repair. Interestingly, BRCA1 deficient cells were shown to mount an adaptive response to cisplatin pre-treatment by upregulating PRIMPOL-mediated repriming, thereby counteracting fork reversal and degradation and ensuring cell survival⁸⁶.

Fork protection defects are also a hallmark of FA pathway deficiency^{3,87}. In the absence of FANCD2, aberrant activity of DNA2 was found to underlie defective ICL repair¹⁴, suggesting a role for FA-mediated fork protection at ICL-stalled forks. In line with this, inactivation of fork protection factors such as BOD1L-SETD1A, which operate in the same pathway as FANCD2 in preventing DNA2-mediated degradation of forks, underlies sensitivity to ICL-inducing agents^{13,15}. Similarly, RAD51 mutations identified in individuals with FA-like presentation were shown to cause fork degradation and ICL sensitivity⁸⁸. Importantly, recent work also revealed that

BRCA2 DNA-binding domain (DBD) mutants engender FA-like presentations, sensitivity to ICLs via excessive DNA2-mediated resection, and fork protection defects⁸⁹. Intriguingly, unlike what was observed for BRCA1⁵, fork reversal through SMARCAL1, HLF and ZRANB3 did not play a role in ICL-induced fork resection in these BRCA2 DBD-mutant cells. Conceptually, these findings indicate overlapping functions of the BRCA pathway with the FA pathway of ICL repair, and highlight the importance of BRCA2-RAD51-mediated fork protection in cellular survival upon treatment with ICL-inducing agents.

Recent evidence has linked the restoration of fork protection to synthetic viability in BRCA-deficient backgrounds. Knockdown or genetic ablation of PARP1 was shown to restore viability to mouse embryonic stem cells (mESCs) bearing a homozygous genetic knockout of BRCA2 (BRCA2-KO)⁹⁰. Importantly, it was found that loss of PARP1 had no effect in restoring HR, but rather restored fork protection to these cells. Similarly, loss of either PTIP or RADX, which promotes fork stability in BRCA-deficient cells, also restores synthetic viability to BRCA2-KO mESCs, without rescuing HR^{38,79}.

In line with the role of fork protection in restoring viability, the further enhancement of fork degradation was shown to contribute to synthetic lethality in BRCA-deficient cells. BRCA-deficient cells were found to be hyperdependent on FANCD2 for fork protection and survival^{16,17}. However, FANCD2 was also found to enhance the recruitment of POLQ to damaged DNA, thereby promoting alternative end-joining¹⁷, in line with a role for POLQ in enhancing the survival of BRCA-deficient cells. Indeed, BRCA-deficient tumors were found to be dependent on POLQ-mediated alternative-NHEJ for survival^{91,92}. Loss of CTIP function, which underlies fork degradation, also synergizes with the loss of BRCA1, resulting in a further exacerbation of fork degradation and synthetic sickness in BRCA1-deficient cells⁴⁴. Similar to FANCD2, the

deubiquitinase USP1 was found to be required for fork protection in BRCA1 deficient cells, and loss of USP1 triggered lethality in these cells⁹³. Lastly, loss of PRIMPOL results in fork degradation and exacerbates the growth defects of BRCA1-mutant cells⁸⁶. Collectively, these observations highlight the importance of fork protection in determining cellular fitness in the context of BRCA deficiency.

Fork stability and PARPi sensitivity

Restoration of fork stability often correlates with resistance to PARPi (Fig. 1.3A). Restoration of fork stability by abrogating fork reversal was shown to ameliorate PARPi sensitivity in BRCA1-deficient cells⁵. Similarly, RADX depletion, which restores fork protection in BRCA-deficient cells without rescuing HR, also restores PARPi resistance in BRCA2-deficient cells⁷⁹. Furthermore, treatment with olaparib in concert with HU further enhances fork degradation in BRCA2-deficient cells⁹⁴. The amelioration of PARPi sensitivity upon restoration of fork protection appears in many cases to be context-dependent. For example, abrogation of fork reversal has not been documented to improve survival upon PARPi treatment in BRCA2-deficient cells. On similar lines, RADX inactivation, though restoring fork protection to BRCA1-deficient cells, does not impact the survival of these cells upon treatment with PARPi⁴. These observations indicate that conventional fork protection, while a contributing factor, may not be the primary determinant of PARPi sensitivity.

A specific context in which PARPi sensitivity correlates with fork protection defects is that of the activation of ssDNA-induced innate immune response. Nucleolytic processing of stalled replication forks was shown to induce activation of the cGAS-STING pathway triggered by the presence of cytosolic ssDNA⁹⁵. Furthermore, PARPi treatment was shown to trigger the

expression of interferon-stimulated genes and activation of the cGAS-STING pathway in BRCA2-deficient cells, owing to the presence of cytosolic DNA⁹⁶. Similarly, in mouse models of BRCA1-deficient ovarian cancer, the cGAS-STING pathway was found to be critical for PARPi-dependent reduction of tumor size⁹⁷. It is therefore possible that, in the context of an intact innate immune signaling, restored fork protection becomes an important component of acquired PARPi resistance. Indeed, in orthotopic transplantation mouse models, acquired PARPi resistance of BRCA2-deficient tumors was found to coincide with restoration of fork stability³⁸. This suggests that fork protection is a potential mechanism by which tumors avoid immune surveillance and become resistant to PARPi *in vivo*.

A significant body of work identified restoration of DSB repair as a major mechanism of acquired PARPi resistance. Our recent work showed that loss of E2F7 promotes PARPi resistance in BRCA2-deficient cells, and this correlates with both fork protection, and HR restoration⁸⁰. BRCA2 DBD mutants which display fork protection defects (likely explaining their MMC sensitivity), also show sensitivity to PARPi⁸⁹. While moderately compromised, HR was not abolished in these cells. Moreover, we recently showed that loss of the acetyltransferase TIP60 confers PARPi resistance to BRCA2-deficient cells through the restoration of accurate end-joining DSB repair⁸³. In BRCA1-deficient cells, loss of 53BP1 or of the Shieldin complex, which is a critical effector of 53BP1-mediated NHEJ, restores HR and PARPi resistance^{37,98-104}. Collectively, these findings underline the importance of intact DSB repair as a major determinant of PARPi resistance (Fig. 1.3A).

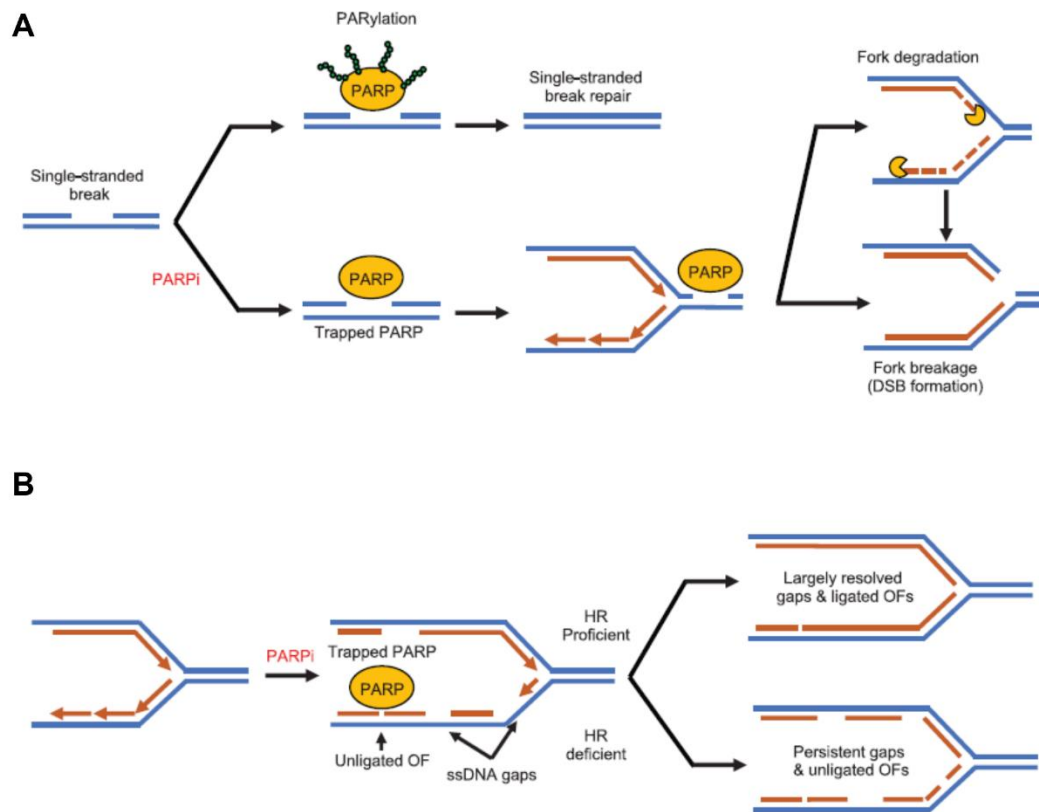


Figure 1.3: Proposed mechanisms of PARPi-mediated cellular lethality in BRCA-deficient cells. The original models proposed fork degradation and DSB-induction as major mechanisms contributing to PARPi-mediated synthetic lethality in BRCA-deficient cells. Specifically, PARPi-induced trapping of PARP1/2 on the chromatin poses obstacles to replication fork progression thereby causing replication stress which putatively results in fork degradation and/or fork cleavage (**A**). A proposed alternative model suggests ssDNA gap induction as the major mechanism underlying PARPi-mediated cellular lethality. In HR-deficient cells, PARPi can potentially create persistent ssDNA gaps by inhibiting timely fork slowing in the face of replication stress as well as interfering with the resolution of ribonucleotide excision intermediates owing to PARP-trapping. PARPi can also interfere with the resolution of Okazaki fragment ligation by inhibiting lagging strand gap-filling and cause the potential accumulation of trapped PARP at unligated Okazaki fragment intermediates. A combination of persistent ssDNA gaps and unligated Okazaki fragments may lead to cellular lethality in HR-deficient cells (**B**).

Another mechanism implicated in PARPi-mediated cytotoxicity is the trapping of PARP1 and PARP2 proteins on the chromatin. Trapped PARP1/2 could directly pose obstacles to DNA

replication, and thereby potentially underlie fork degradation and DSB formation (Fig. 1.3A, B). The cytotoxic effects of trapped-PARP lesions were first described in DT40 chicken lymphoblasts, where the genetic depletion of PARP1 was found to suppress PARPi sensitivity¹⁰⁵. Furthermore, recent studies revealed that loss of ALC1 drives PARPi sensitivity in HR-deficient cells by prohibiting the release of trapped PARP1 and PARP2 from chromatin¹⁰⁶⁻¹⁰⁸. Genome-wide CRISPR screens have recently uncovered misincorporated ribonucleotides as a major source of PARP-trapping lesions¹⁰⁹. Specifically, TOP1-mediated cleavage of misincorporated ribonucleotides was shown to underlie PARPi sensitivity in RNASEH2-knockout cells, suggesting a role of TOP1 cleavage products in engaging and subsequently trapping PARP1. PARP-trapping was also shown to contribute to the transcriptional repression of p21 leading to an unbridled increase in fork speed, which could potentially exacerbate the effect of trapped-PARP lesions encountered by the replication fork¹¹⁰.

We recently showed that PCNA-K164R cells, which have fork protection defects, are not sensitive to PARPi but instead exacerbate the PARPi sensitivity of BRCA-deficient cells²². This further indicates that fork protection is unlikely to be a universal determinant of PARPi resistance. Instead, we found that lack of PCNA ubiquitination synergizes with BRCA deficiency in suppressing the accumulation of ssDNA gaps, which correlates with the synergistic sensitivity to PARPi. This raises the possibility that persistent ssDNA gaps, rather than defects in fork protection, are responsible for PARPi sensitivity. This is further corroborated by recent work showing that PARPi treatment results in formation of replication associated gaps, potentially exacerbating the predisposition to gap formation of BRCA-deficient cells (Fig. 1.3B)^{64,111}. In these studies, PARPi resistance was found to be associated with increased capacity to suppress PARPi-induced gaps. Furthermore, restoration of gap suppression in the absence of fork protection was sufficient to confer PARPi resistance to BRCA2- or FA-deficient cells. The role of

HR in suppressing ssDNA gaps is supported by the findings that RAD51 is required for post-replicative gap filling in response to bulky DNA lesions or the absence of translesion synthesis^{1,112,113}. However, the precise mechanism underlying the formation of PARPi-induced gaps remains unclear. One possibility could be related to the role of PARP1 in mediating fork slowing and reversal upon encountering replication stress¹¹⁴. As BRCA-deficient cells are defective in fork slowing/reversal and gap-filling^{8,22,40,64}, unrestrained fork progression upon PARPi treatment could give rise to an accumulation of spontaneously occurring gaps resulting from endogenous replication stress in these cells. Another putative source of PARPi-induced ssDNA gaps is TOP1 cleavage products of misincorporated ribonucleotides¹⁰⁹, which could become persistent due to the inhibition of ssDNA gap repair by PARP1. In both situations, the persistence of newly acquired replication-associated gaps could become exacerbated in the absence of BRCA-mediated post-replicative repair. Indeed, studies in *X. laevis* egg extracts established a role for RAD51 and BRCA2 in suppressing gaps both at the junctions of replication forks, as well as MRE11-dependent gaps behind them^{1,8}, thus solidifying a bona fide connection between the BRCA/RAD51-mediated HR and novel gap evasion.

An unexpected role for PARP1 and PARP2 in ensuring the ligation of Okazaki fragments which escaped conventional ligation during S-phase DNA synthesis was recently revealed¹¹⁵. Perturbation of Okazaki fragment maturation through chemical inhibition of FEN1 in PARP1/2-deficient cells was found to cause lethality. These observations suggest that an aberrant accumulation of unligated Okazaki fragments could itself be toxic to cells. Recent work including ours suggests that the inability to mitigate replication associated gaps, for example upon loss of PCNA ubiquitination, causes lagging strand synthesis defects through the preferential accumulation of lagging strand-associated gaps likely owing to frequent repriming by Pol α ^{22,116,117}. This indicates the possibility that, upon PARPi treatment, ssDNA gaps preferentially

accumulate on the lagging strand in the absence of gap-filling pathways such as the BRCA pathway. Persistent lagging strand gaps undergoing delayed gap-filling in BRCA-deficient cells could later necessitate the engagement of PARP1/2 at unligated Okazaki fragment substrates. In this situation, PARPi could further exacerbate the prevalence of toxic unligated Okazaki fragments as well as lead to PARP-trapping lesions at these substrates, resulting in selective cytotoxicity in these cells.

In conclusion, while fork protection may confer PARPi-resistance in certain backgrounds, it is possible that mechanisms which allow cells to evade catastrophic DSB-induction, PARP-trapping and ssDNA gap accumulation comprise the major channels by which PARPi resistance is restored.

Concluding Remarks

In the past decade, replication fork degradation has emerged as a major mechanism underlying cancer-associated genome instability. Fork protection and its determinants have gained prominence in the context of BRCA deficiency. This is due to the fact that fork degradation observed in BRCA-deficient cells revealed fork protection as a major mechanism by which the BRCA pathway ensures genome stability. These findings are especially significant since they reveal a protective function of the BRCA pathway against replication stress, which is frequently encountered by cells undergoing DNA replication. Due to the relatively ubiquitous nature of replication stress, as opposed to DSBs – which represent the most severe form of DNA damage – replication fork protection can be regarded as a more clinically relevant mechanism by which genome stability is maintained by the BRCA pathway. In recent years, fork protection has also emerged as a major determinant cell survival and chemosensitivity, highlighting the inability

to protect replication forks as a therapeutic vulnerability in BRCA-deficient cancers. Therefore, gaining a better understanding of the underpinnings of fork stability has important implications in the etiology of BRCA-deficient cancers as well as other cancers susceptible to fork degradation.

Recent efforts in characterizing fork protection defects have yielded not only a better understanding of how the BRCA pathway orchestrates fork protection, but also revealed a multitude of other factors which govern fork stability. Importantly, these newly-emerging factors belong to pathways which either cooperate with the BRCA pathway or act independently of it in protecting replication forks. In this review, we examined these factors on the basis of their dependence on RAD51 to orchestrate fork protection, and the mechanisms of fork resection they protect against (MRE11, DNA2-WRN). We further examined the downstream effects of the loss of fork protection upon the inactivation of these pathways on genome stability, as well as the impact of their combined inactivation with the BRCA pathway on cell viability. We also explored the emerging role of nucleosome remodeling and chromatin dynamics as determinants of stalled fork resection. Importantly, histone modifications and nucleosome remodeling may have a direct impact on the accessibility of nucleases to stalled fork substrates, thereby influencing fork resection.

The inability to protect replication forks is associated with a vulnerability to treatment with chemotherapeutics in BRCA-deficient cells. Conversely, the artificial restoration of fork stability in BRCA-deficient cells has been shown to restore chemoresistance to these cells. This highlights the challenges in the treatment of BRCA-deficient cancers. In the last section, we examined mechanisms underlying the restoration of fork stability to BRCA-deficient cells. These include: restoration of the RAD51 fork protective function, inactivation of replication fork reversal, increasing the reliance of BRCA-deficient cells on proteins which bolster fork stability

(such as FANCD2, USP1 and PRIMPOL). Finally, we evaluated fork degradation as a mechanism contributing to PARPi-mediated synthetic lethality. Recent findings showed that fork degradation, though often associated with PARPi sensitivity, may not be universally causative of PARPi-mediated cellular lethality. Instead, a more significant correlation may be found between PARPi sensitivity and the inability to mitigate replication-associated ssDNA gaps. These gaps may arise as a result of the effect of PARPi in suppressing key functions of PARP1 in mediating replication fork slowing upon stress encounter, as well as inducing PARP-trapping as a result of the aborted resolution of misincorporated ribonucleotides during DNA replication. We suggest an importance of unligated Okazaki fragments as lesions potentially contributing to PARPi-mediated cellular lethality. Collectively, these observations imply a complex role of fork protection in determining progression as well as therapeutic outcomes in BRCA-mutant cancers. Furthermore, the breadth of the emergent determinants of fork stability discussed here, may indicate a more significant role of fork stability in cancer etiology than previously anticipated.

Chapter 2

Uncovering the Role of PCNA-Ubiquitination in Maintaining Replication Fork Integrity

Rationale

DNA replication is initiated at discrete replication origins and occurs in a continuous manner on the leading strand, catalyzed by DNA polymerase Pol ϵ . In contrast, lagging strand replication needs frequent re-priming by the Pol α -primase complex, followed by processive DNA synthesis by Pol δ . This results in short RNA-primed DNA fragments known as Okazaki fragments (OFs). An essential component of the replication machinery is the homotrimeric ring-shaped protein Proliferating Cell Nuclear Antigen (PCNA), which encircles and slides along the DNA during DNA synthesis. PCNA is loaded at replication origins by the RFC1-5 complex, and unloaded upon replication termination by an alternative complex in which ATAD5 (Elg1 in yeast) replaces RFC1^{23,118}. During DNA synthesis, PCNA interacts with the replicative polymerases on each strand and enhances their processivities^{119,120}. On the lagging strand PCNA recruits the Flap endonuclease (FEN1) which cleaves the RNA primer displaced by Pol δ , and DNA ligase 1 (LIG1) which seals the resulting nick to complete OF maturation (OFM)¹²¹. Concomitant with DNA replication, PCNA promotes chromatinization of the newly synthesized DNA by recruiting the chromatin assembly factor CAF-1 and other histone chaperones^{122,123}. These interactions are mediated by a motif termed PCNA-interacting peptide (PIP)-box^{119,124}.

Unrepaired DNA lesions, secondary DNA structures, and other difficult to replicate sequences, can induce the arrest of the replicative polymerases, causing replication stress^{125,126}. In response to replication stress, PCNA is mono-ubiquitinated by the RAD18 ubiquitin-ligase at lysine 164 (K164). This modification promotes a switch from the replicative polymerase to

specialized low-fidelity polymerases, which preferentially bind ubiquitinated-PCNA (UbiPCNA)^{30,31,119,120,127,128}. These polymerases bypass replication obstacles to ensure efficient DNA replication, a process known as translesion synthesis (TLS)^{129,130}.

In vertebrate cells, mono-ubiquitination is the prevalent form of modified PCNA, although poly-ubiquitination can also be detected^{52,53,131}. While PCNA ubiquitination is induced upon replication stress, basal levels of mono-ubiquitinated PCNA can be detected in S-phase cells under unperturbed growth conditions^{30,52,53}. This suggests that, in human cells, PCNA ubiquitination may play an important but so far elusive role in controlling replication fork progression and genome stability during normal S-phase. In the following sections we examine the role of PCNA-ubiquitination during unperturbed DNA replication as well as its role in determining the stability of stalled replication forks. We further study the impact of PCNA-ubiquitination in ensuring efficient OFM, PCNA unloading, and replication coupled nucleosome assembly and the role of these processes in influencing the stability of replication forks during stress. Lastly, we also study the impact of PCNA-ubiquitination loss on fork stability and post-replicative gap accumulation in the context of BRCA-deficiency, as well its potential role in influencing the survivability of BRCA-deficient cells upon treatment with the PARP-inhibitor Olaparib.

Results

Generation of PCNA-K164R mutant cells

As PCNA is essential for cell proliferation, previous studies investigating the role of PCNA ubiquitination in human cell lines relied on siRNA-mediated depletion of endogenous

PCNA coupled with transfection of a K164R mutant or PCNA-ubiquitin fusion polypeptides 6. However, the residual expression from the endogenous PCNA locus and the artificial overexpression of the PCNA variants can complicate the analyses. In order to overcome these limitations, we employed CRISPR/Cas9 gene editing to introduce the K164R homozygous mutation in the endogenous PCNA gene, in 293T and RPE1 cell lines. Monoclonal cultures were initially screened for loss of PCNA ubiquitination by western blot using an antibody specific for ubiquitinated PCNA. Several K164R mutant 293T clones were obtained. However, the level of unmodified PCNA in these clones was reduced compared to the parental line, as shown for the clone KR5, in Fig. A1. The genome of 293T cells is considered pseudotriploid¹³². Cloning of individual PCNA alleles from the KR5 cell line followed by Sanger sequencing revealed, in addition to PCNA-K164R allele(s), other alleles in which the PCNA gene was inactivated through introduction of small insertions or deletions. To exclude phenotypes caused by reduced PCNA expression and off-target effects of CRISPR/Cas9, we created an isogenic pair by re-expressing wildtype PCNA or the K164R mutant in the KR5 clone through a lentiviral expression system. The resulting cell lines, termed 293T-WT and 293T-K164R (or KR) from here on, show similar levels of unmodified PCNA between themselves and when compared to the parental cell line (Fig. 2.1A; Fig. A1). In contrast to 293T cells, RPE1 cells are near-diploid¹³³. Two RPE1 clones harboring the PCNA-K164R mutation endogenously were generated (Fig. 2.1B). Both clones showed similar levels of unmodified PCNA as the parental line. Sequencing of the genomic region confirmed that, in both clones, both PCNA alleles were homozygously edited with the desired mutation, and thus they were used for subsequent experiments without the complementation employed for 293T cells.

sensitive to DNA damaging agents that induce single-stranded DNA lesions, such as UV and cisplatin (Fig. 2.1D, E).

Replication stress and increased fork speed in PCNA- K164R cells

Under unperturbed growth conditions, KR clones showed lower proliferation rates (Fig. 2.2A), and a reduced proportion of cells undergoing DNA synthesis (Fig. 2.2B). As this pattern was reminiscent of cells experiencing increased levels of endogenous replication stress¹³⁵, we next investigated expression of DNA damage markers. We observed that, under normal growth conditions, KR cells showed increased levels of CHK2 phosphorylation (Fig. 2.2C) and 53BP1 chromatin foci (Fig. 2.2D,E), indicating DNA damage accumulation. These findings suggest that PCNA ubiquitination-deficient cells are unable to resolve endogenous replication stress, resulting in DNA damage accumulation under unperturbed growth conditions.

To evaluate the role of PCNA ubiquitination in replication fork progression, we employed the DNA fiber combing assay to measure replication dynamics in K164R cells. Under unperturbed growth conditions, both 293T-K164R and RPE1-K164R cells showed longer nascent tract length and increased replication fork speed (Fig. 2.3A, B). Previously, it was shown that the ZRANB3 translocase is recruited by K63-linked polyubiquitinated PCNA to mediate slowing of replication forks in the presence of replication stress³⁸. In line with this, we found that 293T-K164R cells were unable to efficiently reduce fork speed in the presence of low levels (0.4mM) of the replication fork stalling agent hydroxyurea (HU) (Fig. 2.3C). This raises the possibility that the longer nascent tracts observed in KR cells under normal growth conditions may simply reflect the loss of ZRANB3 recruitment to stressed replication forks. To address this, we depleted ZRANB3 in wildtype cells. This did not result in longer nascent tracts (Fig. A2A, B), arguing

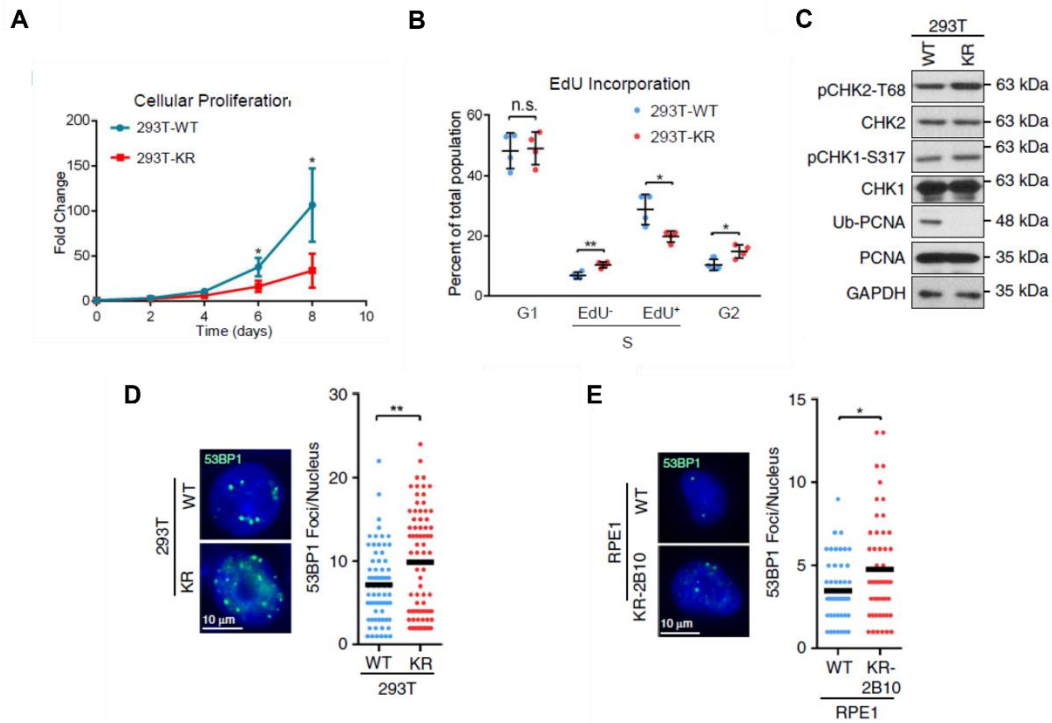


Figure 2.2: Endogenous replication stress in PCNA-K164R cells. (A) Reduced rate of proliferation of 293T-K164R cells as measured by the ATP-based CellTiter-Glo assay. The average of three independent experiments with standard deviations indicated as error bars is shown. Asterisks indicate statistical significance (t-test, two tailed, unequal variance). (B) Reduced EdU incorporation and increased G2 accumulation in 293T-K164R cells as measured by EdU/PI flow cytometry. The average of three independent experiments with standard deviations indicated as error bars is shown. Asterisks indicate statistical significance (t-test, two tailed, unequal variance). (C) 293T-K164R cells exhibit increased CHK2-T68 phosphorylation. (D), (E) Increased 53BP1 foci formation in 293T-K164R (D) and RPE1-K164R cells (E). At least 50 cells were quantified for each condition. The mean values are marked on the graph, and asterisks indicate statistical significance (t-test, two-tailed, unequal variance). Representative micrographs are also shown.

against a role for ZRANB3-mediated fork slowing in controlling fork speed under normal growth conditions.

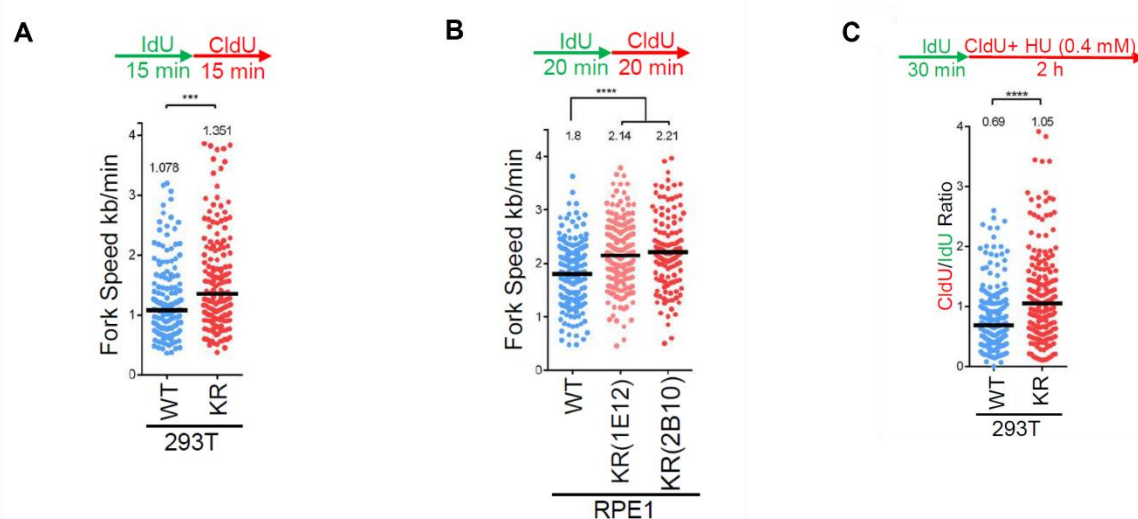


Figure 2.3: Increased fork speed in PCNA-K164R cells. (A), (B) DNA fiber combing experiments showing increased fork speed in 293T-K164R (A) and RPE1-K164R (B) cells. Each $1\mu\text{m}$ in fiber length was set to correspond to 2 kilobases of DNA. Median values are marked on the graph and listed at the top. Asterisks indicate statistical significance (Mann-Whitney test, two-sided). Schematic representations of the assay conditions are also presented. DNA fiber combing experiment showing reduced fork slowing in 293T-K164R cells upon low-level replication stress exposure (C). The ratio of CldU to IdU tract lengths is presented, with the median values marked on the graph and listed at the top. Asterisks indicate statistical significance (Mann-Whitney test, two-sided). A schematic representation of the assay conditions is also presented.

PCNA ubiquitination protects stalled forks from degradation

To investigate if the abnormal replication fork characteristics described above are associated with defects in fork stability, we measured replication fork integrity in the presence of acute replication stress. Treatment with 4mM HU resulted in degradation of the nascent DNA tract in both 293T-K164R and RPE1-K164R cells, but not in the respective control cells (Fig. 2.4A-D). Nascent tract degradation was observed under two different experimental conditions: when HU was added for 3h in between the IdU and CldU pulses and the IdU tract length was measured (Fig. 2.4A, B), and when HU was added for 4.5h after consecutive incubations with

thymidine analogs and the ratio of CldU to IdU tract-lengths was calculated (Fig. 2.4C, D). HU-induced nascent strand degradation has been extensively described in the context of BRCA deficiency, where it is dependent on the activity of the MRE11 nuclease²⁻⁴. Surprisingly, MRE11 inhibition using the inhibitor mirin did not suppress nascent tract degradation in KR cells (Fig. 2.4C, D; Fig. A3A-C), indicating that a different fork degradation pathway operates in these cells. We further ruled out the involvement of other nucleases previously involved in nascent tract degradation, including EXO1, CTIP, and MUS81^{10,136} (Fig. A3D, E). In contrast, inhibition of the nuclease DNA2 with the specific inhibitor C5, or siRNA-mediated knockdown of DNA2, completely restored nascent tract length in both 293T-K164R and RPE1-K164R cells (Fig. 2.4C, D; Fig. A3F, G), indicating that DNA2 is the nuclease responsible for fork degradation upon loss of PCNA ubiquitination. The WRN helicase has been previously described as a cofactor for DNA2 in nascent tract degradation⁶. In line with this, WRN depletion also rescued HU-induced fork degradation in KR cells (Fig. A3F, G).

The K164 residue of PCNA is subjected not only to ubiquitination, but also to SUMOylation^{137,138}. Depletion of the ubiquitin-ligase RAD18 recapitulated the PCNA-K164R phenotype, as it resulted in DNA2-mediated nascent tract degradation (Fig. A4A-C). Depletion of the SUMO-conjugating enzyme UBC9 did not affect fork stability (Fig. A4A, B). Finally, depletion of the ubiquitin-ligase UBC13, involved in PCNA poly-ubiquitination by K63-linked ubiquitin chains^{119,127} also resulted in DNA2-mediated nascent tract degradation (Fig. A4D-F). These findings indicate that K164 modification by ubiquitin, rather than SUMO, is necessary for replication fork protection.

Next, we investigated the impact of DNA2-mediated fork degradation on genomic instability. HU treatment induced 53BP1 foci preferentially in KR cells compared to WT. Importantly, DNA2 inhibition suppressed HU-induced 53BP1 foci formation in KR cells (Fig. 2.4E). Similar results were obtained for RPA foci (Fig. A4G). We also measured DSB formation using the neutral comet assay. Similar to the 53BP1 foci results, this experiment indicated that HU induces DSBs at higher rates in KR cells, which depends on DNA2 activity (Fig. 2.4F). These findings argue that, in KR cells, DNA2-mediated processing of stalled replication forks results in DSB formation and genomic instability.

Impact of fork reversal enzymes on fork degradation in K164R cells

In BRCA-deficient cells, nascent tract degradation by MRE11 occurs upon fork reversal^{5,8-10}. We investigated if fork reversal is also required for nascent tract degradation in KR cells. Fork reversal depends on RAD51 and the translocases HLTF, ZRANB3, and SMARCAL1^{5,9,10,139,140}. Depletion of RAD51 restored nascent tract integrity (Fig. 2.5A; Fig. A5A), indicating that fork reversal by RAD51 is also a prerequisite for nascent strand degradation in KR cells. We next investigated the involvement of translocases HLTF, ZRANB3 and SMARCAL1. Previously, individual depletion of each of these factors was shown to completely restore fork protection in BRCA-deficient cells, suggesting that they act in concert to perform fork reversal^{5,48}. In contrast, in KR cells we observed differential impact of translocase depletion. Loss of HLTF did not restore fork protection, whereas ZRANB3 depletion partially rescued nascent tract degradation, and complete rescue was observed after depleting SMARCAL1 (Fig. 2.5B; Fig. A5B). These findings demonstrate that, unlike in BRCA-mutant cells, fork reversal

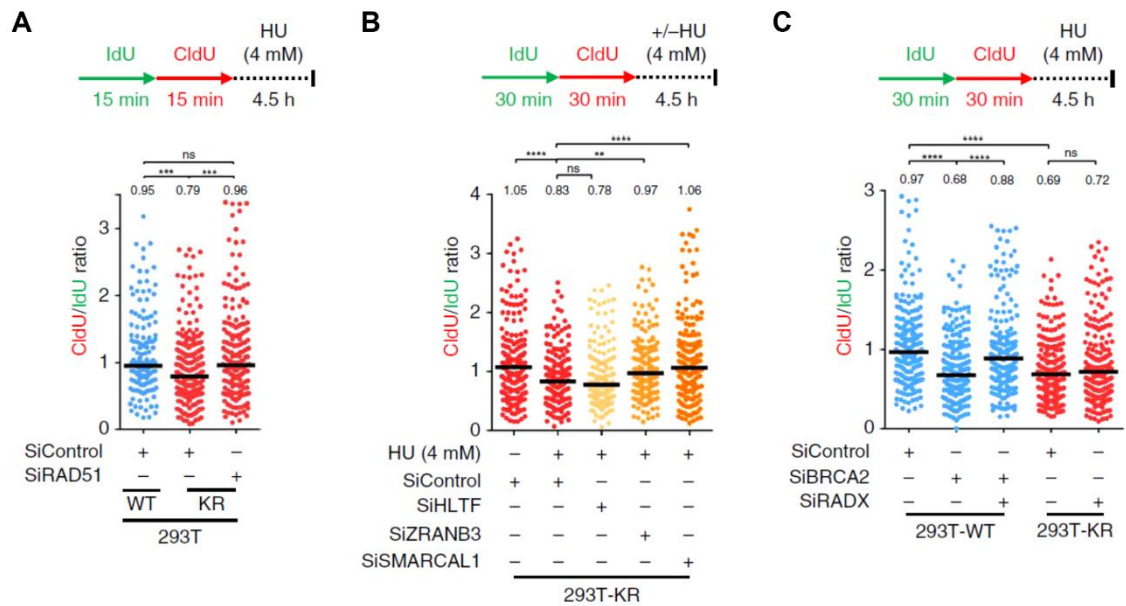


Figure 2.5: Factors involved in fork reversal are required for nascent strand degradation in PCNA-K164R cells. (A) RAD51 depletion suppresses HU-induced nascent strand degradation in 293T-K164R cells. The ratio of CldU to IdU tract lengths is presented, with the median values marked on the graph and listed at the top. Asterisks indicate statistical significance (Mann–Whitney test, two-sided). A schematic representation of the fiber combing assay conditions is also presented. (B) Impact of DNA translocases HLTF, ZRANB3, and SMARCAL1 on HU-induced nascent strand degradation in 293T-K164R cells. The ratio of CldU to IdU tract lengths is presented, with the median values marked on the graph and listed at the top. Asterisks indicate statistical significance (Mann–Whitney test, two-sided). A schematic representation of the DNA fiber combing assay conditions is also presented. (C) Knockdown of RADX suppresses HU-induced nascent strand degradation in BRCA2-deficient cells, but not in 293T-K164R cells. The ratio of CldU to IdU tract lengths is presented, with the median values marked on the graph and listed at the top. Asterisks indicate statistical significance (Mann–Whitney test, two-sided). A schematic representation of the assay conditions is also presented.

in PCNA-K164R cells depends on SMARCAL1 and partially on ZRANB3 and does not involve HLTF activity. It was previously shown that fork reversal by ZRANB3 depends on UBC13-catalyzed poly-ubiquitination of PCNA, which recruits ZRANB3 to stalled forks^{50,51}. However, ZRANB3 knockdown partially rescued HU-induced nascent tract degradation in UBC13-depleted cells (Fig. A5C), similar to its effect in PCNA-K164R cells. In contrast, ZRANB3 knockdown fully suppressed nascent tract degradation in BRCA2-depleted cells (Fig. A5C), as previously

shown^{5,9}. These findings suggest that ZRANB3-mediated fork reversal is only partially dependent on PCNA poly-ubiquitination, and it is not completely abolished in the absence of this modification.

Besides its role in fork reversal, RAD51 is also critical for the protection of reversed forks. The inability to stabilize RAD51 at stalled replication forks renders them susceptible to nucleolytic processing^{2-4,8}. To test if the fork protection defect observed in KR cells is caused by defective RAD51 loading on reversed forks, we depleted RADX. RADX antagonizes RAD51 accumulation at stalled forks, and its depletion results in enhanced RAD51 binding to reversed forks^{4,79}. While RADX knockdown suppressed nascent tract degradation in BRCA2-deficient cells, it failed to restore fork protection in KR cells (Fig. 2.5C; Fig. A5D), arguing that the nascent tract degradation in KR cells is not caused by deficient RAD51-mediated fork protection.

Previously, DNA2-mediated nascent tract degradation was described in cells depleted of RECQL1, which restarts stalled replication forks upon prolonged fork arrest (treatment with 4mM HU for 6h)⁶. To test if the fork protection defect in KR cells is caused by defective RECQL1-mediated fork restart, we depleted RECQL1 in both WT and KR cells. Under experimental conditions used to detect nascent tract degradation in KR cells (4mM HU for 4.5h), we did not observe any impact of RECQL1 knockdown in either WT or KR cells (Fig. A5E, F). These findings argue against an involvement of RECQL1 in the fork protection defect observed in KR cells.

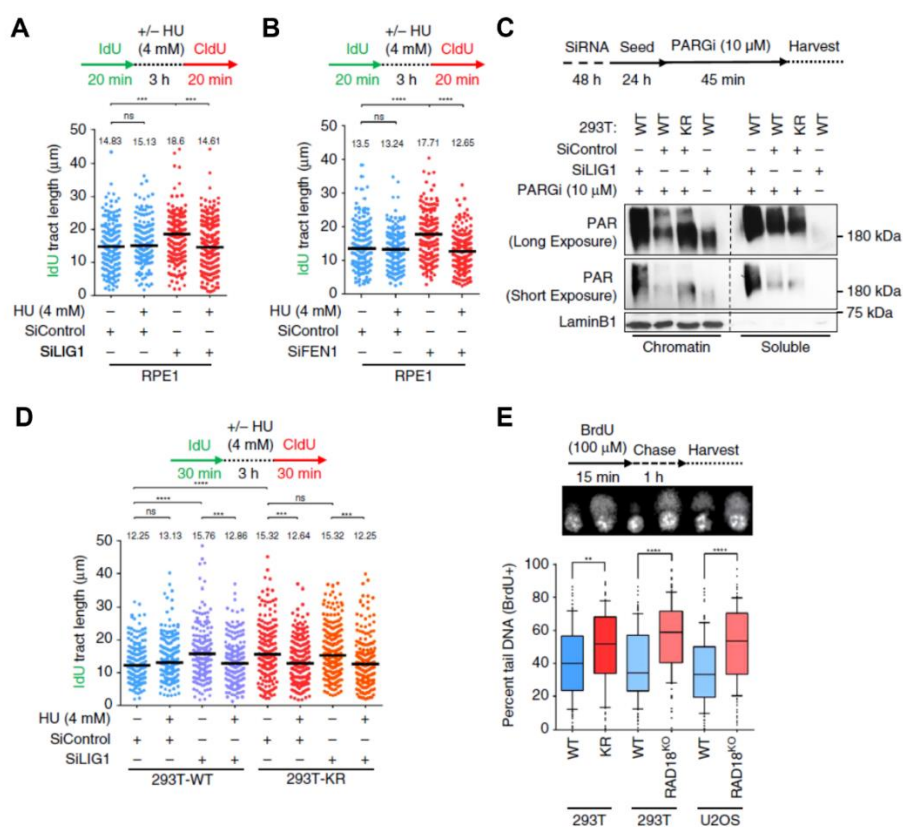


Figure 2.6: Defective Okazaki fragment maturation results in nascent strand degradation. (A), (B) DNA fiber combing assays showing that depletion of *LIG1* (A) or *FEN1* (B) results in faster replication fork progression under normal conditions and induce nascent strand degradation upon fork arrest. The quantification of the IdU tract length is presented, with the median values marked on the graph and listed at the top. Asterisks indicate statistical significance (Mann–Whitney test, two-sided). Schematic representations of the assay conditions are also presented. (C) Chromatin fractionation experiment showing increased PAR chain formation in KR cells under normal growth conditions, indicative of defective Okazaki fragment maturation. Cells were treated as indicated with a PARG inhibitor (PARGi) for 45 min prior to harvesting to block PAR chain removal. *LIG1* depletion was used as positive control for defective Okazaki fragment maturation. Chromatin-associated LaminB1 was used as loading control. (D) Loss of *LIG1* is epistatic with the PCNA-K164R mutation for fork progression and HU-induced nascent strand degradation in 293T cells. The quantification of the IdU tract length is presented, with the median values marked on the graph and listed at the top. Asterisks indicate statistical significance (Mann–Whitney test, two-sided). A schematic representation of the assay conditions is also presented. (E) BrdU-alkaline comet assay showing accumulation of ssDNA gaps under normal replication conditions in 293T-K164R and RAD18-knockout 293T and U2OS cells. At least 100 cells were quantified for each condition. Center line indicates the median, bounds of box indicate the first and third quartile, and whiskers indicate the 10th and 90th percentile. Asterisks indicate statistical significance (t-test, two-tailed, unequal variance). A schematic representation of the assay conditions, and representative micrographs, are also presented.

Okazaki fragment ligation underlies fork protection

The ~30% increase in fork speed observed in KR cells is reminiscent of cells depleted of DNA replication factors involved in OFM such as *LIG1* and *FEN1*^{110,141}. Consistent with these findings, we also observed that depletion of *LIG1* or *FEN1* results in longer nascent tracts (Fig. 2.6A, B; Fig. A6A). Thus, we investigated if perturbing OFM also results in nascent DNA degradation upon fork stalling. Under identical conditions as those used for detecting nascent tract degradation in KR cells (4mM HU for 3h), *LIG1* or *FEN1* depletion showed a similar fork protection defect (Fig. 2.6A, B). These findings indicate that defects in OF maturation result in nascent DNA degradation upon replication stress.

Using synthetic genetic array analyses in yeast, we previously uncovered a genetic similarity between the *PCNA-K164R* mutation and inactivation of lagging strand synthesis factors. Moreover, previous work in fission yeast uncovered a lagging strand synthesis defect in *PCNA-K164R* cells¹⁴². Coupled with the fork protection defect similarities described above, these findings raise the question of whether *PCNA-K164R* cells have defects in OF maturation. Previously, it was shown that *LIG1* depletion in human cells results in increased poly-ADP-ribose (PAR) chain formation on chromatin, as detected upon inhibition of poly(ADP-ribose) glycohydrolase (*PARG*) by a specific inhibitor¹¹⁵. As increased chromatin PAR chain formation may represent a marker of OFM defects, we measured PAR chain formation in KR cells. Similar to *LIG1* depletion, PAR chain formation was enhanced in KR cells (Fig. 2.6C). Confirming that PAR chains are caused by accumulation of unligated Okazaki fragments, their formation was suppressed upon short treatment with emetine, an inhibitor of lagging strand synthesis which prevents formation of Okazaki fragments, uncoupling leading and lagging strand replication¹¹⁵ (Fig. A1.6B). These findings argue that *LIG1*-mediated Okazaki fragment ligation is

compromised in PCNA-K164R cells. Importantly, depletion of LIG1 or FEN1 but did not further exacerbate nascent strand degradation, nor did it further increase fork speed, in KR cells (Fig. 2.6D; Fig. A6C, D). This epistatic interaction indicates that LIG1-mediated OFM and PCNA ubiquitination may operate in the same fork protection genetic pathway.

As PCNA ubiquitination recruits non-canonical polymerases to DNA, we hypothesized that upon endogenous replication stress, the inability to recruit specialized polymerases in KR cells may result in accumulation of single stranded gaps which could hinder OF ligation on the lagging strand. To test this, we performed an alkaline comet assay on cells labeled with BrdU, allowing us to specifically detect single stranded gaps in newly replicated DNA. KR cells showed an increase in DNA gap formation under normal replication conditions, as did RAD18-knockout cells (Fig. 2.6E; Fig. A6E, F). Previously, the TLS polymerase Polk was shown to be recruited by ubiquitinated PCNA to perform gap filling during nucleotide excision repair (NER)¹⁴³. POLK depletion resulted in nascent tract degradation, which was partially dependent on DNA2 (Fig. A6G, H). In contrast, depletion of the REV1 polymerase did not affect fork stability (Fig. A6I, J). These findings show that PCNA ubiquitination suppresses accumulation of under-replicated DNA, which may otherwise interfere with OF ligation on the lagging strand.

PCNA retention on chromatin drives fork degradation

We next investigated how OFM defects interfere with fork stability. Previous work in yeast showed that PCNA is removed from DNA by Elg1 upon DNA Ligase I (Cdc9 in yeast) – mediated joining of OF²³. Indeed, knockdown of ATAD5 or LIG1 in 293T cells resulted in increased number of PCNA chromatin foci (Fig. 2.7A; Fig. A7A, B). Importantly,

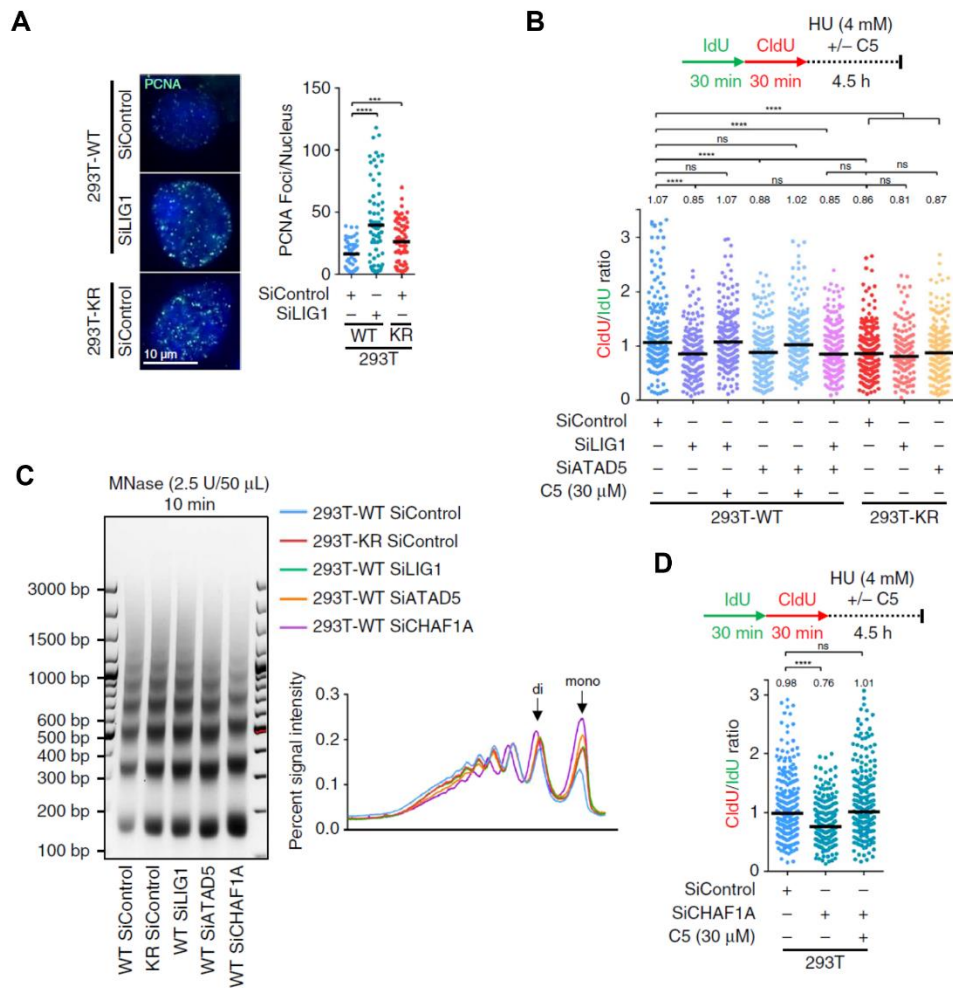


Figure 2.7: Abnormal retention of PCNA on chromatin drives replication fork degradation by altering nucleosome deposition. (A) PCNA immunofluorescence showing increased PCNA retention on chromatin in 293T-K164R cells, or upon LIG1 depletion. At least 65 cells were quantified for each condition. The mean values are marked on the graph, and asterisks indicate statistical significance (t-test, two-tailed, unequal variance). Representative micrographs are also shown. **(B)** ATAD5 knockdown results in DNA2-mediated nascent strand degradation upon HU-induced replication fork arrest, which is epistatic to the K164R mutation. The ratio of CldU to IdU tract lengths is presented, with the median values marked on the graph and listed at the top. Asterisks indicate statistical significance (Mann–Whitney test, two-sided). **(C)** Micrococcal nuclease sensitivity assay showing altered nucleosome deposition in 293T-K164R cells, as well as upon depletion of LIG1, ATAD5, or CHAF1A. A quantification of the signal intensity is also shown. **(D)** CHAF1A depletion results in HU-induced degradation of nascent DNA by DNA2 nuclease. The ratio of CldU to IdU tract lengths is presented, with the median values marked on the graph and listed at the top. Asterisks indicate statistical significance (Mann–Whitney test, two-sided).

293T-K164R cells also showed increased number of PCNA chromatin foci under otherwise unperturbed conditions (Fig. 2.7A), indicating prolonged PCNA retention on chromatin. DNA fiber-combing experiments showed that, similar to LIG1 depletion, ATAD5 knockdown in WT cells results in HU-induced degradation of the nascent strand by DNA2 (Fig. 2.7B). However, ATAD5 knockdown in KR cells or in LIG1-depleted cells did not further exacerbate the fork protection defect, indicating that ATAD5 participates in the UbiPCNA–LIG1 genetic pathway of fork protection. These findings show that increased PCNA retention on chromatin caused by defects in OF ligation or PCNA unloading, results in nascent tract degradation upon fork arrest and reversal.

Elg1-deficient yeast cells exhibit nucleosome assembly defects, ascribed to sequestration of the PCNA-interacting CAF-1 histone chaperone in PCNA complexes on chromatin, which reduces CAF-1 availability for chromatin assembly at the replication fork²⁴. In line with this, depletion of ATAD5 in human cells was shown to result in accumulation of PCNA chromatin structures which contain CAF-1 but do not actively perform DNA synthesis¹¹⁸. Thus, we investigated if nucleosome deposition is altered upon inactivation of the UbiPCNA–LIG1–ATAD5 genetic pathway. Micrococcal nuclease (MNase) sensitivity assays showed that chromatin was more accessible to nucleolytic digestion in KR, LIG1-depleted, and ATAD5-depleted cells (Fig. 2.7C), consistent with a reduction in nucleosome compaction⁷⁵. This defective nucleosome packaging mirrors that observed upon depletion of the CAF-1 complex subunit CHAF1A (Fig. 2.7C, Fig. A7C), suggesting that retention of PCNA on chromatin in KR cells, or upon LIG1 or ATAD5 depletion, sequesters CAF-1 away from active nucleosome deposition sites and thus interferes with its chromatin assembly function. CHAF1A depletion resulted in DNA2-mediated nascent tract degradation upon HU treatment (Fig. 2.7D), similar to what we previously observed upon inactivation of the UbiPCNA–LIG1–ATAD5 genetic pathway.

Altogether, these findings indicate that in KR cells, enhanced PCNA retention on chromatin results in altered nucleosomal packaging likely due to aberrant CAF-1 localization (Fig. 2.7C; Fig. A.1.7D). This nucleosomal packaging defect renders stalled forks susceptible to DNA2-mediated degradation under acute replication stress (Fig. 2.7D; Fig. A7E).

Loss of PCNA ubiquitination enhances the effects of BRCA-deficiency

In BRCA-deficient cells, fork protection correlates with resistance to cisplatin and PARPi^{5,38,79}. BRCA2 depletion in KR cells enhanced nascent tract degradation upon HU treatment (Fig. 2.8A), indicating that they operate separately to maintain fork stability. Moreover, a synergistic increase in 53BP1 foci formation was observed in BRCA2-depleted KR cells under normal growth conditions (Fig. 2.8B). Next, we investigated if loss of BRCA2 potentiates the replication-dependent DNA damage observed in KR cells, using the BrdU alkaline comet assay. BRCA2 depletion did not affect the amount of DNA damage accumulated in newly replicated DNA during DNA synthesis (1h chase time after BrdU pulse), in either WT or KR cells (Fig. 2.8C). However, 5 hours after DNA synthesis, BRCA2-depleted KR cells retained a significant amount of damage in BrdU-positive DNA, compared to BRCA2-depleted WT cells or BRCA2-proficient cells (Fig. 2.8C). Neutral comet assays indicated that this DNA damage accumulating in BRCA2-depleted KR cells under normal growth conditions is not represented by DSBs (Fig. A8A). Overall, these findings indicate that ssDNA gaps which accumulate during DNA replication under normal conditions in PCNA-K164R cells, can be repaired through a BRCA2-dependent mechanism.

As replication fork stability may represent an important component of the response to PARPi in BRCA-deficient cells^{5,38,79}, we next investigated the impact of PCNA ubiquitination

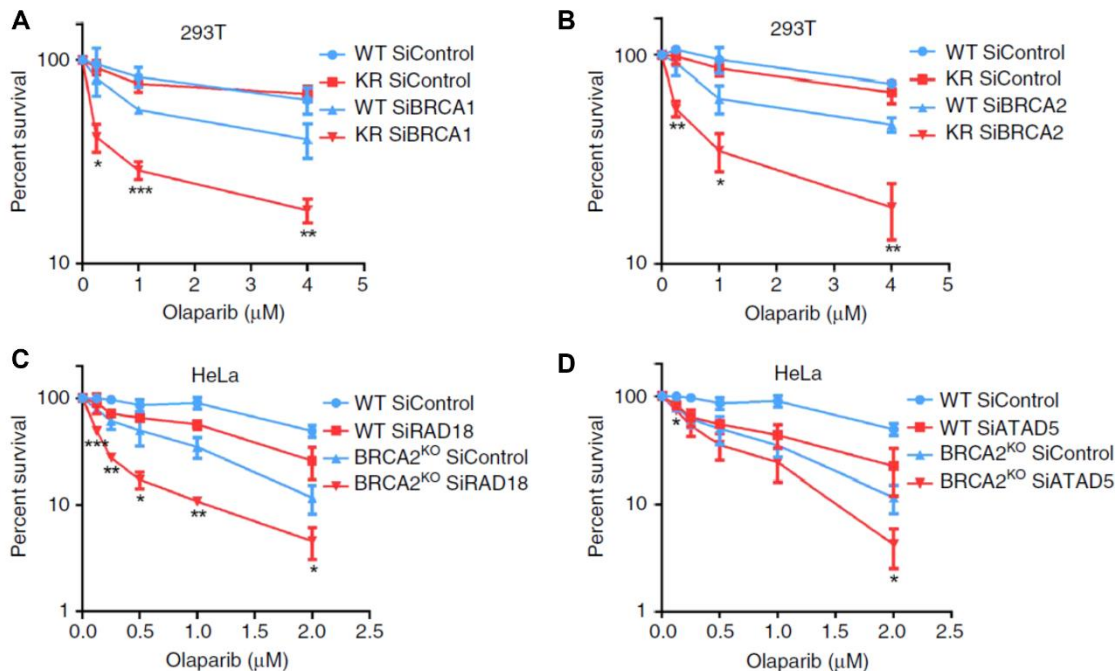


Figure 2.9: Loss of PCNA-ubiquitination sensitizes BRCA-deficient cells to PARP-inhibition. (A), (B) Clonogenic survival experiments showing that loss of PCNA ubiquitination does not result in olaparib sensitivity, but it drastically increases the olaparib sensitivity of BRCA1-depleted (A) and BRCA2-depleted (B) cells. The average of three experiments, with standard deviations indicated as error bars, is shown. Asterisks indicate statistical significance (t-test, two-tailed, unequal variance) comparing WT siBRCA1/2 to KR siBRCA1/2. (C), (D) Clonogenic survival experiments showing that depletion of RAD18 (C) or ATAD5 (G) increases the olaparib sensitivity of BRCA2-knockout HeLa cells. The average of three experiments, with standard deviations indicated as error bars, is shown. Asterisks indicate statistical significance (t-test, two-tailed, unequal variance) comparing BRCA2^{KO} siControl to BRCA2^{KO} siRAD18/siATAD5.

Moreover, knockdown of other components of the PCNA ubiquitination-dependent fork protection pathway described here, namely RAD18 and ATAD5, also enhanced the olaparib sensitivity of BRCA2-knockout HeLa cells (Fig. 2.9C, D). These findings show that PCNA ubiquitination provides an alternative mechanism for fork protection and replication stress suppression in BRCA-deficient cells and determines PARPi sensitivity in these cells.

Chapter 3

Lagging Strand Gap Suppression Connects BRCA-Mediated Fork Protection to Nucleosome Assembly by Ensuring PCNA-Dependent CAF-1 Recycling

Rationale

RAD18-mediated ubiquitination of PCNA at the lysine 164 (K164) residue is a prominent response of eukaryotic cells to replication stress. This modification enables the post-replicative repair (PRR) of ssDNA gaps through translesion synthesis (TLS)^{30,127,128,144,145}. In the previous section we generated PCNA-K164R mutant human cell lines, completely deficient in PCNA ubiquitination, and demonstrated an essential role of ubiquitinated PCNA in preventing the nucleolytic degradation of stalled replication forks. Mechanistically, we showed that fork degradation in PCNA-K164R cells is caused by the accumulation of lagging strand gaps, which sequester PCNA as OF ligation is impaired. Since CAF-1 forms a tight complex with PCNA, it is also sequestered in these PCNA complexes in the wake of replication forks, thus impeding replication-coupled nucleosome assembly in these cells and priming stressed forks for nucleolytic degradation.

Recent publications have revealed a previously underappreciated role of the BRCA-RAD51 pathway in suppressing the accumulation of replication-associated single stranded DNA (ssDNA) gaps. Gap mitigation by the BRCA pathway occurs through two distinct mechanisms: 1) by restraining fork progression during replication stress, thereby suppressing excessive PRIMPOL-mediated fork repriming^{64,146-148}; and 2) by promoting RAD51-dependent PRR of gaps^{1,8,112,149}. Importantly, replication-associated gaps have been connected to PARP inhibitor (PARPi) sensitivity in BRCA-deficient cells^{64,111,147,150}. Interestingly, Okazaki fragment processing defects have also been identified in BRCA-deficient cells^{111,150}.

In this section we investigate the role of BRCA-RAD51 mediated gap suppression in ensuring replication fork stability. We assess the impact of BRCA-deficiency on lagging strand DNA synthesis during replication stress, its subsequent influence on PCNA-CAF1 recycling and the associated putative nucleosome assembly defects in priming stalled replication forks for degradation. We additionally characterize an alternative nucleosome assembly pathway dependent on HIRA and the histone H3 isoform H3.3 in restoring fork stability to BRCA-deficient cells upon the genetic inactivation of CHAF1A. We further define nucleosome assembly as an underlying determinant of replication fork stability.

Results

CAF-1 inactivation rescues fork stability in BRCA-deficient cells

We previously showed that replication-coupled nucleosome assembly mediated by CAF-1 is critical for the stability of stalled replication forks. We therefore sought to investigate the effect of CAF-1 inactivation on fork stability in cells deficient in either BRCA1 or BRCA2 function. To assess fork stability, we subjected cells to consecutive labeling with the nucleotide analogs IdU and CldU, respectively, for 30 minutes each followed by fork arrest with 4mM hydroxyurea (HU) for 4 hours. Fork stability was investigated by measuring the ratios of CldU tract lengths to adjacent IdU tract lengths, allowing us to control for potential changes in fork speed brought about by CAF-1 inactivation. Strikingly, depletion of CHAF1A (the largest subunit of the CAF-1 complex, also known as p150) fully restored fork stability to HeLa-BRCA2^{KO} as well as to RPE1-p53KOBRC1A^{KO} cells, while causing fork degradation in their respective BRCA proficient counterparts (Fig. 3.1A, B; Fig. B1A, B). To rule out potential siRNA off-target effects, we employed CRISPR/Cas9 to knock-out CHAF1A in 293T and HeLa

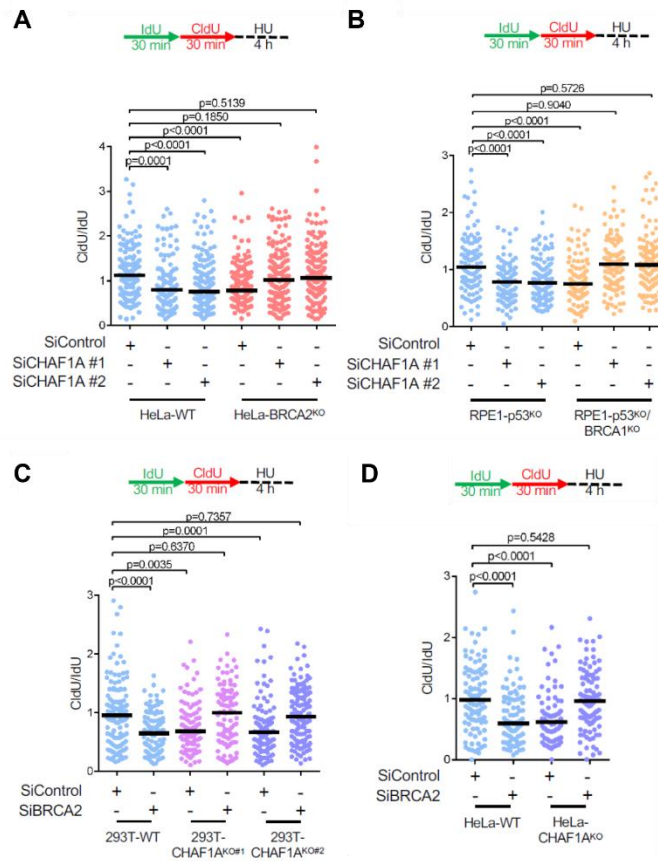


Figure 3.1: Loss of CAF-1 promotes fork stability in BRCA-deficient cells. (A), (B) DNA fiber combing assays showing that CHAF1A depletion results in HU-induced fork resection in wildtype cells, but suppresses this degradation in BRCA2-knockout HeLa cells (A) and in BRCA1-knockout RPE1 cells (B). The ratio of CldU to IdU tract lengths is presented, with the median values marked on the graph. The p-values (Mann-Whitney test) are listed at the top. Schematic representations of the DNA fiber combing assay conditions are also presented. (C), (D) DNA fiber combing assays showing that CHAF1A knockout in 293T (C) or HeLa (D) cells results in HU-induced fork degradation, which is suppressed by BRCA2 knockdown. The ratio of CldU to IdU tract lengths is presented, with the median values marked on the graph. The p-values (Mann-Whitney test) are listed at the top. Schematic representations of the DNA fiber combing assay conditions are also presented.

cells (Fig. B1 C, D). Similar to CHAF1A depletion using siRNA, both 293T and HeLa CHAF1A-knockout (CHAF1A^{KO}) cells displayed fork degradation upon HU treatment (Fig. 3.1C, D). Importantly, BRCA2 depletion caused fork degradation in wildtype, but not in CHAF1A^{KO} HeLa and 293T cells (Fig. 3.1 C, D; Fig. B1E, F). These findings indicate that loss of CAF-1 promotes fork degradation in wildtype cells but suppresses this degradation in BRCA-deficient cells.

Restoration of RAD51 loading on chromatin promotes fork protection in BRCA-deficient settings^{4,80}. We therefore sought to assess the impact of CHAF1A inactivation on chromatin-bound RAD51 levels in BRCA1 and BRCA2-depleted cells. Upon treatment with the topoisomerase I inhibitor camptothecin (CPT), depletion of CHAF1A did not affect RAD51 foci formation in BRCA-proficient HeLa cells and failed to ameliorate the reduction in RAD51 foci formation observed in BRCA1 and BRCA2 depleted cells (Fig. 3.2A, B; Fig. B1G). Treatment with the RAD51 inhibitor B02 was previously shown to elicit nascent DNA resection at stalled forks in BRCA-proficient cells^{4,5}. In line with this, treatment with B02 resulted in HU-induced fork degradation in wildtype HeLa and 293T cells; In contrast, B02 did not cause fork degradation in HeLa-BRCA2^{KO} cells depleted of CHAF1A (Fig. 3.2C), or in 293T-CHAF1A^{KO} cells depleted of BRCA2 (Fig. 3.2D). Collectively, these results indicate that CHAF1A inactivation restores fork stability to BRCA-deficient cells in a RAD51-independent manner. Reversal of stalled replication forks is an essential prerequisite to nascent DNA resection in BRCA-deficient cells^{5,8-10}. Thus, we investigated if the suppression of fork degradation observed upon CHAF1A depletion in BRCA-deficient cells simply reflects a defect in fork reversal.

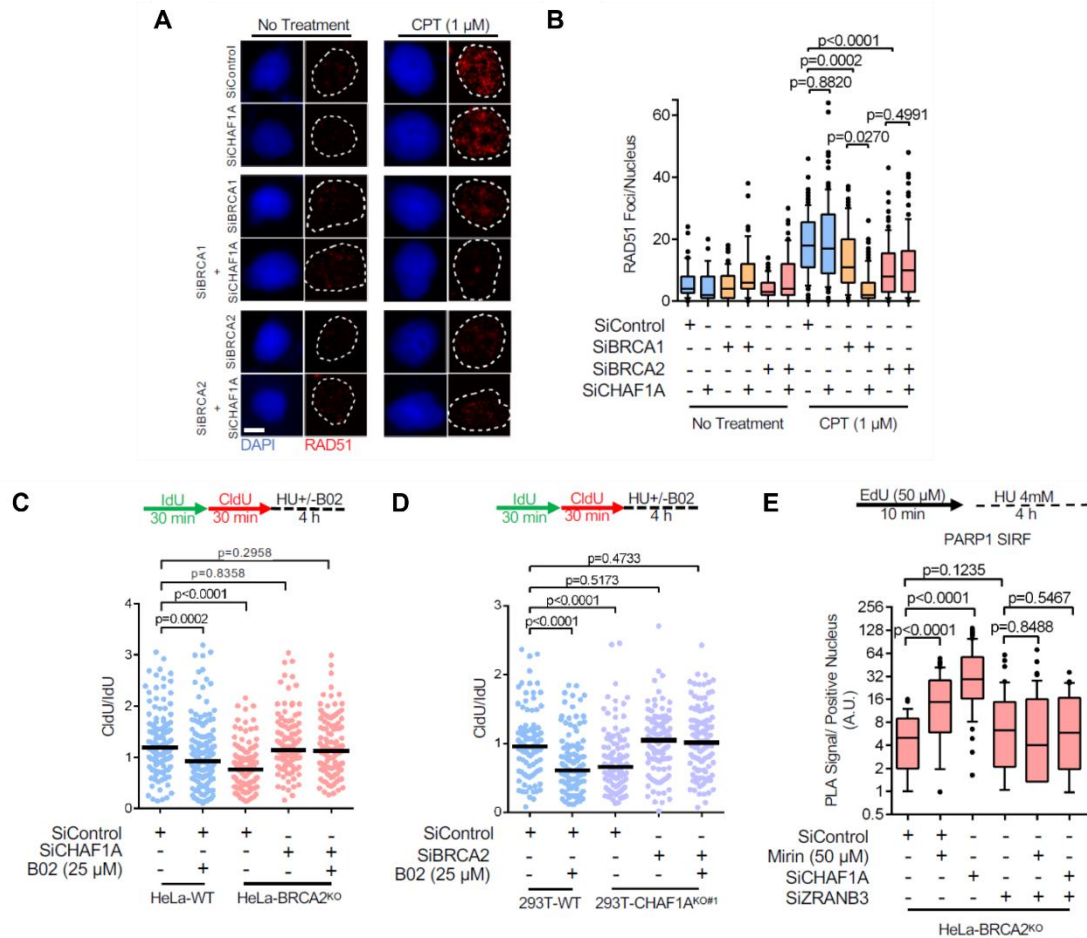


Figure 3.2: CHAF1A loss restores fork stability to BRCA-deficient cells in a RAD51-independent manner. (A), (B) RAD51 immunofluorescence experiment showing that CHAF1A depletion does not restore CPT-induced RAD51 foci in BRCA1 or BRCA2-depleted cells. HeLa cells were treated with 1 μ M CPT for 1h followed by media removal and chase in fresh media for 3h. Representative micrographs (A) and quantifications (B) are shown (scale bar represents 10 μ m). At least 50 cells were quantified for each condition. The median values are represented on the graph, and the p-values (Mann-Whitney test) are listed at the top. (C), (D) Inhibition of RAD51 by B02 treatment does not restore HU-induced fork degradation in CHAF1A-depleted HeLa-BRCA2^{KO} cells (C), or in BRCA2-depleted 293T-CHAF1A^{KO} cells (D). The ratio of CldU to IdU tract lengths is presented, with the median values marked on the graph. The p-values (Mann-Whitney test) are listed at the top. Schematic representations of the DNA fiber combing assay conditions are also presented. E. SIRF assay showing that PARP1 binding to nascent DNA is increased upon CHAF1A depletion in HeLa-BRCA2^{KO} cells, indicating stabilization of reversed replication forks. At least 40 positive cells were quantified for each condition. The p-values (Mann-Whitney test) are listed at the top. A schematic representation of the SIRF assay conditions is also presented.

PARP1 is a critical enabler of fork reversal¹¹⁴. The presence of PARP1 at nascent DNA has been previously used as an indirect readout for fork reversal⁴⁶. Under prolonged replication arrest, stable reversed replication forks are marked by PARP1. In contrast, forks undergoing resection lose nascent DNA on regressed arms and no longer retain the structural configuration resembling four-way junctions, thus precluding the presence of PARP1. We therefore used the SIRF (in situ detection of proteins at replication forks) assay, a proximity ligation-based approach (PLA)^{5,151}, to assess PARP1 binding to nascent DNA upon HU treatment. To account for potential baseline discrepancies arising from variabilities in EdU uptake due to gene knockdowns or drug treatments, we normalized the PARP1-biotin PLA signal in each condition using the fluorescence signal from the corresponding biotin-biotin control (signifying EdU uptake). Similar to inhibition of MRE11 using mirin, depletion of CHAF1A increased PARP1 levels at nascent DNA in HeLa BRCA2^{KO} cells (Fig. 3.2E; Fig. B1H, I). Importantly, abolishing fork reversal by depleting the fork remodeling translocase ZRANB3 restored PARP1 levels to similar levels across all conditions, indicating no baseline differences in PARP1 recruitment to nascent DNA (Fig. 3.2E; Fig. B1H, I). These results suggest that loss of CHAF1A does not preclude fork reversal, but rather promotes the stability to reversed forks in BRCA deficient cells.

Loss of CAF-1 averts DNA damage and drives chemoresistance in BRCA deficient cells

Previous work showed that fork degradation drives DNA damage-induced chromosomal rearrangements in BRCA-deficient cells^{2,3,38}. Thus, we next investigated if CHAF1A inactivation could avert DNA damage accumulation in BRCA-deficient cells.

We assessed replication- coupled DNA damage by immunofluorescence detection of γ H2AX in cells treated with CPT, known to elicit nascent strand degradation⁵.

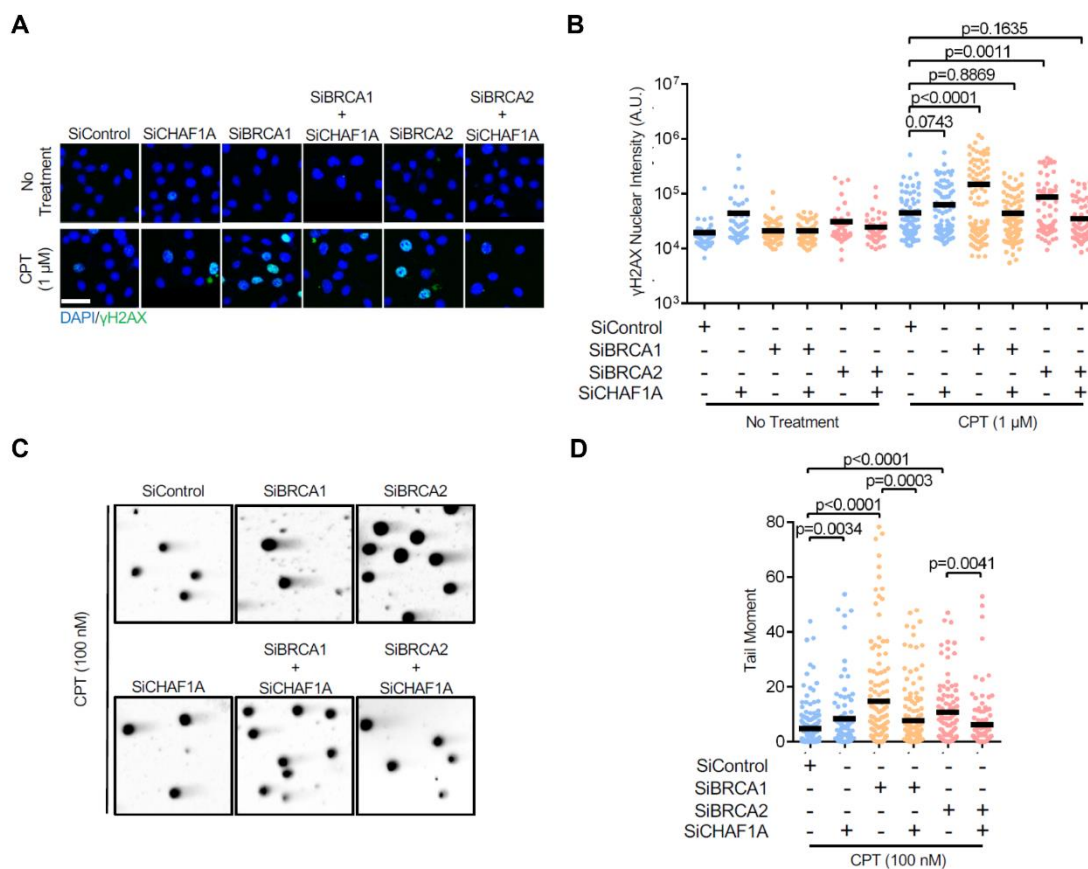


Figure 3.3: Loss of CAF-1 suppresses genomic instability in BRCA-deficient cells. (A), (B). γ H2AX immunofluorescence experiment showing that CHAF1A depletion suppresses CPT-induced DNA damage accumulation in BRCA1 or BRCA2-depleted cells. HeLa cells were treated with 1 μ M CPT for 1h followed by media removal and chase in fresh media for 3h. Representative micrographs (scale bar represents 10 μ m) (A) and quantifications (B) are shown. At least 50 cells were quantified for each condition. The mean values are represented on the graph, and the p-values (t-test, two-tailed, unequal variance) are listed at the top. (C), (D). Neutral comet assay showing that CHAF1A depletion suppresses CPT-induced DSB formation in BRCA1 or BRCA2-depleted cells. HeLa cells were treated with 100nM CPT for 4h. Representative micrographs (C) and quantifications (D) are shown. At least 85 nuclei were quantified for each condition. The mean values are represented on the graph, and the p-values (t-test, two-tailed, unequal variance) are listed at the top.

Indeed, while BRCA1 and BRCA2-depleted HeLa cells exhibited increased γ H2AX levels upon CPT treatment, γ H2AX levels were ameliorated upon co-depletion of CHAF1A (Fig. 3.3A, B; Fig. B2A). We also measured the accumulation of DNA double stranded breaks (DSBs) in these cells, using the neutral comet assay. Similar to γ H2AX induction, treatment with CPT resulted in increased comet tail moments in BRCA1 and BRCA2-depleted HeLa cells, which was rescued upon co-depletion of CHAF1A (Fig. 3.3C, D). These findings show that restoration of fork stability to BRCA-deficient cells upon CHAF1A depletion is associated with suppression of DNA damage accumulation in these cells.

Restoration of fork stability is considered a driver of chemoresistance in BRCA-deficient cells³⁸. By employing clonogenic survival assays, we next investigated the impact of CHAF1A inactivation in BRCA-deficient cells on cisplatin sensitivity. CHAF1A co-depletion significantly rescued cisplatin sensitivity in HeLa cells depleted of BRCA1 or BRCA2 (Fig. 3.4A, B). Cisplatin chemotherapy is the mainstay therapeutic approach in ovarian cancer treatment. We thus investigated if CHAF1A levels impact the chemosensitivity of BRCA-mutant ovarian tumors in clinical samples. Analyses of survival and matched genotype and expression data from TCGA datasets indicated that CHAF1A expression can stratify the survival of individuals with BRCA2-mutant ovarian tumors: high CHAF1A expression trended towards increased survival, while low CHAF1A expression trended towards reduced survival (Fig. B2B). This is in line with our clonogenic survival results showing that CHAF1A depletion causes cisplatin resistance in BRCA2-deficient cells. Taken together, these observations suggest that CHAF1A inactivation can enable BRCA-deficient cells to avert replication-coupled DNA damage, thereby driving chemoresistance and potentially exacerbating adverse clinical outcomes in patients with BRCA1/2 mutated cancers.

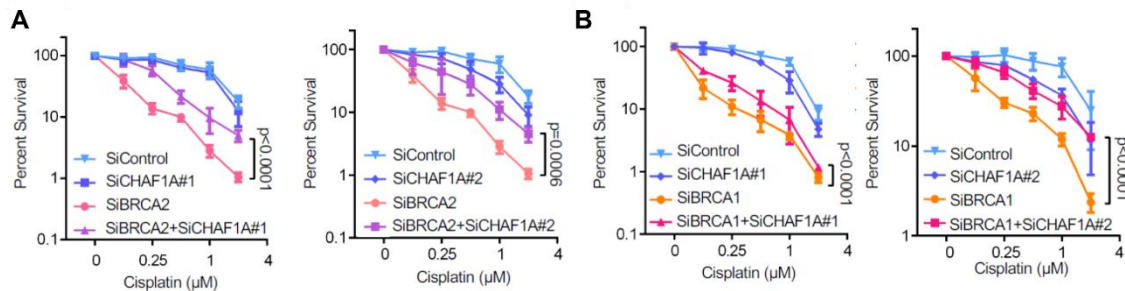


Figure 3.4: CHAF1A inactivation drives chemoresistance in BRCA-deficient cells. (A), (B) Clonogenic survival experiments showing that CHAF1A co-depletion in BRCA2-knockdown (A) or BRCA1-knockdown (B) HeLa cells promotes cisplatin resistance. The average of three experiments, with standard deviations indicated as error bars, is shown. Asterisks indicate statistical significance (two-way ANOVA).

Nucleosome assembly ensures replication fork protection

Since the cellular function of CAF-1 is in nucleosome deposition, we next sought to investigate if nucleosome assembly is a general determinant of fork stability in BRCA-deficient cells. The histone chaperone Anti-Silencing Factor 1 (ASF1) operates upstream of two distinct nucleosome assembly mechanisms: a CAF-1 dependent co-replicative process depositing the H3 isoform H3.1, and replication-independent processes involving the histone chaperones HIRA and DAXX, depositing the H3.3 isoform^{152–155}. To test if inactivating ASF1 rescues fork stability in BRCA-deficient cells, we depleted ASF1A (one of the two human ASF1 paralogs) either alone, or in conjunction with BRCA1 or BRCA2 in HeLa cells. ASF1A knockdown elicited nascent DNA resection in BRCA-proficient cells, but, in contrast to CHAF1A depletion, failed to rescue fork resection in cells depleted either of BRCA1 or BRCA2 (Fig. 3.5A; Fig. B3A).

This suggests that alternative ASF1-dependent nucleosome assembly pathways could compensate

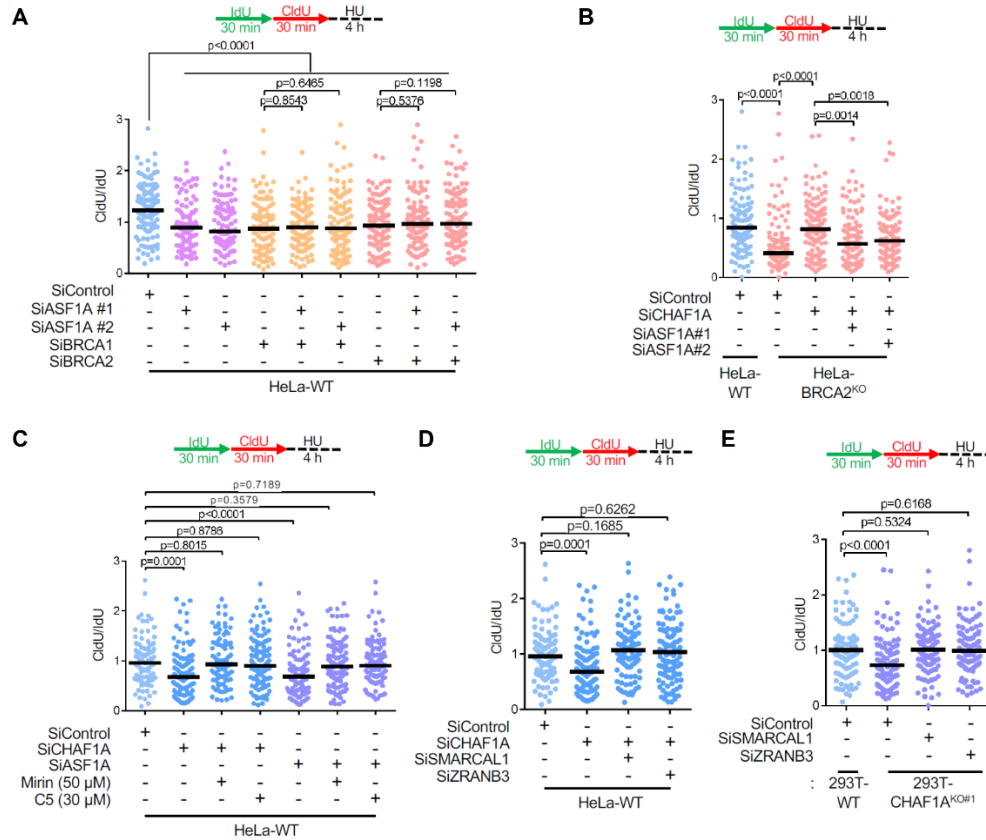


Figure 3.5: Determinants of CHAF1A-mediated fork protection.

(A) DNA fiber combing assay showing that ASF1A depletion results in HU-induced fork degradation in wildtype cells, but does not affect this degradation in BRCA1 or BRCA2-depleted HeLa cells. The ratio of CldU to IdU tract lengths is presented, with the median values marked on the graph. The p-values (Mann-Whitney test) are listed at the top. A schematic representation of the DNA fiber combing assay conditions is also presented. (B) DNA fiber combing assay showing that ASF1A co-depletion restores HU-induced fork degradation in CHAF1A-knockdown HeLa-BRCA2^{KO} cells. The ratio of CldU to IdU tract lengths is presented, with the median values marked on the graph. The p-values (Mann-Whitney test) are listed at the top. A schematic representation of the DNA fiber combing assay conditions is also presented. (C) DNA fiber combing assay showing that inhibition of nucleases MRE11 (by treatment with mirin) or DNA2 (by treatment with C5) suppresses HU-induced fork degradation caused by CHAF1A or ASF1A loss in HeLa cells. The ratio of CldU to IdU tract lengths is presented, with the median values marked on the graph. The p-values (Mann-Whitney test) are listed at the top. A schematic representation of the DNA fiber combing assay conditions is also presented. (D), (E) DNA fiber combing assay showing that depletion of DNA translocases SMARCAL1 and ZRANB3 suppresses HU-induced fork degradation caused by CHAF1A knockdown in HeLa cells (D) or in CHAF1A^{KO} 293T cells (E). The p-values (Mann-Whitney test) are listed at the top. A schematic representation of the DNA fiber combing assay conditions is also presented.

for CHAF1A inactivation in BRCA-deficient cells, to restore fork stability. Indeed, co-depleting CHAF1A and ASF1A in HeLa BRCA2^{KO} cells restored fork degradation, suggesting that fork stability upon CHAF1A inactivation in BRCA-deficient cells depends on ASF1 (Fig. 3.5B; Fig. B3B). These results suggest that ASF1-dependent nucleosome assembly is an essential component of fork protection and determines fork stability in the context of BRCA-deficiency.

The observed epistasis between the inactivation of ASF1A and BRCA proteins led us to examine if ASF1-dependent nucleosome assembly elicits fork protection through mechanisms similar to the BRCA pathway. Loss of BRCA1 or BRCA2 function renders stalled forks susceptible to resection by the MRE11 and DNA2 nucleases^{2,3,38,40}. Similar to this, depletion of either CHAF1A or ASF1A in HeLa cells elicited nascent DNA resection, which could be rescued by inhibition of MRE11 or DNA2 using the small molecule inhibitors mirin and C5 respectively (Fig. 3.5C). Next, we tested if fork reversal was also required for fork degradation in this context. Fork degradation in CHAF1A-knockdown HeLa cells, as well as in CHAF1A^{KO} 293T cells, was rescued upon depletion of the fork remodeling enzymes SMARCAL1 and ZRANB3 (Fig. 3.5 D,E; Fig. B3C, D). These results indicate that nucleosome assembly is a general determinant of replication fork stability, and that the inactivation of nucleosome assembly elicits fork resection through mechanisms similar to those operating in BRCA-deficient cells.

Restoration of fork stability upon CAF-1 inactivation in BRCA-deficient cells depends on compensatory nucleosome assembly pathways

ASF1A was shown to be part of two mutually-exclusive nucleosome assembly complexes involving the CAF-1 and HIRA histone chaperones, responsible for the deposition of H3.1 and H3.3 respectively¹⁵⁵. HIRA-mediated histone deposition was previously shown to

compensate for the inactivation of CAF-1-mediated replication-dependent nucleosome assembly¹⁵⁶. Since restoration of replication fork stability is an important component of cell survival in BRCA-deficient cells¹⁵⁷, to gain insights into a potential role for HIRA in rescuing replication fork stability, we assessed if HIRA promotes cell survival in BRCA-deficient cells upon CHAF1A inactivation. We queried publicly available CRISPR screening data for the relative dependence of BRCA1-deficient cells on HIRA and CHAF1A. We observed a linear regression of CHAF1A and HIRA gene dependency scores (CERES; lower scores correspond to higher dependencies), showing that BRCA1-proficient cells tend to dependent on both CHAF1A and HIRA for survival (Fig. 3.6A). This implies a general pattern of reliance on nucleosome assembly pathways. Strikingly, in cells carrying deleterious BRCA1 mutations, a lower survival dependency on CHAF1A correlated with a greater dependency on HIRA and vice-versa, suggesting that BRCA1-deficient cells rely on HIRA for cell survival in the absence of CHAF1A (Fig. 3.6A). It was previously shown that the histone chaperone DAXX can also cooperate with ASF1 in H3.3-dependent nucleosome assembly¹⁵². In contrast to HIRA, an increased dependence on CHAF1A did not correlate with increased DAXX dependency in BRCA1-proficient cells (Fig. 3.6B). Moreover, in BRCA1-deficient cells, an increased dependency on DAXX was not associated with a reduced dependency on CHAF1A (Fig. 3.6B). These observations suggest that upon CHAF1A inactivation, BRCA-deficient cells rely on HIRA and not on DAXX to mediate nucleosome assembly and ensure cell survival.

We next investigated if the recruitment of HIRA to stalled forks was differentially regulated in BRCA-deficient cells. SIRF assays showed that depletion of BRCA1 or BRCA2 results in increased recruitment of HIRA to HU-stalled forks (Fig. 3.6C, D). As a control, siRNA-mediated depletion of HIRA in HeLa cells resulted in an acute decrease in SIRF signal,

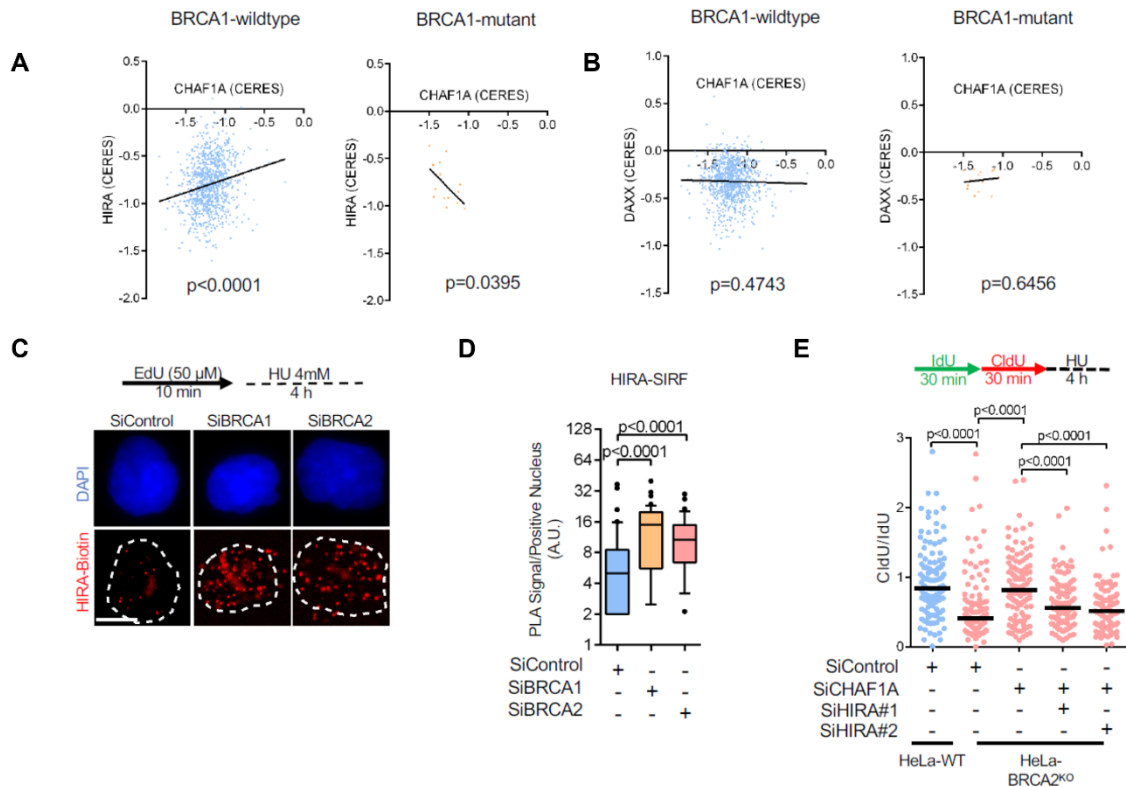


Figure 3.6: Fork protection upon CAF-1 loss in BRCA-deficient cells requires the histone chaperone HIRA. (A), (B) Linear regressions of (A) HIRA Gene Effect (CERES) vs. CHAF1A Gene Effect (CERES) and (B) DAXX Gene Effect vs. CHAF1A Gene Effect (CERES) in Cancer Cell Line Encyclopedia (CCLE) cell lines containing either wildtype BRCA1 or BRCA1 with deleterious mutations are shown. A lower CERES score corresponds to greater survival dependency. (C), (D) SIRF assay showing that HIRA binding to nascent DNA is increased upon BRCA1 or BRCA2 depletion in HeLa cells. Representative micrographs (scale bar represents 10 μ m) (C) and quantifications (D) are shown. At least 40 positive cells were quantified for each condition. The p-values (Mann-Whitney test) are listed at the top. A schematic representation of the SIRF assay conditions is also presented. E. DNA fiber combing assay showing that HIRA co-depletion restores HU-induced nascent strand resection in CHAF1A-knockdown HeLa-BRCA2^{KO} cells. The ratio of CldU to IdU tract lengths is presented, with the median values marked on the graph. The p-values (Mann-Whitney test) are listed at the top. A schematic representation of the DNA fiber combing assay conditions is also presented.

confirming the specificity of this approach in detecting HIRA binding to nascent DNA (Fig.

B4A). Importantly, CHAF1A depletion had no effect on the differential recruitment of HIRA to

stalled forks in BRCA-proficient and BRCA-deficient cells (Fig. B4B), suggesting that BRCA1/2 inactivation and not CHAF1A inactivation guides the differential presence of HIRA at stalled replication forks. In contrast to HIRA, DAXX levels at stalled replication forks in BRCA1/2 depleted cells showed no change compared to BRCA-proficient cells (Fig. B4C), suggesting that HIRA rather than DAXX may be preferentially operational at stalled forks in BRCA-deficient cells.

Based on these findings, we next investigated if the HIRA-H3.3 pathway of nucleosome assembly was responsible for restoring fork stability to BRCA-deficient cells upon CHAF1A loss. Indeed, co-depletion of HIRA or of H3.3 reversed the fork rescue elicited by CHAF1A knockdown in BRCA2^{KO} cells (Fig. 3.6E; Fig. B4D-F). To further assess the fork-protective properties of HIRA, we depleted HIRA in wildtype HeLa cells. Unlike the depletion of ASF1A, CHAF1A, or DAXX, HIRA knockdown did not elicit nascent DNA resection upon fork stalling (Fig. B4G, H), suggesting that HIRA-mediated fork protection is selectively activated during CHAF1A loss in BRCA-deficient cells. Altogether, these findings suggest that loss of CAF-1 triggers HIRA-mediated nucleosome assembly to protect stalled replication forks in BRCA-deficient cells.

BRCA-deficient cells exhibit CAF-1 recycling defects during replication stress

Since HIRA-mediated fork protection in BRCA1/2-deficient cells is triggered only upon the inactivation of CHAF1A, we sought to track the dynamics of CHAF1A at stalled forks in these cells. Replication fork stalling is accompanied by the unloading of PCNA and CAF-1^{79,158}.

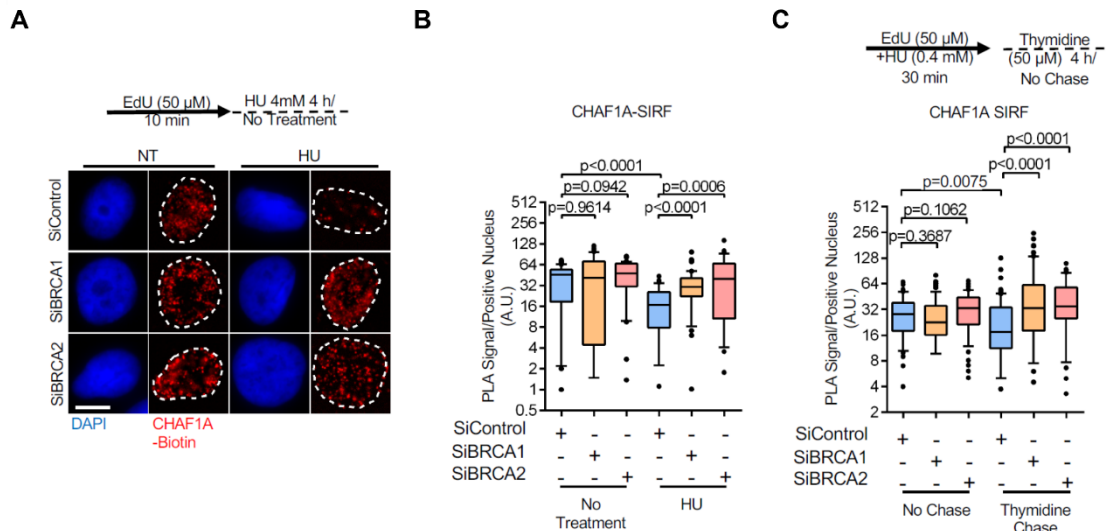


Figure 3.7: CAF-1 unloading defects in BRCA-deficient cells. (A), (B) SIRF assay showing that CHAF1A unloading from nascent DNA upon replication fork arrest is deficient in BRCA1 or BRCA2-depleted HeLa cells. To induce fork arrest, cells were treated with 4mM HU after EdU labeling. Representative micrographs (scale bar represents 10 μ m) (A) and quantifications (B) are shown. At least 30 positive cells were quantified for each condition. The p-values (Mann-Whitney test) are listed at the top. A schematic representation of the SIRF assay conditions is also presented. (C) SIRF assay showing that, in BRCA1 or BRCA2-depleted HeLa cells, CHAF1A is retained on nascent DNA behind the replication fork after recovery from replication stress. Cells were labeled with EdU in the presence of low-dose HU (0.4mM for 30mins) to induce replication stress, washed, and chased for 4h in fresh media containing 50 μ M thymidine. At least 35 positive cells were quantified for each condition. The p-values (Mann-Whitney test) are listed at the top. A schematic representation of the SIRF assay conditions is also presented.

SIRF experiments showed similar CHAF1A levels at unperturbed replication forks in BRCA-proficient and BRCA1/2- depleted HeLa cells (Fig. 3.7A, B; Fig. B5A). However, upon HU-induced replication arrest, BRCA-proficient cells showed lower levels of CHAF1A on EdU labeled DNA, while CHAF1A levels remained virtually unchanged in BRCA1/2-depleted cells (Fig. 3.7A, B), suggesting a potential defect in CAF-1 unloading from stalled forks in BRCA-

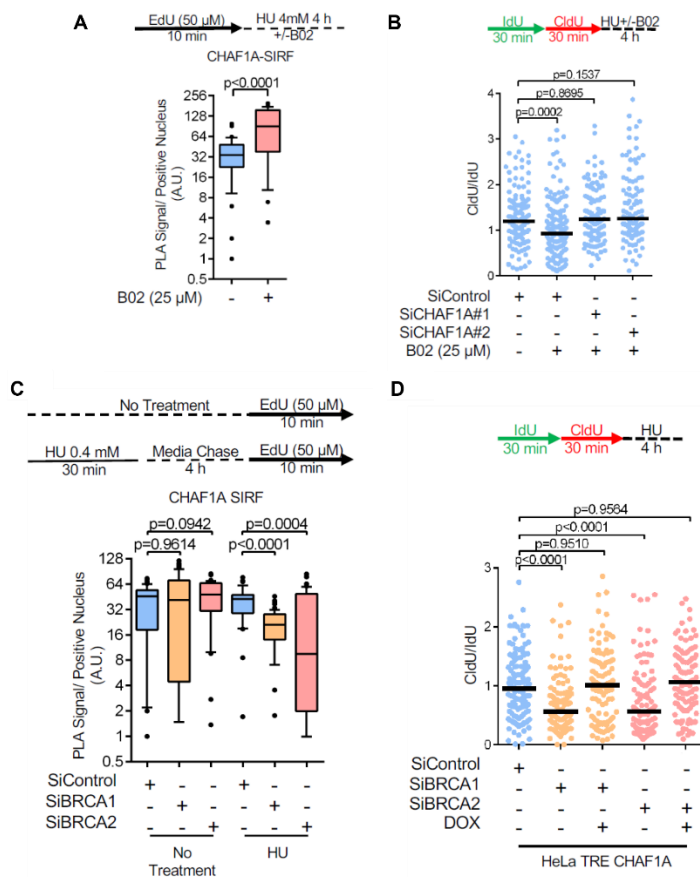


Figure 3.8: BRCA-deficient cells exhibit CAF-1 recycling defects. (A) SIRF assay showing that simultaneous treatment with 25 μ M B02 and 4mM HU elicits CHAF1A unloading defects in HeLa cells. At least 25 positive cells were quantified for each condition. The p-values (Mann-Whitney test) are listed at the top. A schematic representation of the SIRF assay conditions is also presented. (B) DNA fiber combing assay showing that CHAF1A knockdown restores fork protection to wildtype HeLa cells treated with the RAD51 inhibitor B02. The ratio of CldU to IdU tract lengths is presented, with the median values marked on the graph. The p-values (Mann-Whitney test) are listed at the top. A schematic representation of the DNA fiber combing assay conditions is also presented. (C) SIRF assay showing that prior replication stress reduces the levels of CHAF1A at ongoing replication forks in BRCA1 or BRCA2-depleted HeLa cells. Cells were subjected to low-dose HU (0.4mM for 30 mins) to induced replication stress, chased in fresh media for 4h to recover from replication stress, then labeled with EdU. At least 40 positive cells were quantified for each condition. The p-values (Mann-Whitney test) are listed at the top. A schematic representation of the SIRF assay conditions is also presented. (E) DNA fiber combing assay showing that CHAF1A overexpression suppresses HU-induced fork degradation in BRCA1 or BRCA2-depleted HeLa cells. CHAF1A expression is under the control of the tetracycline responsive element (TRE), and is induced upon doxycycline (DOX) treatment. The ratio of CldU to IdU tract lengths is presented, with the median values marked on the graph. The p-values (Mann-Whitney test) are listed at the top. A schematic representation of the DNA fiber combing assay conditions is also presented.

deficient cells.

We recently showed that in PCNA ubiquitination-deficient K164R cells, the chromatin unloading of PCNA-CAF-1 complexes is defective since these complexes are retained on spontaneously accumulating ssDNA gaps on the lagging strand, which preclude Okazaki fragment maturation behind replication forks. Interestingly, recent work from several laboratories has demonstrated that BRCA-deficient cells are also prone to gap accumulation during replication stress, owing to their inability to restrain replication fork progression^{40,64,111,146}. Altogether, these findings led us to hypothesize that replication stress-induced ssDNA gap accumulation in BRCA-deficient cells may retain CAF-1 on lagging strands, similar to the situation we previously described in PCNA-K164R cells. To test this, we performed SIRF experiments with EdU labeling in the presence of a low dose of HU which elicits gap formation but does not result in replication fork arrest⁶⁴. While the recruitment of CHAF1A to replication forks remained unchanged, BRCA1/2-depleted cells showed a persistent retention of CHAF1A at EdU-labeled DNA after a 4h thymidine chase (Fig. 3.7C). Importantly, CHAF1A retention defects were not observed in BRCA1/2-depleted cells under endogenous (non-HU treatment) conditions (Fig. B5A). In contrast, the *in-situ* inactivation of RAD51 function using simultaneous treatments with B02 and HU, as opposed to the prior genetic inactivation of BRCA1/2, was enough to elicit CHAF1A unloading defects in BRCA-proficient HeLa cells (Fig. 3.8A). Additionally, HU-induced fork degradation caused by B02 treatment could also be rescued by CHAF1A depletion (Fig. 3.8B), similar to what we observed in BRCA-deficient cells. These findings argue that the inability of BRCA-deficient cells to restrain replication forks during replication stress gives rise to post-replicative ssDNA gaps prior to fork arrest and drives abnormal CHAF1A retention at stalled replication forks.

We previously showed that PCNA-dependent sequestration of CHAF1A at gaps behind replication forks drives nucleosome assembly defects and fork degradation in PCNA ubiquitination-deficient K164R cells. We thus hypothesized that, in BRCA-deficient cells, CAF-1 chromatin retention at replication stress-induced ssDNA gaps left behind forks, reduces its availability at ongoing replication forks; this would cause nucleosome deposition defects, and prime nascent DNA for degradation upon fork stalling. To test this, we pre-treated cells with a low dose of HU, and investigated the recruitment of CHAF1A at EdU labeled DNA after a 4h chase. CHAF1A signal was significantly lower in BRCA1/2-depleted cells than in BRCA-proficient cells (Fig. 3.8C), suggesting that its availability for ongoing replication forks is reduced when ssDNA gaps accumulate behind forks. Moreover, bolstering CHAF1A levels by using a doxycycline inducible overexpression system completely rescued fork stability in cells depleted of BRCA1 and BRCA2 (Fig. 3.8D; Fig. B5B). Taken together, these findings suggest that the retention of CAF-1 at ssDNA gaps behind the replication fork reduces its availability at ongoing replication forks, causing impaired nucleosome assembly which drives fork degradation in BRCA-deficient cells.

Lagging strand gaps cause CAF-1 recycling defects in BRCA-deficient cells

PRIMPOL-mediated repriming has recently been shown to promote ssDNA gap accumulation in BRCA-deficient cells^{86,112,146-149}. We therefore asked if PRIMPOL activity could potentially drive HU-induced gap accumulation in BRCA-deficient cells. We employed the BrdU alkaline comet assay to measure the accumulation of replication-associated ssDNA gaps¹⁵⁹. Importantly, the BrdU alkaline comet assay can detect ssDNA gaps in situations where only one of the complementary nascent DNA strands bears gaps, as opposed to the previously described S1 nuclease-based approach, where the readout necessitates the simultaneous presence of leading

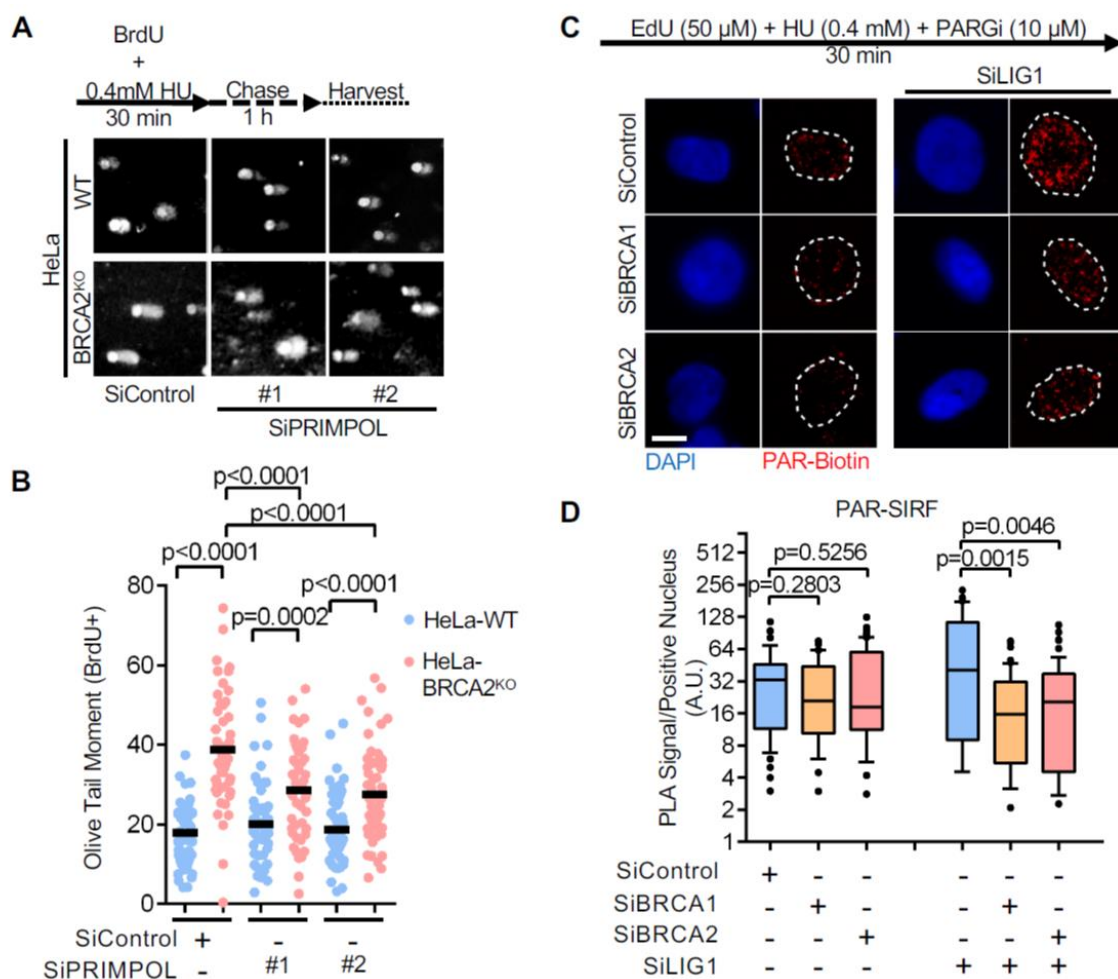


Figure 3.9: Accumulation of lagging strand gaps in BRCA-deficient cells. (A), (B) BrdU alkaline comet assay showing that PRIMPOL depletion reduces, but does not abolish replication stress-induced ssDNA accumulation in BRCA2-knockout HeLa cells, indicating the presence of PRIMPOL-independent gaps. Representative micrographs (A) and quantifications (B) are shown. At least 45 nuclei were quantified for each condition. The mean values are represented on the graph, and the p-values (t-test, two-tailed, unequal variance) are listed at the top. A schematic representation of the assay conditions is also presented. (C), (D) SIRF assay showing that, upon replication stress, LIG1 knockdown induces PAR chain formation in wildtype HeLa cells, but not in BRCA1 or BRCA2-depleted HeLa cells upon treatment with a low dose of HU (0.4mM), indicating the prevalence of lagging strand gaps in these cells. Representative micrographs (scale bar represents 10 μ m) (C) and quantifications (D) are shown. At least 35 positive cells were quantified for each condition. The p-values (Mann-Whitney test) are listed at the top. A schematic representation of the SIRF assay conditions is also presented.

and lagging strand gaps. HeLa-BRCA2^{KO} cells labeled with BrdU in the presence of a low dose of HU exhibited a greater olive tail moment compared to wildtype HeLa cells, indicating the presence of more ssDNA gaps (Fig. 3.9A, B). In line with previous findings, depletion of PRIMPOL with two separate siRNAs completely rescued ssDNA gap formation in HeLa-BRCA2^{KO} cells under a low dose of HU as detected by measuring DNA fibers treated with S1 nuclease (Fig. B6A, B). In addition, we did not observe differences in replication-associated ssDNA gaps in HeLa-BRCA2^{KO} cells under unperturbed DNA replication conditions (Fig. A2.6B). Importantly, in contrast to the S1 nuclease assay, the BrdU alkaline comet assay showed only a partial rescue of HU-induced ssDNA gaps by PRIMPOL depletion in HeLa-BRCA2^{KO} cells (Fig. 3.9 A, B; Fig. B6A). Due to the continuous nature of DNA synthesis on the leading strand, it was previously suggested that PRIMPOL likely serves as a dedicated leading strand primase during replication stress¹⁶⁰. We thus hypothesized that PRIMPOL-independent gaps may in part be explained by gaps on the lagging strand which form in a Pol α -dependent manner.

Unligated Okazaki fragments result in the chromatin accumulation of poly(ADP-ribose) (PAR) chains in S-phase, which can be detected upon inhibition of the poly(ADP-ribose) glycohydrolase (PARG) enzyme¹¹⁵. Indeed, SIRF experiments on cells subjected to PARG inhibition (PARGi) showed that depletion of the OF ligase LIG1 in wildtype cells results in increased PAR chain formation (Fig. B6C, D). We reasoned that, when gaps occur on the lagging strand, the nicked DNA structure which is the substrate of LIG1 during OF ligation is not formed, since DNA synthesis on the OF is not completed. Thus, LIG1 depletion should increase PAR chain signal in cells with completed OF synthesis, but not in cells which accumulate gaps precluding nick formation. Under normal conditions, PAR SIRF experiments showed no difference in PAR chromatin levels in BRCA-proficient and BRCA1/2-depleted cells (Fig. B6C, D). LIG1 depletion yielded a detectable increase in PAR SIRF signal but failed to elicit

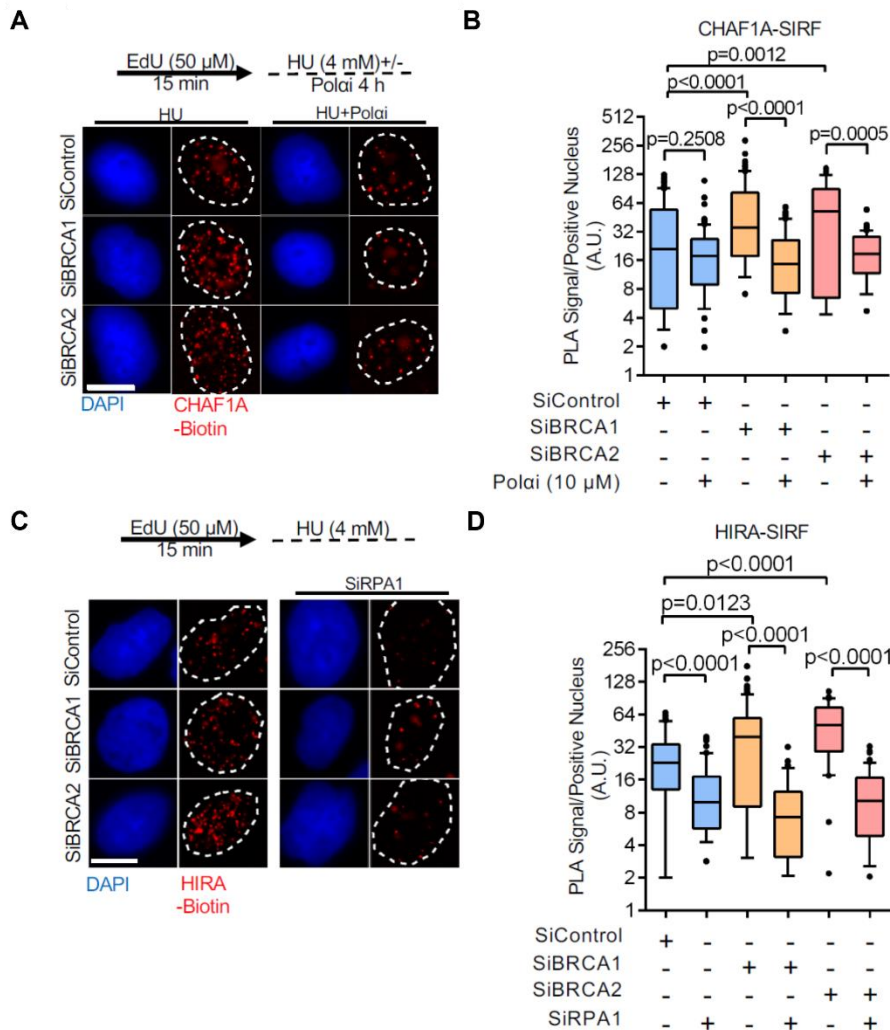


Figure 3.10: Lagging strand gaps drive CHAF1A and HIRA accumulation at stalled forks. (A), (B) SIRF assay showing that Pola inhibition suppresses the increased CHAF1A retention in BRCA1 or BRCA2-depleted HeLa cells. Representative micrographs (scale bar represents 10 μ m) (A) and quantifications (B) are shown. At least 35 positive cells were quantified for each condition. The p-values (Mann-Whitney test) are listed at the top. A schematic representation of the SIRF assay conditions is also presented. (C), (D). SIRF assay showing that RPA1 co-depletion restores HIRA levels to the same levels in wildtype and BRCA1 or BRCA2-knockdown HeLa cells. Representative micrographs (scale bar represents 10 μ m) (C) and quantifications (D) are shown. At least 30 positive cells were quantified for each condition. The p-values (Mann-Whitney test) are listed at the top. A schematic representation of the SIRF assay conditions is also presented.

differences between BRCA-proficient and BRCA1/2-depleted cells, suggesting that Okazaki fragment synthesis remains largely unperturbed in BRCA-deficient cells under normal growth conditions. We next performed SIRF to detect chromatin PAR chains after subjecting cells to EdU labeling under a low dose of HU. Interestingly, HU-induced replication stress resulted in a modest reduction in SIRF signal in BRCA1/2-depleted cells which was drastically exacerbated upon the depletion of LIG1 (Fig. 3.9C, D). This suggests that BRCA-deficient cells accumulate incompletely synthesized Okazaki fragments due to lagging strand gap formation upon encountering HU-induced replication stress. We next sought to directly test if frequent Pol α -mediated repriming during transient HU induced replication stress prior to fork stalling, could drive lagging strand gap accumulation and CAF-1 recycling defects in BRCA-deficient cells. The retinoid ST1926 was previously shown to abolish Pol α activity resulting in replication fork uncoupling at sufficiently high doses¹⁶¹. Indeed, treatment of HeLa cells with 10 μ M ST1926 induced maximal chromatin bound RPA levels within 5 minutes (Fig. B6E, F), indicating a robust and immediate inhibition of Pol α activity. We next performed SIRF on EdU-labeled cells subjected to a high dose of HU in the presence of ST1926. Strikingly, Pol α inhibition, while having a minimal impact on BRCA-proficient cells, completely suppressed CHAF1A retention at stalled forks in BRCA1 and BRCA2-depleted cells (Fig. 3.10A, B). These results suggest that frequent Pol α -mediated lagging strand repriming during replication stress is responsible for the CHAF1A recycling defects in BRCA-deficient cells.

Replication-associated ssDNA gaps are likely to be immediately coated by the RPA complex. Interestingly, the recruitment of HIRA to DNA during transcription has been shown to be dependent on RPA1¹⁶². We wondered if RPA-coated ssDNA could account for the increased presence of HIRA observed at stalled forks in BRCA-deficient cells. Indeed, depletion of RPA1 restored HIRA at stalled forks to similar levels in both BRCA-proficient and BRCA1/2-depleted

cells (Fig. 3.10C, D; Fig. B6G). Taken together, these results suggest that the prevalence of lagging strand gaps, caused by Pol α -dependent repriming, drives the aberrant retention of CAF-1 at stressed replication forks in BRCA-deficient cells. Furthermore, RPA complexes coating ssDNA at these gaps recruit HIRA in the proximity of HU-arrested forks in BRCA-deficient cells.

PCNA unloading ensures CAF-1 mediated fork protection in BRCA-proficient cells

We previously showed that PCNA-K164R cells exhibit PCNA-unloading defects owing to their inability to mitigate lagging strand ssDNA gaps, therefore interfering with CAF-1 recycling at replication forks. Interestingly, similar to BRCA-deficient cells, CHAF1A depletion also rescued fork stability in PCNA-K164R cells (Fig. B7A, B). Thus, we sought to test if PCNA unloading defects cause the CAF-1 retention at stalled forks observed in BRCA-deficient cells. Indeed, similar to what we observed for CHAF1A, SIRF experiments revealed an abnormal retention of PCNA at stalled replication forks in BRCA1/2-depleted cells upon treatment with a high dose of HU (Fig. 3.11A, B). Importantly, Pol α inhibition completely abrogated this abnormal PCNA retention, indicating that lagging strand gaps are responsible for the PCNA unloading defects in BRCA-deficient cells.

Since the results described above suggested that CAF-1 retention on ssDNA gaps promotes fork degradation in BRCA-deficient cells, we next assessed if correcting this defective PCNA unloading could restore fork stability to these cells. Recent work showed that the bromodomain extra-terminal (BET) family of proteins, namely BRD2, BRD3 and BRD4, form complexes with ATAD5 and inhibit its PCNA unloading activity^{163,164}. We reasoned that inactivating these BET proteins would enhance PCNA removal from DNA and thus reverse the

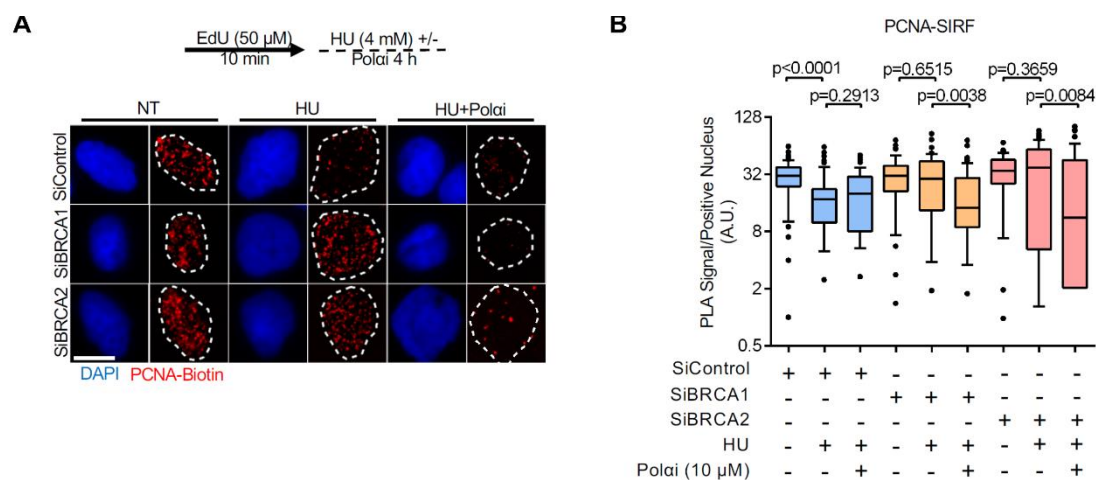


Figure 3.11: BRCA-deficient cells display PCNA unloading defects dependent on Pol α -mediated repriming during replication stress. (A), (B) SIRF assay showing deficient PCNA unloading from nascent DNA upon replication fork arrest in BRCA-depleted HeLa cells. Pola inhibition by treatment with 10 μM ST1926 suppresses this defect, indicating that this PCNA retention on nascent DNA occurs at lagging strand gaps. Representative micrographs (scale bar represents 10 μm) (A) and quantifications (B) are shown. At least 50 positive cells were quantified for each condition. The p-values (Mann-Whitney test) are listed at the top. A schematic representation of the SIRF assay conditions is also presented.

effect of PCNA unloading defects in BRCA-deficient cells. Strikingly, depleting BRD3 and BRD4 restored fork stability to HeLa-BRCA2^{KO} cells (Fig. 3.12A; Fig. A2.7C). Importantly, co-depletion of CHAF1A with either BRD3 or BRD4 restored nascent fork degradation to HeLa-BRCA2^{KO} cells, suggesting that correction of PCNA unloading defects in BRCA-deficient cells restores fork stability in a CAF-1-dependent manner.

To more directly assess the role of PCNA unloading in ensuring fork stability in BRCA-deficient cells, we next created PCNA variants exhibiting reduced chromatin retention. We previously obtained a clonal line in pseudotriploid human 293T cells bearing genetic knockouts

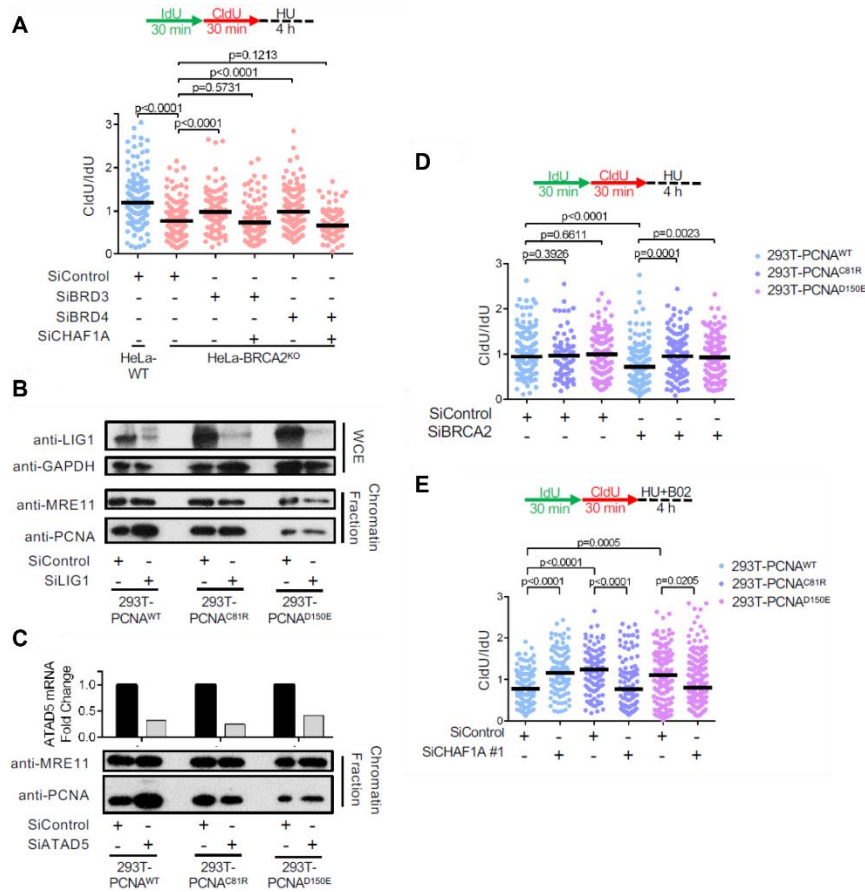


Figure 3.12: Restoring PCNA unloading rescues fork stability in BRCA-deficient cells. (A) DNA fiber combing assay showing that co-depletion of BRD3 or BRD4 restores HU-induced fork degradation in CHAF1A-knockdown HeLa-BRCA2^{KO} cells. The ratio of CldU to IdU tract lengths is presented, with the median values marked on the graph. The p-values (Mann-Whitney test) are listed at the top. A schematic representation of the DNA fiber combing assay conditions is also presented. (B), (C) Chromatin fractionation experiments showing that ATAD5 (B) or LIG1 (C) knockdown increases the chromatin levels of wildtype PCNA, but not those of PCNA-C81R and D150E variants. MRE11 is used as a control for the chromatin fraction. LIG1 depletion is confirmed by western blot. ATAD5 depletion is confirmed by RT-qPCR, since no antibody was available to use to verify depletion by western blot. The average of two technical replicates is shown. (D). DNA fiber combing assay showing that BRCA2 knockdown causes HU induced fork degradation in 293T cells expressing wildtype PCNA, but not in 293T cells expressing PCNA variants with deficient chromatin retention. The ratio of CldU to IdU tract lengths is presented, with the median values marked on the graph. The p-values (Mann-Whitney test) are listed at the top. A schematic representation of the DNA fiber combing assay conditions is also presented. (E) DNA fiber combing assay showing that CHAF1A knockdown suppresses HU-induced fork degradation caused by B02 treatment in 293T cells expressing wildtype PCNA, but not in 293T cells expressing PCNA variants with deficient chromatin retention. The ratio of CldU to IdU tract lengths is presented, with the median values marked on the graph. The p-values (Mann-Whitney test) are listed at the top. A schematic representation of the DNA fiber combing assay conditions is also presented.

of four out of five endogenous PCNA alleles, with the final allele encoding a PCNA-K164R mutation (293T-PCNAK164R(hyp)). Importantly, we showed that these cells exhibit lower endogenous PCNA expression and the stable complementation with wildtype PCNA restored near-wildtype characteristics to these cells, thus establishing their suitability for complementation with potential PCNA mutants. Studies in *S. cerevisiae* have characterized point mutations on PCNA's trimer interface that interfere with stable homotrimer formation^{23,165–167}. We generated two of the corresponding mutations, namely PCNA-C81R and PCNA-D150E, in human PCNA (Fig. B7D). Using a lentiviral expression system, we stably complemented 293T-PCNAK164R(hyp) cells with either PCNA-WT, PCNA-C81R or PCNA-D150E variants (Fig. A2.7E). We next tested if these mutations could ameliorate PCNA unloading defects caused by ATAD5 or LIG1 depletion. As expected, ATAD5 depletion increased chromatin-bound PCNA in 293T-PCNA-WT cells, however, 293T-PCNA-C81R and 293T-PCNA-D150E cells exhibited no increase in PCNA chromatin association upon ATAD5 depletion (Fig. 3.12C). Similarly, LIG1 depletion also increased chromatin-bound PCNA levels in 293T-PCNA-WT cells, in line with Okazaki fragment ligation being a prerequisite for PCNA unloading²³. In contrast, LIG1 knockdown failed to cause PCNA chromatin retention in 293T-PCNA-C81R and 293T-PCNA-D150E cells (Fig. 3.12B). These results confirm that PCNA-C81R and PCNA-D150E mutants have reduced chromatin retention and can correct PCNA unloading defects in human cells.

We next assessed if PCNA-C81R and PCNA-D150E can ameliorate fork degradation in BRCA-deficient cells. Indeed, while both BRCA2 depletion as well as RAD51 inhibition using B02 elicited fork degradation in 293T-PCNA-WT cells, fork stability remained intact in 293T-PCNA-C81R and 293T-PCNA-D150E cells (Fig. 3.12D, E; Fig. B7F). Importantly, while CHAF1A depletion restored fork stability to B02-treated 293T-PCNA-WT cells, it caused fork

degradation in B02-treated 293T-PCNA-C81R and 293T-PCNA-D150E cells. (Fig. 3.12D, E; B7G). These results suggest that, in cells with impaired BRCA/RAD51 function, the restoration of PCNA unloading rescues fork stability by reinstating CAF-1 function at replication forks. Taken together, these observations imply that CAF-1 is a direct effector of the BRCA/RAD51 pathway of fork protection whose function is ensured by lagging strand gap suppression and efficient PCNA unloading (Fig. B8A).

Chapter 4

Discussion

Nucleosome assembly is a determinant of replication fork stability

Replication-coupled nucleosome assembly depends on the PCNA-interacting histone chaperone CAF-1^{168,169}. In the previous sections, we outlined distinct genetic backgrounds susceptible to replication fork degradation, i.e., PCNA-K164R – deficient in PCNA-ubiquitination - and BRCA-deficiency, as exhibiting a functional inactivation of CAF-1 during replication stress. In both backgrounds, CAF-1 inactivation at replication forks was associated with the inability of PCNA-K164R and BRCA-deficient cells to mitigate replication associated gaps, resulting in the inefficient recycling of PCNA-CAF-1 complexes at stressed replication forks. Furthermore, CAF-1 inactivation in BRCA- and PCNA-ubiquitination proficient cells elicited fork degradation through similar mechanisms as previously documented in models of HR deficiency, involving the activity of DNA2 and MRE11 nucleases^{2,3,38}, as well as fork reversal dependent on ZRANB3 and SMARCAL1^{5,8-10}.

CAF-1 mediated nucleosome assembly depends on its interaction with ASF1, which packages H3/H4 heterodimers that are subsequently used by CAF-1 to assemble (H3/H4)₂ tetramers on replicating chromatin¹⁷⁰⁻¹⁷³. CAF-1 preferentially interacts with the canonical histone isoform H3.1¹⁵⁵. ASF1 also participates in replication-independent deposition of histone H3.3, by cooperating with the histone chaperone HIRA^{155,174}. In humans, two ASF1 paralogs exist: ASF1A and ASF1B. Of the two, only ASF1A is capable of interacting with both CAF-1 and HIRA, and appears to do so in a mutually exclusive manner^{155,175,176}. Interestingly, we observed ASF1A inactivation to be epistatic with BRCA1/2 deficiency in eliciting fork

degradation, further suggesting a role for nucleosome assembly as an effector of BRCA-mediated fork stability. In line with this, restoring CAF-1 activity at replication forks in BRCA-deficient cells by either CHAF1A overexpression or the restoration of PCNA-unloading rescued fork stability. Lastly, we uncovered that fork rescue upon the inactivation of CHAF1A in BRCA-deficient cells was dependent on ASF1A and operated through the compensatory HIRA/H3.3 pathway of nucleosome assembly. Fork rescue upon CHAF1A inactivation was also observed in PCNA-K164R cells, which exhibit similar defects in ssDNA gap suppression and PCNA unloading as BRCA-deficient cells. These collective observations are consistent with the previous findings showing that nucleosomes act as a barrier to DNA resection by nucleases⁶⁸ and may reflect a role of nucleosome assembly as a determinant of canonical fork stability mechanisms.

Recently published work revealed a role for CAF-1 and ASF1-dependent nucleosome assembly in promoting HR by mediating RAD51 recruitment to ssDNA through MMS22L-TONSL¹⁷⁷. It is therefore possible that the inactivation of CAF-1 and ASF1 directly results in fork instability by impairing RAD51-mediated fork protection. In the present work, we reveal that fork stability in BRCA-deficient cells upon CHAF1A inactivation occurs in a manner dependent on ASF1A, HIRA and H3.3. Importantly, treatment with the RAD51 inhibitor B02 fails to elicit fork degradation under these conditions, suggesting that HIRA-mediated restoration of fork stability occurs in a RAD51-independent manner. These observations suggest that, in the context of replication stress, nucleosome assembly acts as the major determinant of fork stability and operates independently of the role of RAD51 in mediating HR.

Our observations indicate that the fork protective activity of HIRA only operates when CAF-1 and the BRCA pathway are simultaneously inactivated. Previous studies have revealed a compensatory role of HIRA in filling nucleosome gaps on the genome in the absence of the CAF-

1¹⁵⁶. However, the inactivation of CHAF1A in BRCA-proficient cells does not trigger HIRA mediated fork protection. We speculate that this selective activation of HIRA is caused by its recruitment to RPA-coated ssDNA accumulating in BRCA-deficient cells, proximal to stalled forks. Nevertheless, the activation of HIRA-mediated fork protection still necessitates the inactivation of CHAF1A. A possible explanation for this could be the mutual exclusivity of ASF1A interactions with CAF-1 and HIRA. Indeed, ASF1 has previously been shown to ensure the supply of S-phase (H3.1-containing) histones during replication stress¹⁷⁸. Therefore, it is possible that the absence of CAF-1 relieves ASF1A of its S-phase histone buffering constraints, enabling it to participate in H3.3-dependent nucleosome assembly with HIRA. Furthermore, the RPA-dependent accumulation of HIRA at stalled forks in BRCA-deficient cell may prime HIRA to mediate efficient nucleosome assembly thereby preventing fork degradation upon CAF-1 loss (Fig. B8B).

Inadequate gap evasion during DNA replication contributes to lagging strand synthesis defects

In our work we revealed that PCNA-K164R cells accumulate spontaneous replication-associated gaps during unperturbed DNA replication putatively due to endogenous replication stress. We further found that forks speed and fork stability defects in PCNA-K14R cells operate epistatically with the inactivation of Okazaki fragment maturation factors FEN1 and LIG1. Additionally, in asynchronous cells, PCNA-K164R contributed to enhanced chromatin bound poly(ADP ribose) chains which could be suppressed by the lagging strand synthesis inhibitor emetine, suggesting that PCNA-K164R cells accumulate unligated Okazaki fragments¹¹⁵ arising from unmitigated replication-associated gaps on the lagging strand. Importantly, we found that the resolution of post-replicative gaps in PCNA-K164R cells depended on the BRCA-pathway, thereby suggesting that the BRCA-pathway operates as a parallel pathway to PCNA-

ubiquitination dependent translesion synthesis in mediating ssDNA gap repair. Furthermore, PCNA-K164R, while not eliciting PARPi sensitivity, synergistically sensitized BRCA-deficient cells to the PARP-inhibitor Olaparib, in line with later works revealing persistent ssDNA gaps, potentially those on lagging strands, as lesions that govern PARPi sensitivity in BRCA-deficient cells^{64,111,148,150}. Indeed recent work has revealed that ssDNA arising on lagging strands as a result of FEN1 inactivation, sensitizes cells to PARPi¹⁷⁹.

A recent body of literature revealed a role for the BRCA-RAD51 pathway in suppressing ssDNA gap formation by restraining fork progression during replication stress^{64,111,112,146,148}. In this context, replication-associated gap accumulation is found to occur in a manner dependent on the PRIMPOL primase, which allows for repriming and continued fork progression during replication stress. Recent evidence suggests that PRIMPOL-mediated repriming and subsequent gap induction during replication stress is enhanced in the absence of sufficient fork reversal, a downstream outcome of fork slowing during replication stress^{7,51,86,149,180}. In models of 53BP1 inactivation and partial RAD51 inhibition, BRCA2 was recently documented to participate in the generation of a reversed fork substrate necessary for nucleolytic resection⁴⁰. These collective observations suggest that the BRCA-pathway, through fork restraint and reversal, prevents excessive PRIMPOL-mediated repriming at stressed forks, thereby suppressing ssDNA gap formation.

While active fork restraint ensures BRCA-mediated gap evasion during replication stress, the mechanistic basis of spontaneous gap formation during DNA replication under endogenous conditions in PCNA-K164R cells is less clear. Increased rates of fork progression can potentially underlie replication stress¹¹⁰. Therefore, it is possible that the observed increased fork progression rates in PCNA-K164R cells underlie spontaneous replication-associated gap induction. However,

while depletion of FEN1 and LIG1 increases fork speed to similar levels and in a manner epistatic with PCNA-K164R, LIG1 depletion did not increase replication associated gap accumulation in PCNA-ubiquitination proficient cells (data not shown). This suggests that modest increases in fork speed, as observed in PCNA-K164R or FEN1/LIG1 depleted cells are not sufficient to explain increased replication-associated gap accumulation. The SNF2 family translocases HLTF and ZRANB3 are required for fork slowing and reversal during replication stress^{48,50,51,56,57,180}. Importantly, HLTF is known to catalyze PCNA-ubiquitination^{52,53}, while the fork remodeling activities of ZRANB3 depend on polyubiquitinated PCNA^{50,51}. Our data suggest that that PCNA-K164R cells show no dependence on HLTF and only a partial dependence on ZRANB3 fork reversal. Therefore, it is possible that increased fork speeds upon perturbing Okazaki fragment synthesis and processing necessitate an enhanced involvement of ZRANB3 and HLTF in restricting gaps arising from endogenous replication obstacles in a manner dependent on ubiquitinated PCNA. Loss of ZRANB3 and HLTF activity in the context of abolished PCNA-ubiquitination could therefore explain the increase in replication-associated gap accumulation in PCNA-K164R cells. Notably, we did not observe fork degradation upon ZRANB3 inactivation alone. However, the lack of fork degradation in this context could be reflective of 1) the absence of fork acceleration upon ZRANB3 inactivation; 2) the presence of HLTF activity; 3) the context specificity of ZRANB3 function loss upon abolishing PCNA-ubiquitination vs. the complete inactivation of ZRANB3, which could affect global replication fork reversal. Interestingly, as opposed to ZRANB3 inactivation, suppressing PCNA-polyubiquitination through UBC13 inactivation elicited fork degradation, further supporting a possible context-specific function of ZRANB3 in suppressing fork progression and gap accumulation during replication stress.

Despite the well-documented emerging role of PRIMPOL in gap induction in BRCA-deficient cells, its impact on leading versus lagging strand gap induction is not well understood.

The major experimental approach employed to detect replication-associated gaps involves measuring the shortening of DNA tracts upon treatment with the S1 nuclease, which specifically digests ssDNA substrates, in DNA fiber spreading experiments¹⁸¹. In this assay, for a detectable shortening of replication tracts upon S1 treatment, gaps likely need to be present on both the leading and the lagging strands. In our studies, we show that while PRIMPOL depletion in HeLa-BRCA2^{KO} cells completely abolishes replication tract shortening upon treatment with the S1 nuclease, it only partially suppresses ssDNA gaps detected by the BrdU alkaline comet assay. This raises the question of the mechanism by which PRIMPOL-independent gaps occur. Recent work in reconstituted eukaryotic DNA replication systems revealed that fork progression is disproportionately impeded by leading strand obstacles, while lagging strand obstacles are efficiently bypassed via inherently frequent Pol α -mediated repriming^{116,117}. Repriming by PRIMPOL is thus likely to occur mostly on the leading strand, giving rise to leading strand ssDNA gaps¹⁶⁰. This raises the possibility that the PRIMPOL-independent ssDNA gaps detected in BRCA2-deficient cells by BrdU alkaline comet assays could, in part, be Pol α -dependent lagging strand gaps. Indeed, taking advantage of the fact that S-phase chromatin-bound PAR chains specifically form at fully synthesized but unligated OFs¹¹⁵, we demonstrate that BRCA-deficient cells accumulate lagging strand discontinuities during replication stress.

The unloading of PCNA from lagging strands can only occur upon OF ligation²³. Importantly, we and others have shown that loss of PCNA ubiquitination, which ensures efficient lagging strand synthesis, results in PCNA unloading defects¹⁵⁸. Thus, PCNA unloading represents a surrogate marker for OF synthesis and ligation defects. In our work, we show that PCNA unloading is defective upon replication stress in both PCNA-K164R as well as BRCA-deficient cells. Moreover, PCNA-unloading defects in BRCA-deficient cells, which only manifest in the presence of exogenously added replication stress, can be rescued upon Pol α inhibition, solidifying

their connection to lagging strand synthesis defects. This further supports the notion that incompletely synthesized OFs accumulate in BRCA-deficient cells. Indeed, recent studies have also reported OF processing defects in BRCA-deficient cells^{111,150}. In conclusion, in combination with previous studies, we provide significant evidence that lagging strand gaps comprise a direct and therapeutically relevant consequence of gap evasion defects in PCNA-K164R and BRCA-deficient cells.

PCNA-unloading and CAF-1 recycling connect gap evasion to replication fork stability

The classical FA/BRCA modality of replication fork protection asserts a role for stable RAD51 nucleofilaments on reversed fork arms in acting as a direct obstacle to nuclease mediated resection^{2-4,8,79}. However, recent evidence suggests that RAD51 at replication forks may also assemble at PRIMPOL-dependent gaps that occur proximal to the replication fork experiencing stress¹¹². Further evidence, as discussed above, suggests that the BRCA-pathway possesses a latent role in orchestrating replication fork reversal and, therefore, could participate in restraining forks during replication stress⁴⁰. These observations suggest that the BRCA/RAD51 pathway may actively act at stressed replication forks to 1) restrain uncoupled forks by catalyzing reversal and 2) initiate the rapid repair of post-replicative ssDNA gaps, thereby offering a potential mechanistic explanation for the recently defined role of the BRCA/RAD51-pathway in suppressing replication-associated ssDNA gaps^{1,8,64,111,112,146,148,150}. Through our studies in PCNA-K164R cells, we revealed replication-associated ssDNA gaps as critical enablers of fork instability owing to their direct impact on lagging strand DNA synthesis and the subsequent unloading and recycling of PCNA. In line with this, we also detected PCNA unloading defects in BRCA-deficient cells, and correcting these defects restored fork stability in a CAF-1 dependent

manner. This leads us to speculate that gap-evasion followed by PCNA unloading and CAF-1 recycling may be a major effector mechanism operating downstream of previously characterized fork protection pathways. This raises the possibility that, in addition to the formation of stable RAD51 nucleofilaments on reversed forks, ssDNA gap evasion may be a major accessory of the BRCA/RAD51 pathway of replication fork protection with PCNA-CAF1 recycling and nucleosome assembly as effectors. Interestingly, cells deficient of the PCNA unloader ATAD5 have recently been characterized to be defective in RAD51-mediated fork slowing and reversal¹⁸². It is therefore possible that the initial inability to complete lagging strand synthesis in gap-evasion defective models could entail further fork restraint defects, thereby exacerbating fork instability.

Despite sharing gap suppression and PCNA unloading defects, PCNA-K164R cells and BRCA-deficient cells experience fork degradation through distinct mechanisms. While BRCA-deficient cells display fork degradation through both MRE11 and DNA2 dependent mechanisms, fork degradation in PCNA-K164R cells is independent of MRE11 and depends on DNA2 alone. These divergent mechanisms could potentially arise as a consequence of differences in reversed fork substrates upon fork stalling. We showed that PCNA-K164R cells undergo fork reversal in a manner independent of HLTF and only partially dependent on ZRANB3, as opposed to BRCA-deficient cells that show an equal dependence on SMARCAL1, HLTF and ZRANB3 for fork degradation⁵. As speculated on in the literature review, in PCNA-K164R cells, a near complete dependence on SMARCAL1, which prefers leading strand uncoupled fork substrates, could lead to an asymmetric reversed fork configuration that is only compatible with the 5'-3' exonuclease activity of DNA2, as opposed to MRE11/EXO1 which relies on an initial 3'-5' processing by MRE11 on putatively symmetrical reversed fork substrates prior to long range resection by EXO1^{58,59}. Regardless, the presence of nucleosomes inhibits resection by both EXO1 as well as

DNA2⁶⁸ and thus may act as a deterrent to fork resection by mechanisms inclusive of either one or both of these nucleases.

Future Directions

In BRCA-deficient cells, replication associated gaps are subject to MRE11-dependent processing, leading to gap expansion^{1,8,65,112,149}. These extended gaps underlie the reliance of BRCA-deficient cells on PRR mechanisms and enhance sensitivity to chemotherapeutics and PARPi in these cells^{64,111,148,149}. The effect of nucleosome deposition on limiting the nucleolytic processing of gaps remains to be ascertained. In our work, we showed that CHAF1A inactivation in BRCA-deficient cells promotes the activity of HIRA recruited at ssDNA gaps. Therefore, it is possible that CHAF1A inactivation in BRCA-deficient cells may restrict gap expansion by MRE11 through a mechanism similar to that observed in the context of reversed replication forks. Further studies assessing replication-associated ssDNA gap formation involving BrdU alkaline comet assays and S1 nuclease assays are required to assess this possibility. Additionally, the effect of CHAF1A inactivation on PARPi sensitivity remains to be ascertained as any effect on ssDNA gap expansion upon CHAF1A inactivation is likely to affect the survivability of BRCA-deficient cells to these treatments.

Despite sharing defective PCNA unloading as an underlying mechanism predisposing to fork instability, the concomitant loss of BRCA-function in PCNA-K164R cells results in additive fork degradation. These observations indicate that PCNA-ubiquitination and the BRCA pathway, through their participation in replication associated gap avoidance, likely act as parallel pathways ensuring PCNA recycling. Recent evidence revealed temporal distinctions between gap avoidance pathways dependent on RAD51/template switching and translesion synthesis¹⁴⁹,

suggesting that PCNA recycling may be differentially regulated depending on which gap avoidance pathway is engaged. Through SIRF experiments, we characterized PCNA-CHAF1 recycling defects in BRCA-deficient cells exposed to replication stress (Fig. 3.7A, B, C; Fig 3.11 A, B). However, the kinetics of PCNA unloading in PCNA-K164R cells remain to be precisely defined in mammalian systems. Our observations of spontaneous gap accumulation in PCNA-K164R cells under endogenous conditions suggest that PCNA unloading defects may be operational in these cells independently of exogenous replication stress, leading to global nucleosome assembly defects, in line with what we observed in MNase sensitivity assays in asynchronous 293T PCNA-K164R cells (Fig. 2.8C). SIRF studies in the presence or absence of exogenous replication stress are needed to characterize the precise nature of PCNA unloading defects in PCNA-K164R cells.

Unloading of PCNA depends on the alternative RLC complex involving ATAD5^{118,182}. Interestingly, we observed that while ATAD5 depletion elicited fork degradation in PCNA-WT cells, it did not further enhance fork degradation in PCNA-K164R cells (Fig. 2.8B). Subsequent experiments using BRD3 and BRD4 inactivation to disinhibit ATAD5 activity in BRCA-deficient cells restored fork stability via restored CHAF1A function (Fig. 3.12A), suggesting ATAD5 function is also dysregulated in BRCA-deficient cells during replication stress. Thus, the absence of additive fork degradation upon ATAD5 inactivation in PCNA-K164R cells as opposed to BRCA inactivation in PCNA-K164R cells is counterintuitive to our understanding of how ATAD5 regulates PCNA unloading and fork stability. One possibility underlying these differential effects may be related to the role of ATAD5 in augmenting RAD51-mediated fork reversal through PCNA unloading. It is possible that both PCNA-K164R cells and ATAD5 inactivated cells experience fork reversal defects, thereby restricting the prevalence of fork substrates required for nucleolytic resection upon the combined inactivation of ATAD5 and

PCNA-ubiquitination. Regardless, the precise mechanisms underlying fork degradation upon ATAD5 inactivation such as the involvement of MRE11, as well as the SNF2 family translocases SMARCAL1, ZRANB3 and HLTF remain to be characterized. Furthermore, the effect of ATAD5 inactivation in BRCA-deficient cells remains to be ascertained. Lastly, experiments using PCNA-C81R and PCNA-D150E cells with combinatorial RAD18 and BRCA1/2 inactivation are required to further characterize the universality of PCNA unloading as a mechanism underlying RAD51 and PCNA-ubiquitination dependent fork stability.

Through our work we elucidate nucleosome assembly as a major fork stability mechanism operating through the suppression of ssDNA gaps. However, whether this mechanism of fork stability acts as an accessory to pathways independent of the BRCA proteins or PCNA-ubiquitination is unknown. A classical BRCA-independent fork protection pathway involves the Fanconi anemia family of proteins^{3,15,76}. FA proteins have been extensively characterized to participate in ICL repair, but their role in suppressing ssDNA gap accumulation is less understood. This also raises questions regarding whether nucleosome assembly is important for fork protection via the FA pathway as well. Indeed, latest work suggests that FANCD2 facilitates strand exchange by promoting the binding of RAD51 to ssDNA, in addition to the fact that FANCD2 acts to restrain fork protection during replication stress^{87,183}. Therefore, cells deficient in fork protection through the loss of FA pathway activity may be subject to similar PCNA-CHAF1A recycling constraints as BRCA-deficient cells. Further studies are required to assess this possibility. These studies can be further extended to other RAD51-dependent and RAD51-independent fork protection pathways outlined in the literature review.

In vivo psoralen crosslinking in combination with electron microscopy studies recently revealed that reversed replication forks undergo regular chromatinization and display standard

nucleosome periodicity⁷¹. However, it remains unknown whether nucleosome assembly on reversed forks is essential for replication fork stability as measured by the DNA fiber assay. Using the association of PARP1 with nascent DNA as a proxy for reversed fork prevalence, we showed that HIRA mediated nucleosome assembly upon CHAF1A inactivation stabilizes reversed forks in BRCA-deficient cells (Fig. 3.2E). However, due to the limited resolution of the DNA fiber combing approach, as opposed to electron microscopy, it remains unclear whether the stabilized structures represent fully intact reversed fork structures with unresected reversed arms, or simply a partially resected structure with stable daughter strands only behind replication fork junctions. *In vitro* studies have revealed that stable RAD51 nucleofilaments on structures resembling reversed replication forks antagonize DNA resection^{4,8}. Therefore, further studies employing electron microscopy of psoralen crosslinked replication fork intermediates would be needed to ascertain whether nucleosome assembly is protective of reversed arms in stalled fork structures from nucleolytic resection, and the relative contribution of RAD51 nucleofilaments versus the presence of nucleosomes in ensuring this protection. The bacterial Holliday junction binding protein RuvA, has been used as a proxy for the detection of reversed fork intermediates owing to its preference for X-shaped recombination intermediates as opposed to Y-shaped replication fork junctions¹⁹. Ectopically expressed RuvA constructs used in conjunction with chromatin fractionation or SIRF assays may be employed to further augment electron microscopy studies in ascertaining the nature of stalled fork substrates dependent on nucleosome-dependent protection against resection.

Chapter 5

Materials and Methods

Cell culture techniques

Human 293T, RPE1, HeLa, and U2OS cells were grown in DMEM supplemented with 10% Fetal Calf Serum. To generate PCNA-K164R cells, the gRNA sequences used were: TTTCACCTCCGTCTTTTGCACAGG for 293T cells and GCAAGTGGAGAACTTGGAATGG for RPE1 cells. The sequences were cloned into the pX458 vector (pSpCas9BB-2A-GFP; obtained from Addgene). Cells were co-transfected with this vector and a repair template spanning the K164 genomic locus but containing the K164R mutation (AAA-AGA codon change). Transfected cells were FACS-sorted into 96-well plates using a BD FACSAria II instrument. Resulting monoclonal cultures were screened by western blot for loss of PCNA ubiquitination using an antibody specific for this modification. For verification of positive cell lines, the targeted genomic region was PCR amplified from genomic DNA, cloned into pBluescript, and multiple clones were Sanger-sequenced to ensure that all alleles are identified. In the 293T KR5 clone obtained, no wildtype allele was discovered, and at least one K164R allele was found. In addition, several other alleles bearing insertions or deletions at that position, introducing frameshifts and premature subsequently stop codons, were identified. No truncated forms were detectable by western blot. In RPE cells, only alleles with the K164R mutation were detected. For exogenous PCNA expression, pLV-puro- CMV lentiviral constructs encoding wildtype, K164R, D150E or C81R variant were obtained from Cyagen. Infected cells were selected by puromycin. RPE1-p53^{ko}-BRCA1^{ko} were obtained from Dr. Alan D'Andrea (Dana-Farber Cancer Institute, Boston, MA)⁹³. For doxycycline-induced CHAF1A

overexpression, the pLV[Exp]-Puro-TRE>hCHAF1A lentiviral construct (Cyagen) was used. Infected cells were selected by puromycin.

For RAD18 and CHAF1A gene knockout, the commercially available CRISPR/Cas9 KO plasmids were used (Santa Cruz Biotechnology sc-406099 and sc-402472 respectively). Transfected cells were FACS-sorted into 96-well plates using a BD FACSAria II instrument. Resulting colonies were screened by western blot. The BRCA2-knockout HeLa cells were previously published⁸⁰.

Protein techniques

Denatured whole cell extracts were prepared by boiling cells in 100mM Tris, 4% SDS, 0.5M β -mercaptoethanol. Chromatin fractionation was performed as previously described¹⁸⁴. Briefly, cells were treated with 1% Triton-X and the pellet was isolated using centrifugation at 4°C. Antibodies used for Western blot were: CHAF1A (Cell Signaling Technology 5480); ASF1 (Santa Cruz Biotechnology sc-53171); BRCA1 (Santa Cruz Biotechnology sc-6954); BRCA2 (Calbiochem OP95); ZRANB3 (Invitrogen PA5-65143); SMARCAL1 (Invitrogen PA5-54181); HIRA (Abcam 129169); DAXX (Invitrogen PA5-79137); RPA1 (Cell Signaling Technology 2198); LIG1 (Bethyl A301-136A); MRE11 (GeneTex GTX70212); PCNA (Cell Signaling Technology 2586); ubiquitinated PCNA (Cell Signaling Technology 13439); BRD3 (Bethyl A302-368A); BRD4 (Bethyl A700-005); GAPDH (Santa Cruz Biotechnology sc-47724); CHK2 (Cell Signaling Technology 2662); pCHK2-T68 (Cell Signaling Technology 2661); CHK1 (Cell Signaling Technology 2360); pCHK1-S317 (Cell Signaling Technology 2344); EXO1 (Santa Cruz Biotechnology sc-56092); WRN (Santa Cruz Biotechnology sc-5629); CTIP (Santa Cruz Biotechnology sc-271339); MUS81 (Santa Cruz

Biotechnology sc-47692); RAD18 (Cell Signaling Technology 9040); UBC9 (Santa Cruz Biotechnology sc-10759); RAD51 (Santa Cruz Biotechnology sc-8349); ZRANB3 (Bethyl A303-033A); HLTF (Santa Cruz Biotechnology sc-398357); RECQL1 (Santa Cruz Biotechnology sc-166388); PAR chains (ENZO ALX-804-220); LaminB1 (Abcam ab16048); LIG1 (Santa Cruz Biotechnology sc-271678); REV1 (Santa Cruz Biotechnology sc-393022); POLK (Santa Cruz Biotechnology sc-166667); Vinculin (Santa Cruz Biotechnology sc-73614); FEN1 (Santa Cruz Biotechnology sc-28355); UBC13 (Santa Cruz Biotechnology sc-376470).

Gene knockdowns

For gene knockdown, cells were transfected with Stealth siRNA (Life Tech) using Lipofectamine RNAiMAX reagent. AllStars Negative Control siRNA (Qiagen 1027281) was used as control. Gene knockdown was confirmed by western blot or qRT-PCR, and representative results are shown. The siRNA targeting sequences used were: BRCA2: GAGAGGCCTGTAAAGACCTTGAATT; EXO1: CCTGTTGAGTCAGTATTCTCTTTCA; WRN: TGGGCTCCTGCAGACATTA ACTTAA; CTIP: GGGTCTGAAGTGAACAAGATCATT; MUS81: TTTGCTGGGTCTCTAGGATTGGTCT; RAD18: CATATTAGATGAACTGGTATT; UBC9: TAAACAAGCCTCCTTCCCACGGAGT; RAD51: CCATACTGTGGAGGCTGTTGCCTAT; HLTF: TGCATGTGCATTA ACTTCATCTGTT; ZRANB3: TGGCAATGTAGTCTCTGCACCTATA; SMARCAL1: CACCCTTTGCTAACCCAACTCATAA; RECQL1: ACAGGAGGUGGAAAGAGCTTATGTT; REV1: GAAATCCTTGCAGAGACCAA ACTTA; POLK: CAGCCATGCCAGGATTTATTGCTAA; ATAD5: GGTACGCTTTAAGACAGTTACTGTT; BRCA1: AATGAGTCCAGTTTCGTTGCCTCTG; LIG1: Silencer Select ID s8173/4 (Life Technologies); FEN1: Silencer Select ID s5104

(Life Technologies); CHAF1A#1: Silencer Select ID s19499 (Life Technologies); CHAF1A#2: HSS115231; UBC13 Silencer Select ID: s14595 (Life Technologies); RADX: ON-TARGETplus J-014634-21 (Dharmacon); PRIMPOL #1: GAGGAAACCGTTGTCCTCAGTGTAT (Horizon Discovery); PRIMPOL #2: 39536; ASF1A#1: CAGAGAGCAGTAATCCAAATCTACA; ASF1A#2: s226043; HIRA#1: HSS111075; HIRA#2: HSS186934; DAXX: s3935; H3F3A: s51241; H3F3B: s226272; RPA1: s12127; BRD3: s23901; BRD4: s15544.

Comet assay

For the BrdU alkaline comet assay, cells were incubated with 100 μ M BrdU for in the presence or absence of 0.4mM HU as indicated, followed by media removal, PBS wash, and incubation in fresh media for the indicated times. Cells were harvested and subjected to the alkaline comet assay using the CometAssay kit (Trevigen 4250-050) according to the manufacturer's instructions. Slides were stained with primary anti-BrdU (BD 347580) and secondary Alexa Fluor 568 (Invitrogen A11031) antibodies. Slides were imaged using a Nikon Eclipse TE2000-U microscope. The percent tail DNA or the olive tail moments were calculated using CometScore 2.0 software. For the neutral comet assay, cells were treated as indicated, harvested, and the assay was performed using the CometAssay kit (Trevigen 4250-050) according to the manufacturer's instructions. Slides were imaged and the tail moments were calculated using the CometScore 2.0 software.

DNA fiber assay

Cells were incubated consecutively with 100 μ M CldU and 100 μ M IdU for the indicated times. Hydroxyurea and nuclease inhibitors (50 μ M mirin for MRE11 inhibition or 30 μ M C5¹⁸⁵ for

DNA2 inhibition) were added as indicated. Next, cells were harvested and DNA fibers were obtained using the FiberPrep kit (Genomic Vision EXT-001). DNA fibers were stretched on glass coverslips (Genomic Vision COV-002-RUO) using the FiberComb Molecular Combing instrument (Genomic Vision MCS-001). Slides were incubated with primary antibodies (Abcam 6326 for detection of CldU; BD 347580 for detection of IdU; Millipore Sigma MAB3034 for detection of DNA), washed with PBS, and incubated with Cy3, Cy5, or BV480 –coupled secondary antibodies (Abcam 6946, Abcam 6565, BD Biosciences 564879). Following mounting, slides were imaged using a Leica SP5 confocal microscope. At least 70 tracts were quantified for each sample.

S1 nuclease fiber spreading assay

The S1 nuclease treatment in combination with DNA fiber spreading for the detection of replication-associated ssDNA gaps was done as previously described¹⁸¹. Briefly, exponentially growing cells were labeled with 100 μ M IdU and 100 μ M CldU for the indicated times in the presence or absence of 0.4mM HU. After labeling, cells were washed with PBS and permeabilized with CSK100 buffer (100mM NaCl, 10mM MOPS pH 7, 3mM MgCl₂, 300mM sucrose, 0.5% Triton X-100) for 10 minutes at room temperature. Permeabilized cells were subjected to subsequent washes with PBS and S1 nuclease buffer (30mM sodium acetate, 10mM zinc acetate, 5% glycerol, 50mM NaCl, pH 4.6). Nuclei were then treated with either 20U/ml S1 nuclease (Invitrogen 18001016) or S1 buffer without nuclease for 30 minutes at 37°C. After treatment, nuclei were washed with PBS, collected in PBS with 0.1% BSA, and centrifuged at 7000 RPM for 5 minutes. The pelleted nuclei were resuspended in PBS, and 2 μ L of the solution was spotted on microscopy slides, followed by lysis with 8 μ L lysis buffer (200mM Tris–HCl pH 7.5, 50mM EDTA, 0.5% SDS) and spreading. Slides were allowed to dry, followed by fixation

with methanol and acetic acid (3:1) for 5 minutes, followed again by drying. Dried slides were rinsed in distilled water and denatured with 2.5M HCL for 90 minutes. Slides were then washed with PBS followed by staining and imaging in accordance with the DNA fiber combing protocol outlined above. At least 45 tracts were quantified for each condition.

Functional assays

For Clonogenic survival experiments, 1000-2000 cells (depending on plating efficiency) were seeded in 6-well plates. For UV sensitivity, cells were treated 24 h after seeding. For cisplatin and olaparib treatment, cells were seeded in indicated drug concentrations for 24 and 72 h respectively, followed by media change. Two weeks later, colonies were stained with Crystal violet. For time-course proliferation experiments, 500 cells were seeded in wells of 96-well plates, and cellular viability was scored at indicated days using the CellTiterGlo reagent (Promega G7572). EdU incorporation was assayed using the Click-iT Plus kit (Invitrogen C10633) according to the manufacturer's instructions.

Translesion synthesis SupF assay

The SupF assay was performed as previously described¹³⁴. Cells were transfected with UVC-irradiated (1000J/m²) pSP189 (SupF) plasmid. Three days later, the plasmid was recovered using a miniprep kit (Promega), DpnI digested and transformed into MBM7070 indicator bacteria. Transformants were selected on plates containing 1mM IPTG and 100µg/ml X-gal. The ratio of white (mutant) to total (blue + white) colonies was scored as mutation frequency.

Immunofluorescence

In the first study, cells were seeded on sterile glass coverslips coated with Poly-L Lysine (Sigma P8920) as per manufacturer's instructions and allowed to incubate for 24h. For RPA and 53BP1 foci detection, cells were fixed with 3.7% paraformaldehyde for 15min, followed by three washes with PBS. Cells were then permeabilized with 0.5% Triton X-100 for 10min. After two washes with PBS, slides were blocked with 3% BSA in PBS for 15min, followed by incubation with the primary antibody diluted in 3% BSA in PBS, for 2h at room temperature. After three washes with PBS, the secondary antibody was added for 1h. Slides were mounted with DAPI-containing Vectashield mounting medium (Vector Labs). For PCNA foci detection, cells were pre-extracted with 0.5% Triton X-100, followed by one PBS wash and methanol fixation for 30min at -20°C. After two washes with PBS, cells were blocked with 3% BSA in PBS for 15min. Primary and secondary antibody treatments as well as mounting were performed as mentioned above. Primary antibodies used for immunofluorescence were: 53BP1 (Bethyl A300-272A); RPA32 (Abcam ab2175); PCNA (Cell Signaling Technology 2586). Secondary antibodies used were AlexaFluor 488 or AlexaFluor 568 (Invitrogen A11001, A11008, A11031, and A11036). Slides were imaged using a DeltaVision Elite microscope. The number of foci/nucleus was quantified using ImageJ software. For the PCNA immunofluorescence, in order to remove non-S-phase cells, only cells with at least 2 foci, corresponding to the top three quartiles in wildtype, were included in the quantification.

In the second study, for RAD51 and γ H2AX staining, cells were seeded in either 4-well or 8-well chamber slides and allowed to incubate for 24hrs. Following this, cells were subjected to indicated drug treatments, followed by washing with PBS, extraction with 5% Triton-X for 10 min and then fixed with ice-cold methanol for 30min. The cells were incubated with primary antibodies for either 1hr at 37°C or overnight at 4°C. Secondary antibody treatment for carried out

at 37°C for 1hr. Antibodies were diluted in 3% BSA. Primary antibodies used were: RAD51 (Abcam ab133534); gH2AX (Millipore 05-636); RPA2 (Abcam ab2175). Secondary antibodies used were AlexaFluor 488 or AlexaFluor 568 (Invitrogen A11001, A11008, A11031, and A11036). Slides were imaged using a DeltaVision Elite microscope. The nuclear intensity or foci/nucleus was quantified using ImageJ software.

In situ analysis of protein interactions at replication forks (SIRF)

Cells were seeded in 8-well chamber slides at 50% confluency. The following day, cells were labeled with 50 μ M 5-Ethynyl-2'-deoxyuridine (EdU) and treated with HU and other drugs as indicated. Cells were then extracted with 0.5% Triton-X in PBS for 10 minutes at 4°C, followed by fixation with 4% formaldehyde in PBS for 15 minutes. Fixed samples were then blocked with 3% BSA in PBS at 37°C. After blocking, samples were subjected to a Click-iT reaction with Biotin Azide for 30 minutes, followed by incubation with primary antibodies in 1% BSA and 0.05% Triton-X in PBS at 4°C overnight. Primary Antibodies used were: Biotin (mouse: Jackson ImmunoResearch 200-002-211; rabbit: Bethyl Laboratories A150-109A); PARP1 (Cell Signaling Technology 9542); CHAF1A (Cell Signaling Technology 5480); HIRA (Abcam 129169); DAXX (Invitrogen PA5-79137); PAR (R&D systems 4335-MC-100); PCNA (Cell Signaling Technology 13110). Following primary antibody treatment, cells were subjected to the PLA reaction using the Duolink kit (Millipore Sigma) according to the manufacturer's instructions. Nuclear fluorescence signal was acquired using a DeltaVision Elite fluorescence microscope. For data analysis, cells positive for PLA fluorescence signal between biotin and the protein of interest were identified and the PLA foci were counted. To control for variabilities in EdU uptake, foci counts of each sample were normalized to the respective biotin-biotin control

using the geometric mean of the PLA fluorescence signal from positive cells and represented as PLA signal.

Cellular gene dependency analyses

Cellular dependency data was obtained from the DepMap Public 21Q3 dataset using the DepMap portal (depmap.org/portal). Gene knockout effects (CERES) from project Achilles CRISPR screens were obtained for BRCA1-wildtype cell lines and for cell lines bearing a deleterious mutation for BRCA1 in accordance to the Cancer Cell Line Encyclopedia Project (CCLE)¹⁸⁶⁻¹⁸⁸. CHAF1A and HIRA gene effects were then plotted as a regression for BRCA1-wildtype and BRCA-mutant samples. P-values for the likelihood of non-zero slopes were ascertained.

TCGA dataset analyses

Genomic, transcriptomic, and survival data for ovarian cancer samples (Cancer Genome Atlas Research Network, 2011), part of The Cancer Genome Atlas (TCGA), were obtained from cBioPortal¹⁸⁹. Survival datasets were sorted by BRCA2-status and all BRCA2-mutant samples were used for subsequent analyses. Samples were divided into two groups based on CHAF1A expression status in the patient tumor samples: high (0-50th percentile) and low (51st-100th percentile). Mantel-Cox log ranked t test was used for statistical analyses of the data sets using Prism software.

Quantification of gene expression by real-time quantitative PCR (RT-qPCR)

Total mRNA was purified using TRIzol reagent (Life Tech). To generate cDNA, 1µg RNA was subjected to reverse transcription using the RevertAid Reverse Transcriptase Kit (Thermo Fisher Scientific) with oligo-dT primers. Real-time qPCR was performed with PerfeCTa SYBR Green SuperMix (Quanta), using a CFX Connect Real-Time Cycler (BioRad). The cDNA of GAPDH gene was used for normalization. Primers used were: H3F3A for: TCTGGTGCGAGAAATTGCTC; H3F3A rev: TCTTAAGCACGTTCTCCACG; H3F3B for: CGAGAGATTCGTCGTTATCAG; H3F3B rev: TGACTCTCTTAGCGTGGATG; ATAD5 for: AGGAAGAGATCCAACCAACG; ATAD5 rev: ATGTTTCGAAGGGTTGGCAG; GAPDH for: AAATCAAGTGGGGCGATGCTG; GAPDH rev: GCAGAGATGATGACCCTTTTG; PRIMPOL for: TTCTACTGAAGTGCCGATACTGT; PRIMPOL rev: TGTGGCTTTGGAGGTTACTGA; RADX for: ATGATGTGACGATCTCAGATGGG; RADX rev: CCCCTGGCCTATCCTTTTCTC.

Micrococcal nuclease sensitivity assay

Cells were trypsinized, washed with PBS and lysed with cold NP-40 lysis buffer (10mM Tris-HCL, 10mM NaCl, 3mM MgCl₂, 0.5% NP-40, 0.15mM spermine and 0.5mM spermidine) for 5min. The resulting nuclei were washed once and resuspended in MNase digestion buffer (10mM Tris-HCl, 15mM NaCl, 60mM KCl, 1mM CaCl₂, 0.15mM spermine and 0.5mM spermidine). Resuspended cells were digested with 2.5U MNase in digestion buffer for the indicated times. The reaction was stopped by adding an equal volume of the MNase stop buffer (100mM EDTA, 10mM EGTA, 15mM NaCl, 60mM KCl and 2% SDS) followed by proteinase K digestion (final concentration of 0.0375µg/µl) at 37°C overnight. DNA was isolated using phenol-

chloroform extraction and subsequently subjected to RNase A digestion. Samples were run on 1.6% agarose gels and visualized using GelRed. Signal intensities were quantified using Icy software (Institut Pasteur).

Appendix A

Supplementary Information to Chapter 2

Figure A1

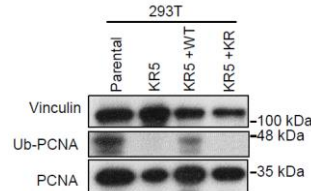


Figure A1: Generating isogenic 293T PCNA-WT and PCNA-K164R cells. Western blot showing PCNA and ubiquitinated PCNA levels in parental and the KR5 clone obtained through CRISPR/Cas9-mediated editing of the PCNA gene in 293T cells. The KR5 clone was complemented by re-expression of wildtype or K164R PCNA from a lentiviral construct, to restore normal PCNA levels.

Figure A2

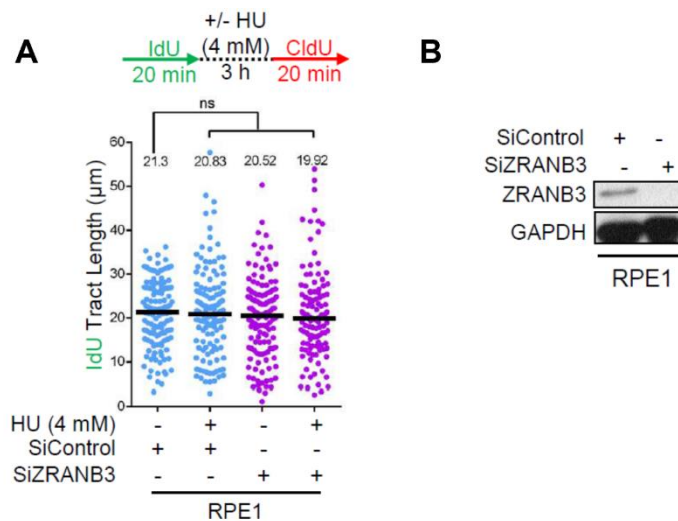


Figure A2: Fork degradation does not depend on ZRANB3 loss of function. (A) ZRANB3 depletion does not affect fork speed under normal growth conditions, or nascent strand degradation upon fork arrest. The quantification of the IdU tract length is shown, with the median values marked on the graph and listed at the top. Statistical significance (Mann-Whitney test, two-sided) and a schematic representation of the DNA fiber combing assay conditions are also presented. (B) Western blot showing ZRANB3 depletion upon siRNA-mediated knockdown.

Figure A3

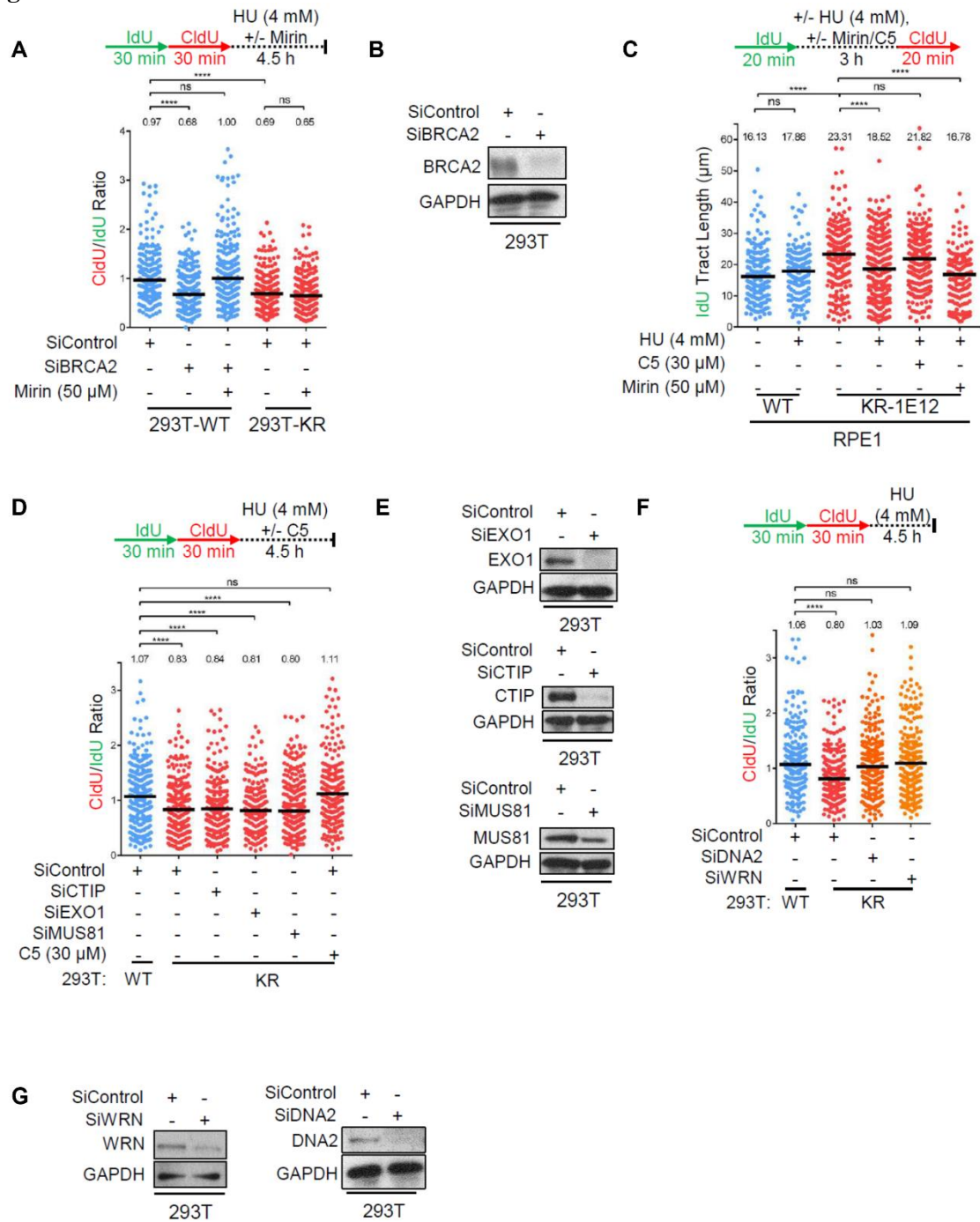


Figure A3: DNA2 degrades stalled replication forks in PCNA-K164R cells. (A) MRE11 inhibition by mirin suppresses HU-induced nascent strand degradation in BRCA2-knockdown cells, but not in 293T-K164R cells. The ratio of CldU to IdU tract lengths is presented, with the median values marked on the graph and listed at the top. Statistical significance (Mann-Whitney test, two-sided) and a schematic representation of the DNA fiber combing assay conditions are also presented. (B) Western blot showing BRCA2 depletion upon siRNA-mediated knockdown. (C) DNA2 inhibition by C5, but not MRE11 inhibition by mirin, suppresses HU-induced nascent strand degradation in RPE1-K164R cells. The quantification of the IdU tract length is shown, with the median values marked on the graph and listed at the top. Statistical significance (Mann-Whitney test, two-sided) and a schematic representation of the DNA fiber combing assay conditions are also presented. (D) Depletion of nucleases CTIP, EXO1, and MUS81 does not suppress HU-induced nascent strand degradation in 293T-K164R cells. The ratio of CldU to IdU tract lengths is presented, with the median values marked on the graph and listed at the top. Statistical significance (Mann-Whitney test, two-sided) and a schematic representation of the DNA fiber combing assay conditions are also presented. (E) Western blots showing CTIP, EXO1, and MUS81 depletion upon siRNA-mediated knockdown. (F) Knockdown of DNA2 or WRN suppresses the HU-induced nascent strand degradation in 293T-K164R cells. The ratio of CldU to IdU tract lengths is presented, with the median values marked on the graph and listed at the top. Statistical significance (Mann-Whitney test, two-sided) and a schematic representation of the DNA fiber combing assay conditions are also presented. (G) Western blots showing DNA2 and WRN depletion upon siRNA-mediated knockdown.

Figure A4

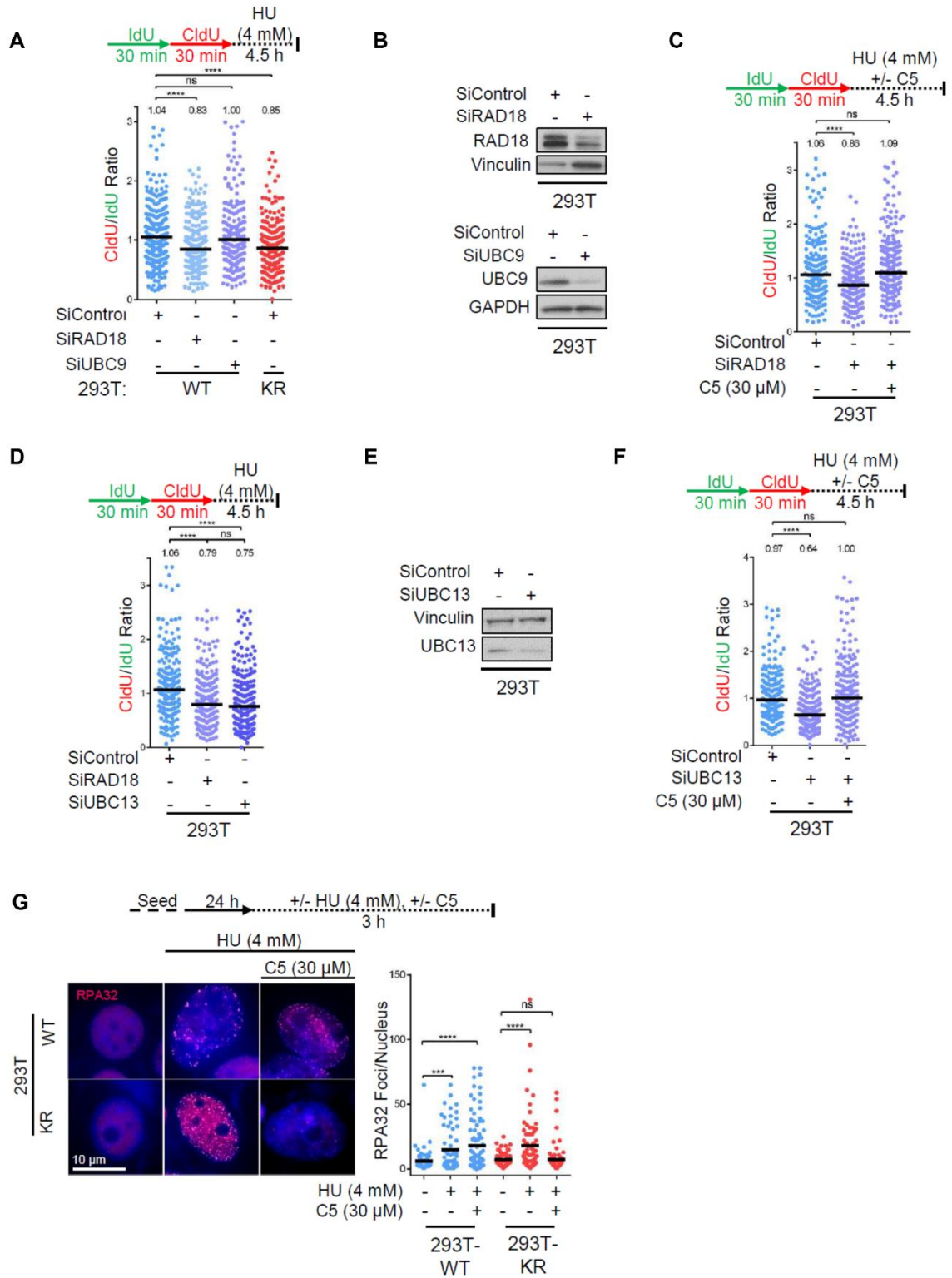


Figure A4: Impact of PCNA modification by ubiquitin or SUMO on fork stability. (A) Depletion of RAD18, but not of UBC9, results in HU-induced nascent strand degradation. The ratio of CldU to IdU tract lengths is presented, with the median values marked on the graph and listed at the top. Asterisks indicate statistical significance (Mann-Whitney test, two-sided). A schematic representation of the DNA fiber combing assay conditions is also presented. (B) Western blots showing RAD18 and UBC9 depletion upon siRNA-mediated knockdown. (C) Depletion of RAD18 results in HU-induced nascent strand degradation mediated by DNA2. The ratio of CldU to IdU tract lengths is presented, with the median values marked on the graph and listed at the top. Asterisks indicate statistical significance (Mann-Whitney test, two-sided). A schematic representation of the DNA fiber combing assay conditions is also presented. (D) Depletion of UBC13 results in HU-induced nascent strand degradation, similar to depletion of RAD18. The ratio of CldU to IdU tract lengths is presented, with the median values marked on the graph and listed at the top. Asterisks indicate statistical significance (Mann-Whitney test, two-sided). A schematic representation of the DNA fiber combing assay conditions is also presented. (E) Western blot showing UBC13 depletion upon siRNA-mediated knockdown. (F) Depletion of UBC13 results in HU-induced nascent strand degradation mediated by DNA2. The ratio of CldU to IdU tract lengths is presented, with the median values marked on the graph and listed at the top. Asterisks indicate statistical significance (Mann-Whitney test, two-sided). A schematic representation of the DNA fiber combing assay conditions is also presented. (G) Immunofluorescence experiment showing that HU-induced RPA32 foci formation is suppressed by DNA2 inhibition in 293T-K164R cells, but not in wildtype cells. At least 75 cells were quantified for each condition. The mean values are marked on the graph, and asterisks indicate statistical significance (t-test, two-tailed, unequal variance). Representative micrographs are also shown.

Figure A5

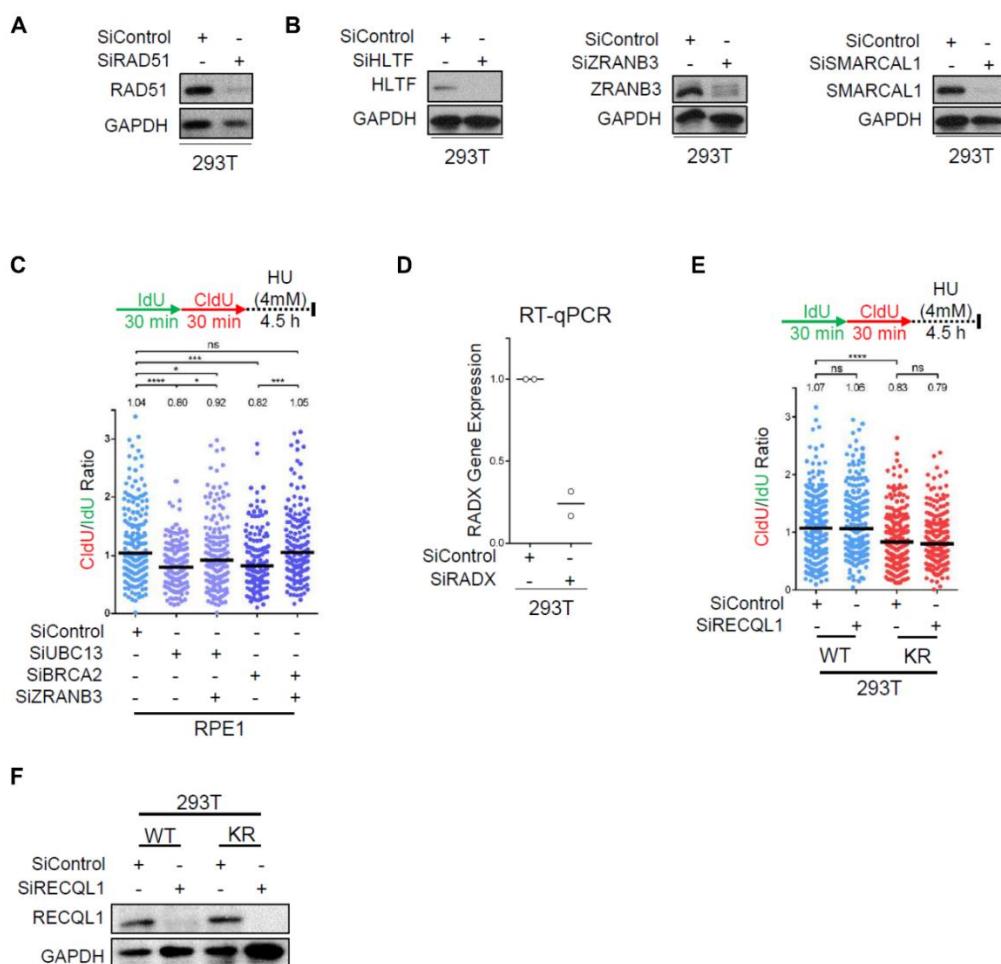


Figure A5: Impact of fork reversal on nascent strand degradation in PCNA-K164R cells.

(A) Western blot confirming RAD51 depletion upon siRNA-mediated knockdown. (B) Western blots showing depletion of HLTF, ZRANB3 and SMARCAL1 upon siRNA-mediated knockdown. (C) Knockdown of ZRANB3 fully suppresses HU-induced nascent tract degradation in BRCA2-depleted RPE1 cells, but only partially suppresses HU-induced nascent tract degradation in UBC13-depleted cells. The ratio of CldU to IdU tract lengths is presented, with the median values marked on the graph and listed at the top. Asterisks indicate statistical significance (Mann-Whitney test, two-sided). A schematic representation of the assay conditions is also presented. (D) RT-qPCR experiment showing reduction in RADX mRNA levels upon siRNA-mediated knockdown. Two technical replicates are shown, with the lines representing the means. (No antibody was available to us for verifying the depletion by Western blot.) (E) RECQL1 is not involved in the nascent tract degradation observed in K164R cells upon HU exposure, as its knockdown does not induce fork degradation in wildtype cells, and does not affect the degradation observed in KR cells. The ratio of CldU to IdU tract lengths is presented, with the median values marked on the graph and listed at the top. Asterisks indicate statistical significance (Mann-Whitney test, two-sided). A schematic representation of the assay conditions is also presented. (F) Western blot confirming RECQL1 depletion upon siRNA-mediated knockdown.

Figure A6

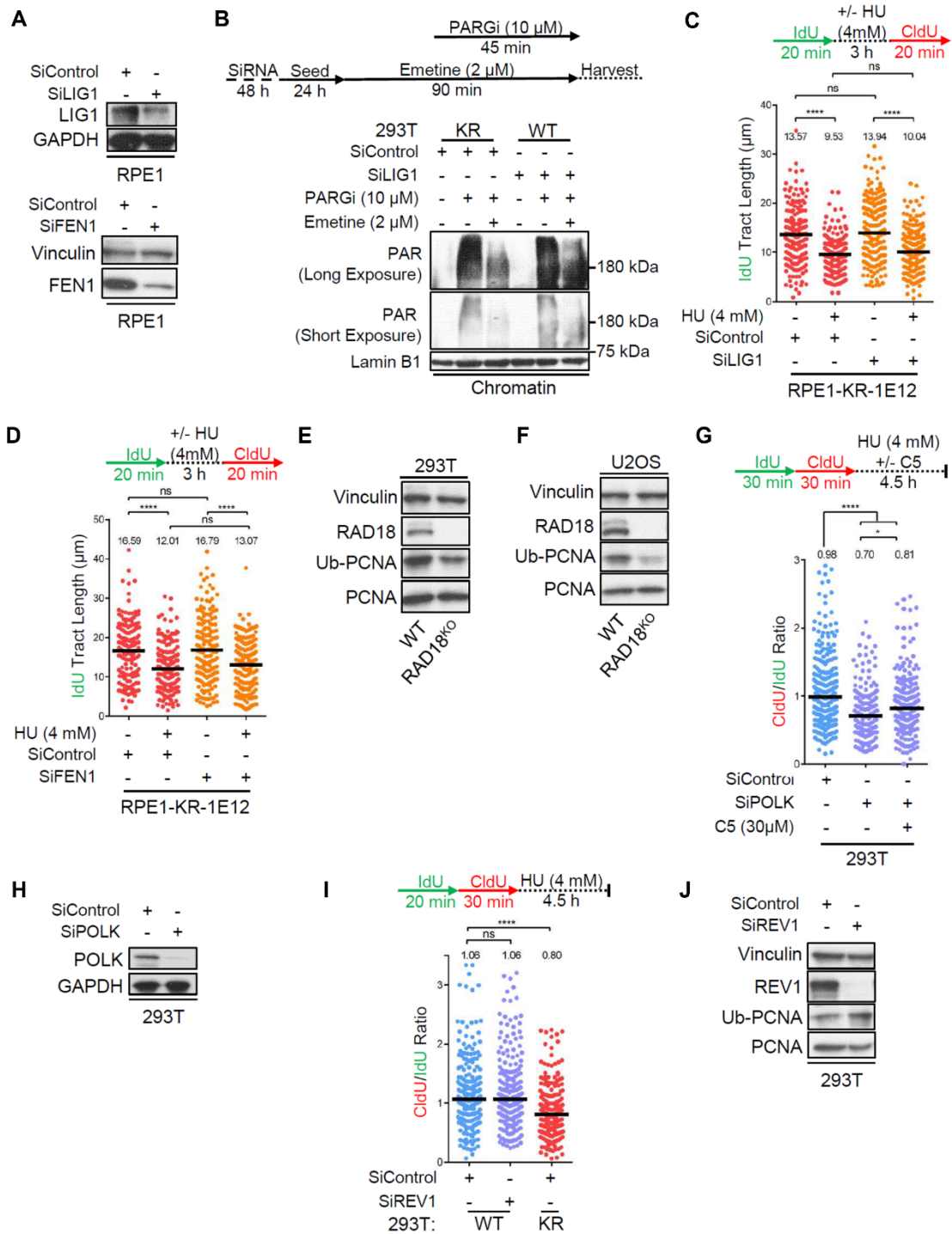


Figure A6: Impact of Okazaki fragment maturation factors and TLS polymerases on replication fork protection. (A) Western blots confirming LIG1 and FEN1 depletion upon siRNA-mediated knockdown. (B) Chromatin fractionation experiment showing that PAR chain formation in PCNA-K164R and LIG1-depleted 293T cells is suppressed upon incubation with 2 μ M emetine for 90 min. Cells were treated as indicated with a PARG inhibitor (PARGi) for 45min prior to harvesting to block PAR chain removal. Chromatin-associated LaminB1 was used as loading control. (C), (D) DNA fiber combing assay showing that LIG1 (C) or FEN1 (D) depletion in RPE1 cells does not further increase fork progression rate and HU-induced degradation in K164R cells. The quantification of the IdU tract length is presented, with the median values marked on the graph and listed at the top. Asterisks indicate statistical significance (Mann-Whitney test, two-sided). A schematic representation of the assay conditions is also presented. (E), (F) Western blots showing the loss of RAD18 expression in 293T (E) and U2OS (F) RAD18-knockout cells, as well as the level of PCNA ubiquitination in these cells. (G) POLK depletion results in HU-induced nascent strand degradation which is partially dependent on DNA2 enzymatic activity. The ratio of CldU to IdU tract lengths is presented, with the median values marked on the graph and listed at the top. Asterisks indicate statistical significance (Mann-Whitney test, two-sided). A schematic representation of the fiber combing assay conditions is also presented. (H) Western blot confirming POLK depletion upon siRNA-mediated knockdown. (I) DNA fiber combing assay showing that REV1 depletion does not cause degradation of arrested replication forks. The ratio of CldU to IdU tract lengths is presented, with the median values marked on the graph and listed at the top. Asterisks indicate statistical significance (Mann-Whitney test, two-sided). A schematic representation of the assay conditions is also presented. (J) Western blot confirming REV1 depletion upon siRNA-mediated knockdown.

Figure A7

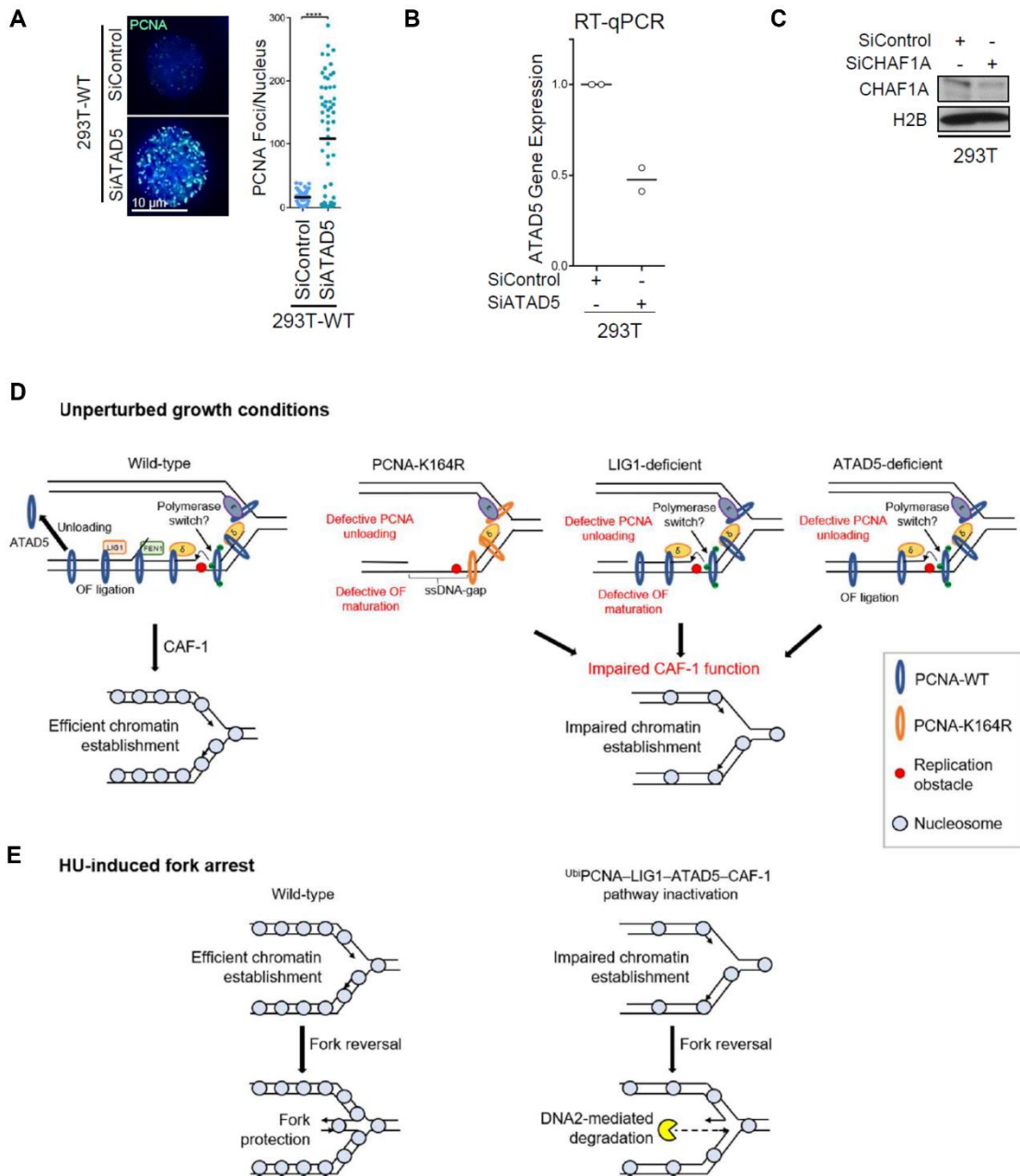


Figure A7: PCNA chromatin retention in ATAD5-depleted cells and consequences on fork stability. (A) Immunofluorescence experiment showing increased PCNA chromatin retention upon ATAD5 depletion. At least 65 cells were quantified for each condition. The mean values are marked on the graph, and asterisks indicate statistical significance (t-test, two-tailed, unequal variance). Representative micrographs are shown. (B) RT-qPCR experiment showing reduction in ATAD5 mRNA levels upon siRNA-mediated knockdown. Two technical replicates are shown, with the lines representing the means. (C) Western blot confirming CHAF1A depletion upon siRNA mediated knockdown. (D), (E) Proposed model depicting the ub_i PCNA–LIG1–ATAD5–CAF-1 genetic pathway. Under unperturbed growth conditions (D), PCNA ubiquitination is required for efficient lagging strand synthesis by mediating gap-filling behind progressing replication forks. Forks arrested at endogenous lesions, whether on the lagging or leading strand, require PCNA ubiquitination-mediated TLS for restart. On the leading strand (not shown), repriming downstream of the lesion (perhaps by PrimPol) mediates replication restart in the absence of PCNA ubiquitination. In contrast, on the lagging strand, continuous initiation of new Okazaki fragments by Pola allows unhindered movement of the replication fork, alleviating the need for downstream repriming. In the absence of PCNA ubiquitination, persistent gaps are formed between the lesion and the previous OF. These gaps interfere with OF maturation and subsequent PCNA unloading. By sequestering the CAF-1 chromatin assembly complex, PCNA retention on the lagging strand alters the efficiency of chromatin establishment which results in replication forks encountering a sparse chromatin organization. As nucleosomal spacing regulates OF priming, inactivation of the ub_i PCNA–LIG1–ATAD5–CAF-1 pathway results in longer OFs which initiate further ahead of lagging strand synthesis. HU treatment (E) induces fork arrest and reversal. In PCNA-K164R, cells fork reversal is reduced but forks that do reverse, through the activity of SMARCAL1 and potentially ZRANB3, have an asymmetric structure with a 5'-overhang in the regressed arm because of the increased length of the OF fragment previously generated. This abnormal reversed fork structure is a preferred substrate for DNA2, leading to uncontrolled resection.

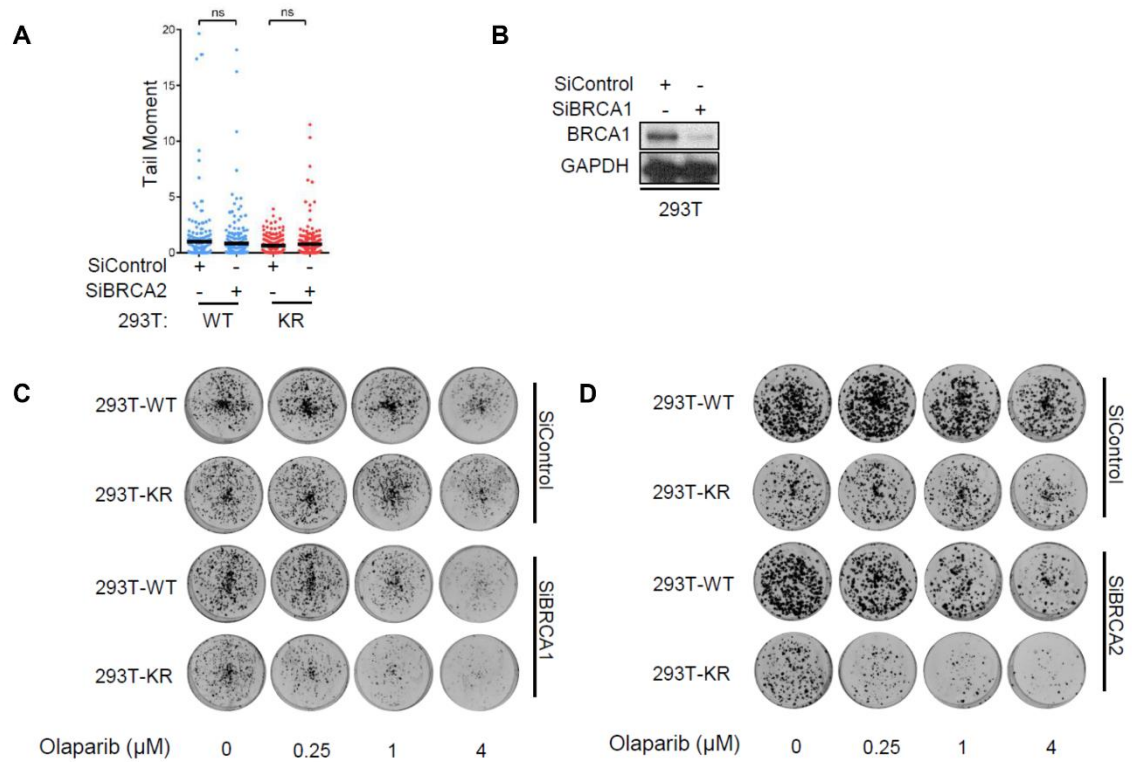
Figure A8

Figure A8: Genetic interaction between PCNA ubiquitination and the BRCA pathways. (A) Neutral comet assay showing no increase in DSBs upon BRCA2 knockdown in 293T-K164R cells under normal growth conditions. At least 100 cells were quantified for each condition. The mean values are marked on the graph, and asterisks indicate statistical significance (t-test, two-tailed, unequal variance). (B) Western blot showing BRCA1 depletion upon siRNA-mediated knockdown. (C), (D) Representative images of the clonogenic assays showing increased olaparib sensitivity of BRCA1-depleted (C) or BRCA2-depleted (D) 293TK164R cells.

Appendix B

Supplementary Information to Chapter 3

Figure B1

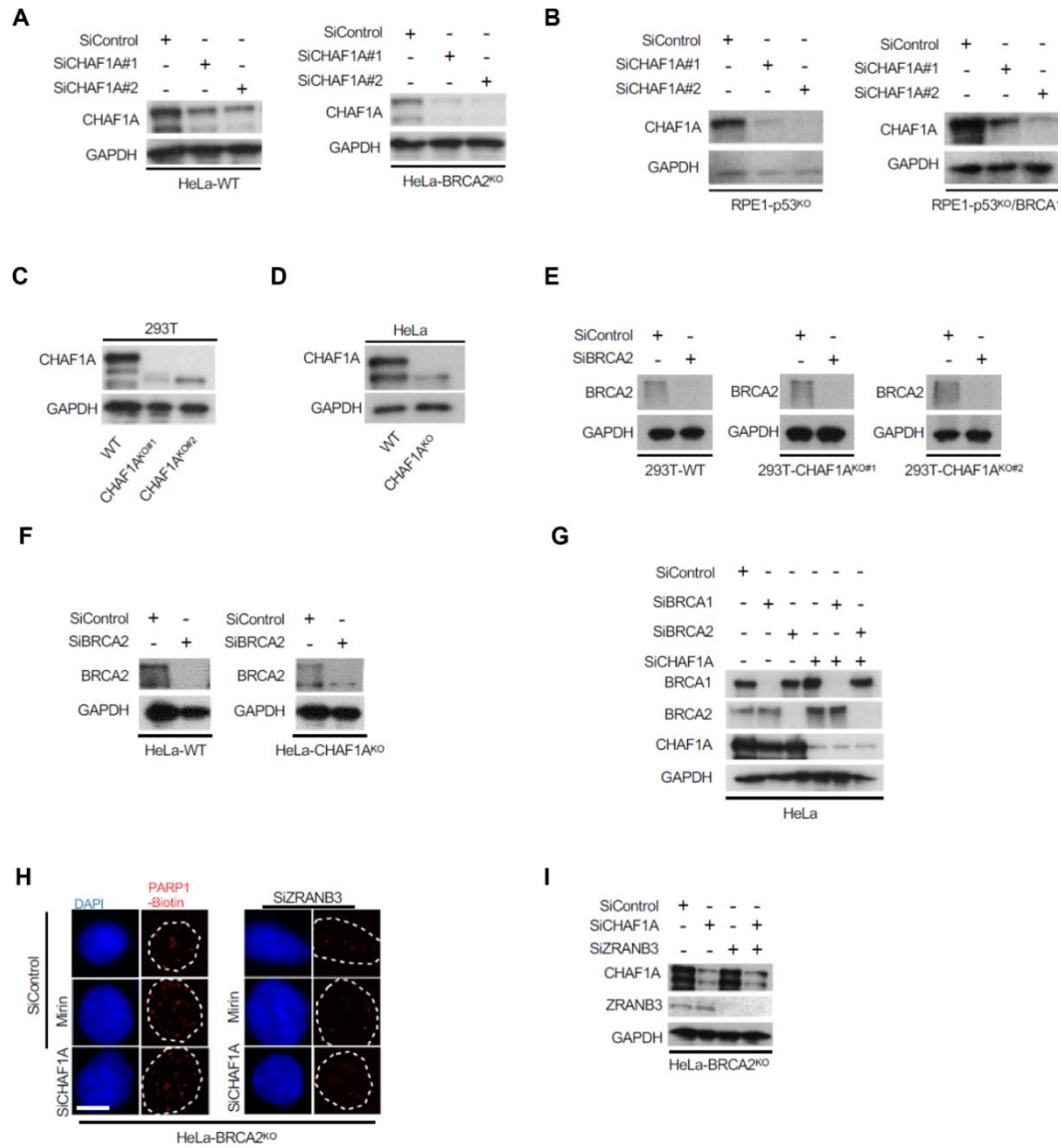


Figure B1: Confirmation of gene knockdowns. (A), (B) Western blots showing CHAF1A depletion in BRCA2-knockout HeLa cells (A) and in BRCA1-knockout RPE1 cells (B). (C), (D) Western blots showing CHAF1A knockdown in 293T (C) and HeLa (D) cells. (E), (F) Western blots showing BRCA2 depletion in CHAF1A-knockout 293T (E) and HeLa (F) cells. (G) Western blots showing CHAF1A co-depletion with BRCA1 or BRCA2 in HeLa cells. (H) Representative micrographs of the PARP1 SIRF experiment (scale bar represents 10µm). (I) Western blots showing CHAF1A co-depletion with ZRANB3 in HeLa-BRCA2^{KO} cells.

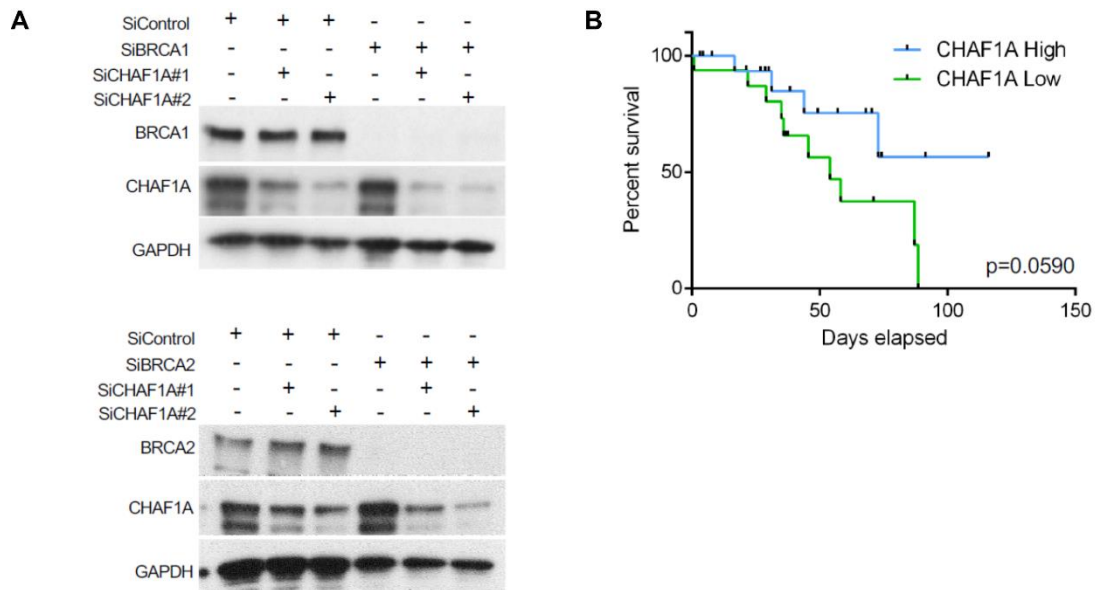
Figure B2

Figure B2: Impact of CAF-1 loss in BRCA-deficient cells. (A) Western blots showing CHAF1A co-depletion with BRCA1 or BRCA2 in HeLa cells. (B) Analyses of BRCA2-mutant ovarian TCGA cancer dataset showing that high CHAF1A levels are associated with increased survival, while low CHAF1A levels are associated with reduced survival. Mantel-Cox log ranked t test was used for statistical analyses (n=14, p=0.0590). The difference observed is not significant, likely because of the small number of BRCA2-mutant samples in the dataset.

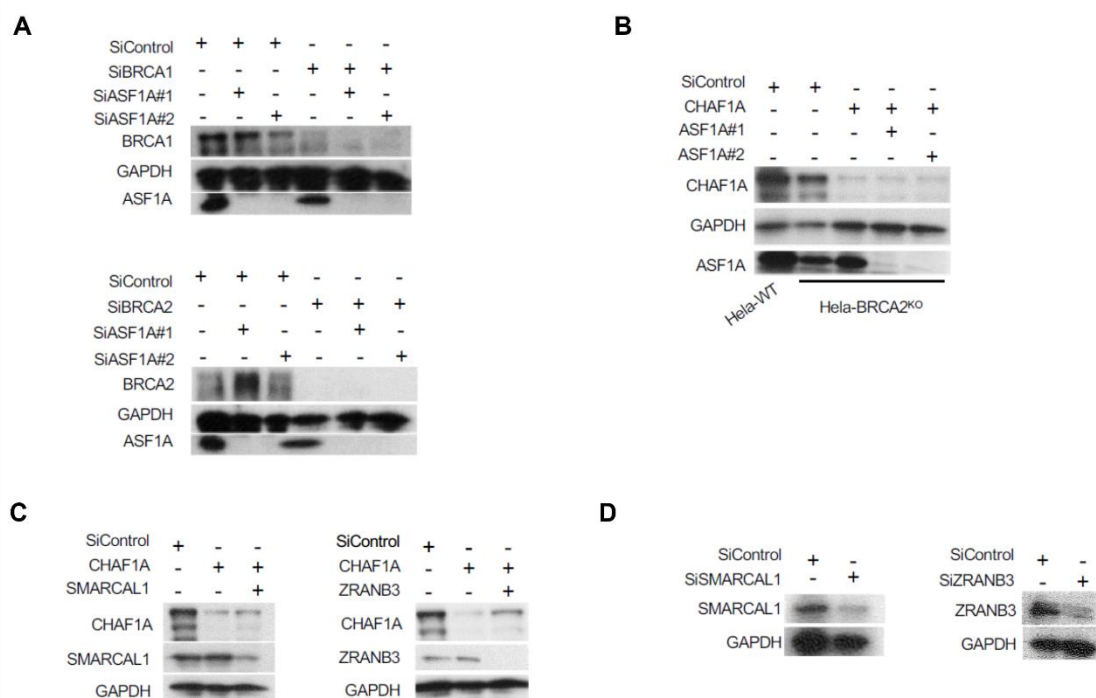
Figure B3

Figure B3: Confirmation of gene knockdowns. (A) Western blots showing ASF1A co-depletion with BRCA1 or BRCA2 in HeLa cells. (B) Western blots showing ASF1A co-depletion with CHAF1A in HeLa-BRCA2KO cells. (C) Western blots showing CHAF1A co-depletion with SMARCAL1 or ZRANB3 in HeLa cells. (D) Western blots showing ZRANB3 and SMARCAL1 depletions in 293T-CHAF1A.

Figure B4

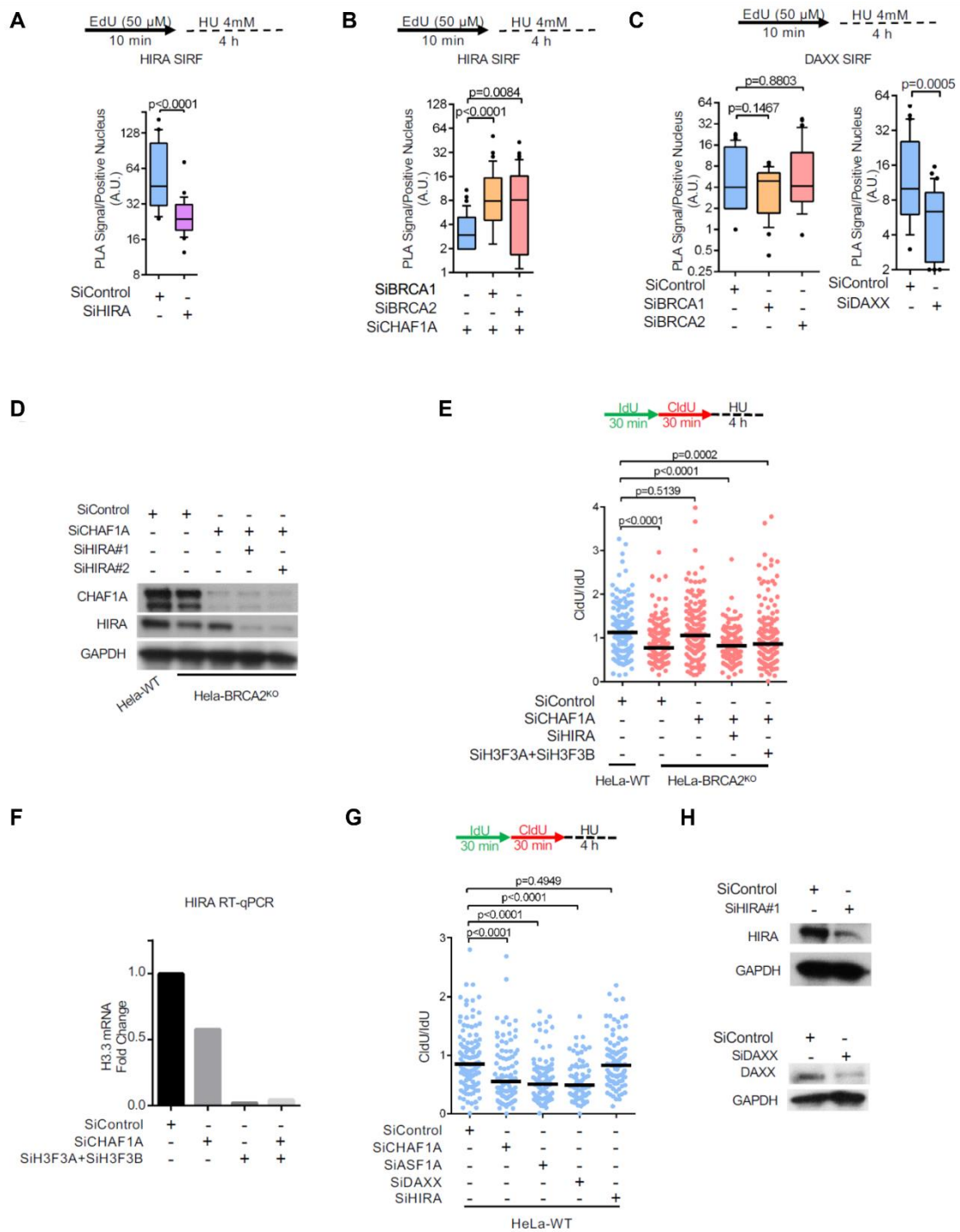


Figure B4: Impact of nucleosome deposition by HIRA on BRCA-deficient cells. (A) SIRF assay confirm that the HIRA PLA signal is specific since it is reduced upon HIRA depletion by siRNA. At least 20 positive cells were quantified for each condition. The p-values (Mann-Whitney test) are listed at the top. A schematic representation of the SIRF assay conditions is also presented. (B) SIRF assay showing the impact of CHAF1A co-depletion on HIRA binding to nascent DNA in BRCA1 or BRCA2-knockdown HeLa cells. At least 65 cells were quantified for each condition. The p-values (Mann-Whitney test) are listed at the top. A schematic representation of the SIRF assay conditions is also presented. (C) SIRF assay showing that DAXX binding to nascent DNA is unchanged upon BRCA1 or BRCA2 depletion in HeLa cells. DAXX depletion by siRNA reduces the PLA signal, confirming its specificity. A schematic representation of SIRF assay conditions is also presented. At least 30 positive cells were quantified for each condition. The p-values (Mann-Whitney test) are listed at the top. A schematic representation of the SIRF assay conditions is also presented. (D) Western blots showing HIRA co-depletion with CHAF1A in HeLa-BRCA2^{KO} cells. (E) DNA fiber combing assays showing that co-depletion of HIRA or of H3.3-encoding genes H3F3A and H3F3B restores HU induced nascent strand degradation in CHAF1A-depleted HeLa-BRCA2^{KO} cells. The ratio of CldU to IdU tract lengths is presented, with the median values marked on the graph. The p-values (Mann-Whitney test) are listed at the top. A schematic representation of the DNA fiber combing assay conditions is also presented. (F) RT-qPCR experiment showing reduction in H3F3A and H3F3B mRNA levels upon siRNA-mediated knockdown. The average of two technical replicates is shown. (No antibody was available to us for verifying the depletion by Western blot.) (G), (H) DNA fiber combing assays showing the impact of the depletion of histone chaperones HIRA and DAXX on HU-induced nascent strand degradation in HeLa cells. The ratio of CldU to IdU tract lengths is presented, with the median values marked on the graph (G). The p-values (Mann-Whitney test) are listed at the top. A schematic representation of the DNA fiber combing assay conditions is also presented. Western blots confirming the knockdowns (H) are also presented.

Figure B5

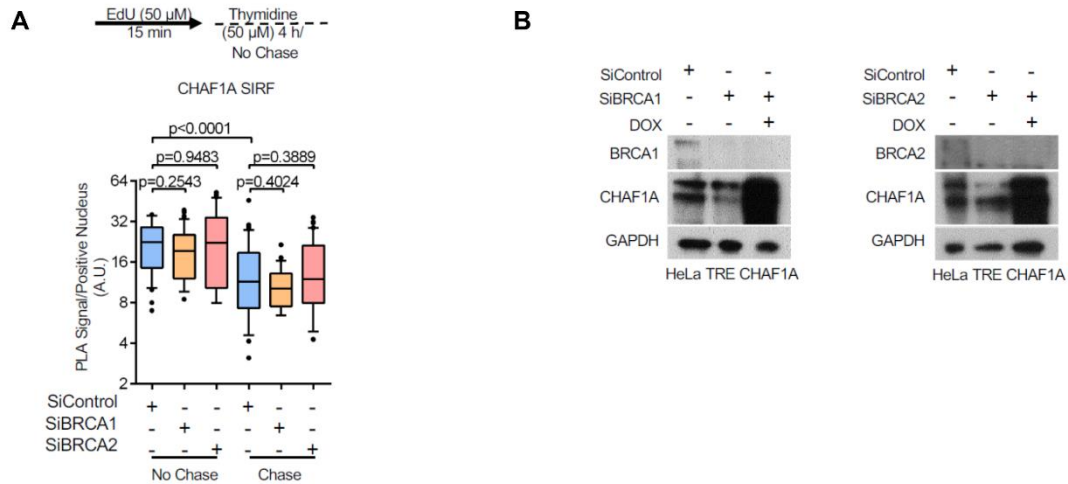


Figure B5: CHAF1A recycling in BRCA-deficient cells. (A) SIRF assay showing that, in the absence of replication stress, CHAF1A recycling is not impaired in BRCA1 or BRCA2-depleted HeLa cells. Cells were labeled with EdU, washed, and chased for 4h in fresh media containing 50 μ M thymidine. At least 25 positive cells were quantified for each condition. The p-values (Mann-Whitney test) are listed at the top. A schematic representation of the SIRF assay conditions is also presented. (B) Western blots showing doxycycline-induced CHAF1A overexpression, and BRCA1 or BRCA2 knockdown in these cells.

Figure B6

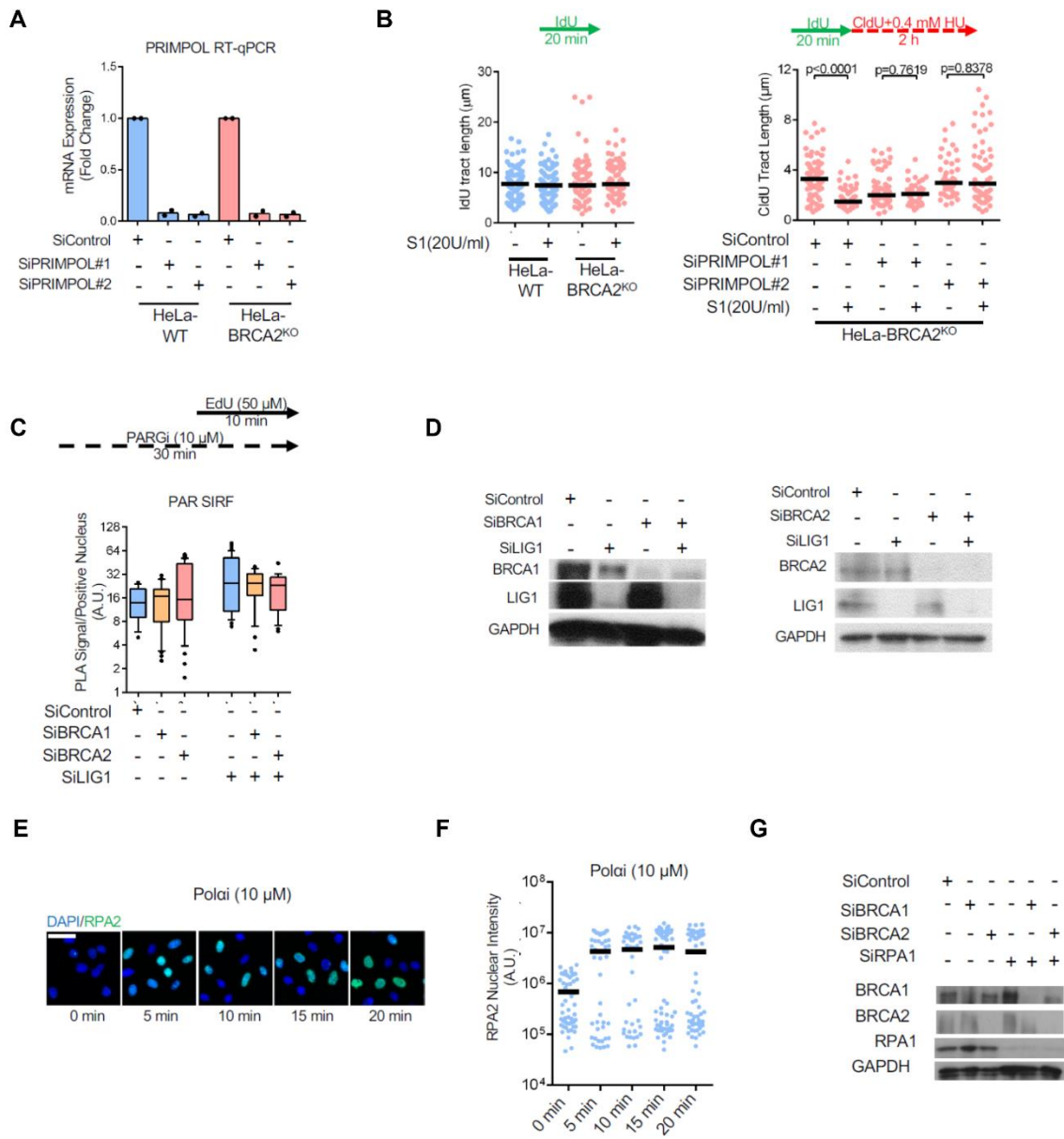


Figure B6: PRIMPOL independent lagging strand synthesis defects in BRCA-deficient cells. (A) RT-qPCR experiment showing reduction in PRIMPOL mRNA levels upon siRNA-mediated knockdown. The average of two biological replicates is shown. (No antibody was available to us for verifying the depletion by Western blot.) (B) S1 nuclease fiber spreading assays showing that fork shortening upon HU-induced replication stress is completely rescued by PRIMPOL depletion in HeLa-BRCA2^{KO} cells. The p-values (Mann-Whitney test) are listed at the top. A schematic representation of the DNA fiber spreading assay conditions is also presented. (C) SIRF assay showing that, under normal growth conditions (in the absence of replication stress), LIG1 knockdown induces PAR chain formation similarly in wildtype and BRCA1 or BRCA2-depleted HeLa cells. At least 25 positive cells were quantified for each condition. A schematic representation of the SIRF assay conditions is also presented. (D) Western blots showing LIG1 co-depletion with BRCA1 or BRCA2 in HeLa cells. (E), (F) immunofluorescence experiment showing the impact of Pol α inhibition by treatment with 10 μ M ST1926 on RPA2 chromatin foci in HeLa cells. Representative micrographs (scale bar represents 50 μ m) (E) and quantifications (F) are shown. At least 40 cells were quantified for each condition. The mean values are represented on the graph. (G) Western blots showing RPA1 co-depletion with BRCA1 or BRCA2 in HeLa cells.

Figure B7

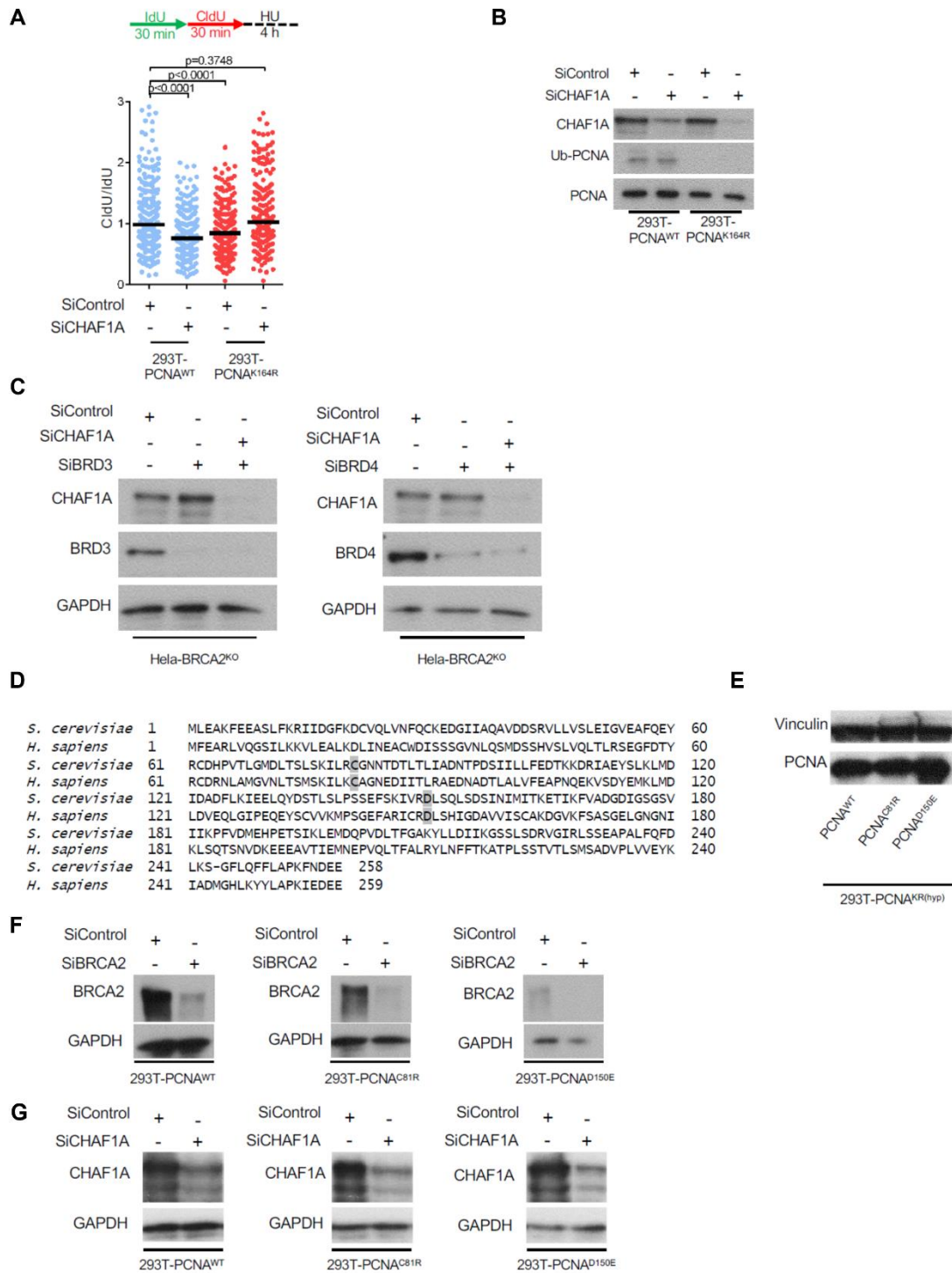


Figure B7: Correcting PCNA unloading defects. (A) DNA fiber combing assays showing that CHAF1A depletion results in HU-induced fork degradation in wildtype cells, but suppresses fork degradation in 293T-PCNA_{K164R} cells. The ratio of CldU to IdU tract lengths is presented, with the median values marked on the graph. The p-values (Mann-Whitney test) are listed at the top. A schematic representation of the DNA fiber combing assay conditions is also presented. (B) Western blots showing CHAF1A depletion in 293T cells. (C) Western blots showing CHAF1A co-depletion with BRCA3 or BRD4 in HeLa-BRCA2^{KO} cells. (D) Alignment of yeast and human PCNA, indicating the PCNA mutations performed. (E) Western blots showing the expression of PCNA variants in PCNA-hypomorph 293T cells. (F) Western blots showing BRCA2 depletion in 293T cells expressing PCNA variants. (G) Western blots showing CHAF1A depletion in 293T cells expressing PCNA variants.

Figure B8

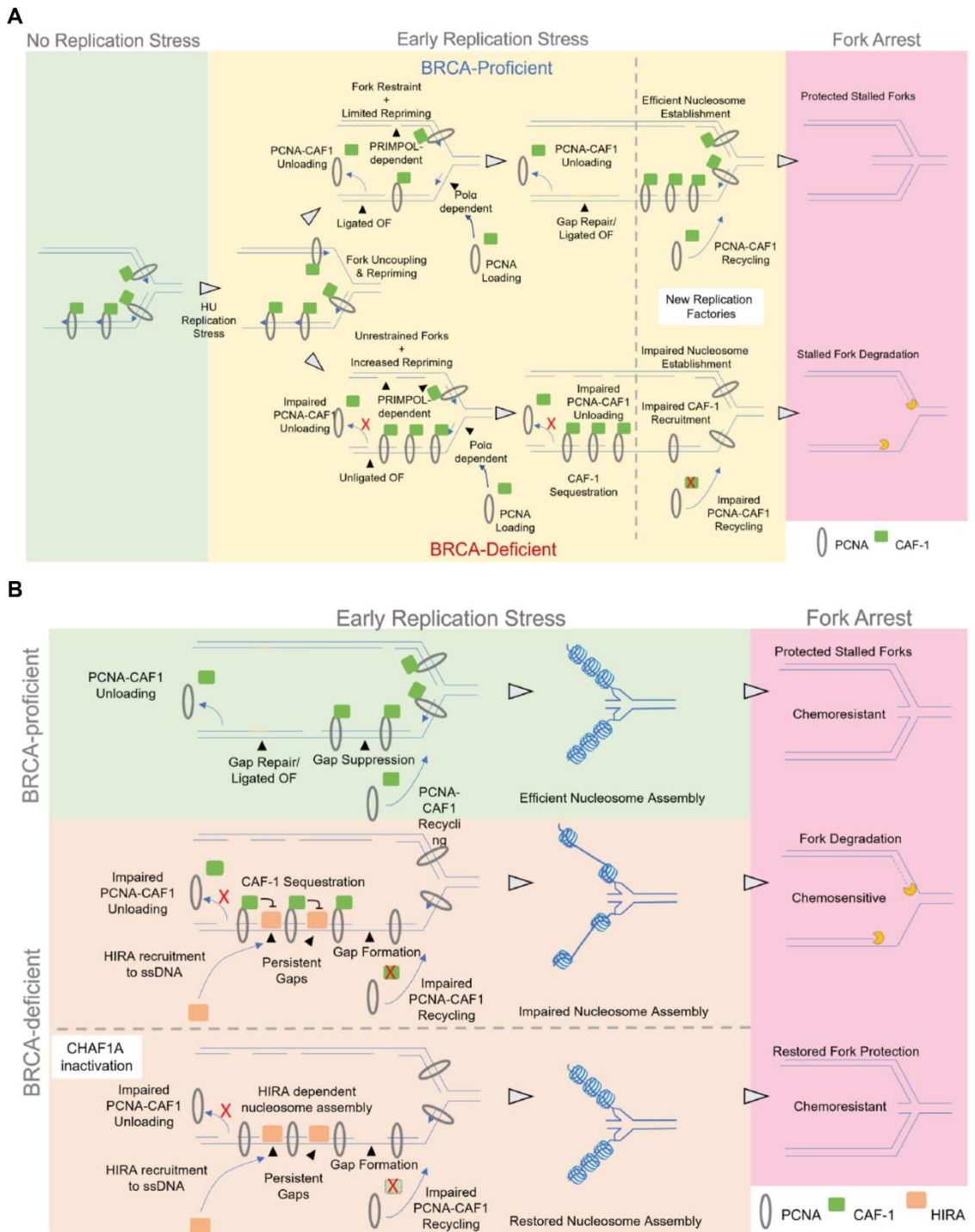


Figure B8: Schematic representations of the proposed models. (A) Model for CAF-1 recycling defects as the underlying factor responsible for fork degradation in BRCA deficient cells. In BRCA-proficient cells, stressed replication forks are slowed, minimizing replication-associated gap formation. BRCA-deficient cells show impaired fork restraint during replication stress, instead undergoing repriming. On the leading strand, forks are reprimed by PRIMPOL leaving behind leading strand gaps. On the lagging strand, forks reprime through Pola-mediated initiation of the subsequent OF, leaving behind lagging strand gaps. Both leading and lagging strand gaps can also be efficiently repaired by BRCA-mediated PRR. On the lagging strand, the BRCA pathway mediates gap suppression and ensures timely OF ligation, allowing unloading of PCNA-CAF-1 complexes and subsequent CAF-1 recycling to ongoing forks. This ensures proper nucleosome assembly, protecting forks from nucleolytic degradation if they arrest and reverse at a later time. In BRCA-deficient cells, gaps on the lagging strand accumulate and retain PCNA-CAF-1 complexes since OF ligation cannot take place. This reduces the availability of CAF-1 at ongoing replication forks, resulting in nucleosome deposition defects. In turn, this predisposes forks to nucleolytic degradation upon their reversal. **(B)** Model for restoration of fork stability and chemoresistance upon CAF-1 loss in BRCA-deficient cells. In wildtype cells, efficient gap repair and subsequent OF ligation allows effective CAF-1 recycling and proper nucleosome assembly. In BRCA-deficient cells, ssDNA gaps accumulate and are coated by RPA, which promotes recruitment of HIRA. However, the presence of CAF-1, sequestered in PCNA complexes at lagging strand gaps, inhibits HIRA activity, possibly by competing for ASF1. Loss of CAF-1 releases HIRA activity, resulting in efficient nucleosome assembly and subsequent fork protection.

References

- (1) Hashimoto, Y.; Ray Chaudhuri, A.; Lopes, M.; Costanzo, V. Rad51 Protects Nascent DNA from Mre11-Dependent Degradation and Promotes Continuous DNA Synthesis. *Nat Struct Mol Biol* **2010**, *17* (11), 1305–1311. <https://doi.org/10.1038/nsmb.1927>.
- (2) Schlacher, K.; Christ, N.; Siaud, N.; Egashira, A.; Wu, H.; Jasin, M. Double-Strand Break Repair-Independent Role for BRCA2 in Blocking Stalled Replication Fork Degradation by MRE11. *Cell* **2011**, *145* (4), 529–542. <https://doi.org/10.1016/j.cell.2011.03.041>.
- (3) Schlacher, K.; Wu, H.; Jasin, M. A Distinct Replication Fork Protection Pathway Connects Fanconi Anemia Tumor Suppressors to RAD51-BRCA1/2. *Cancer Cell* **2012**, *22* (1), 106–116. <https://doi.org/10.1016/j.ccr.2012.05.015>.
- (4) Bhat, K. P.; Krishnamoorthy, A.; Dungrawala, H.; Garcin, E. B.; Modesti, M.; Cortez, D. RADX Modulates RAD51 Activity to Control Replication Fork Protection. *Cell Rep* **2018**, *24* (3), 538–545. <https://doi.org/10.1016/j.celrep.2018.06.061>.
- (5) Taglialatela, A.; Alvarez, S.; Leuzzi, G.; Sannino, V.; Ranjha, L.; Huang, J.-W.; Madubata, C.; Anand, R.; Levy, B.; Rabadan, R.; Cejka, P.; Costanzo, V.; Ciccia, A. Restoration of Replication Fork Stability in BRCA1- and BRCA2-Deficient Cells by Inactivation of SNF2-Family Fork Remodelers. *Mol Cell* **2017**, *68* (2), 414-430.e8. <https://doi.org/10.1016/j.molcel.2017.09.036>.
- (6) Thangavel, S.; Berti, M.; Levikova, M.; Pinto, C.; Gomathinayagam, S.; Vujanovic, M.; Zellweger, R.; Moore, H.; Lee, E. H.; Hendrickson, E. A.; Cejka, P.; Stewart, S.; Lopes, M.; Vindigni, A. DNA2 Drives Processing and Restart of Reversed Replication Forks in Human Cells. *J Cell Biol* **2015**, *208* (5), 545–562. <https://doi.org/10.1083/jcb.201406100>.
- (7) Zellweger, R.; Dalcher, D.; Mutreja, K.; Berti, M.; Schmid, J. A.; Herrador, R.; Vindigni, A.; Lopes, M. Rad51-Mediated Replication Fork Reversal Is a Global Response to

Genotoxic Treatments in Human Cells. *J Cell Biol* **2015**, *208* (5), 563–579.

<https://doi.org/10.1083/jcb.201406099>.

(8) Kolinjivadi, A. M.; Sannino, V.; De Antoni, A.; Zadorozhny, K.; Kilkenny, M.; Técher, H.; Baldi, G.; Shen, R.; Ciccia, A.; Pellegrini, L.; Krejci, L.; Costanzo, V. Smarcal1-Mediated Fork Reversal Triggers Mre11-Dependent Degradation of Nascent DNA in the Absence of Brca2 and Stable Rad51 Nucleofilaments. *Mol Cell* **2017**, *67* (5), 867-881.e7.

<https://doi.org/10.1016/j.molcel.2017.07.001>.

(9) Mijic, S.; Zellweger, R.; Chappidi, N.; Berti, M.; Jacobs, K.; Mutreja, K.; Ursich, S.; Ray Chaudhuri, A.; Nussenzweig, A.; Janscak, P.; Lopes, M. Replication Fork Reversal Triggers Fork Degradation in BRCA2-Defective Cells. *Nat Commun* **2017**, *8* (1), 859.

<https://doi.org/10.1038/s41467-017-01164-5>.

(10) Lemaçon, D.; Jackson, J.; Quinet, A.; Brickner, J. R.; Li, S.; Yazinski, S.; You, Z.; Ira, G.; Zou, L.; Mosammaparast, N.; Vindigni, A. MRE11 and EXO1 Nucleases Degrade Reversed Forks and Elicit MUS81-Dependent Fork Rescue in BRCA2-Deficient Cells. *Nat Commun* **2017**, *8* (1), 860. <https://doi.org/10.1038/s41467-017-01180-5>.

(11) Bhowmick, R.; Minocherhomji, S.; Hickson, I. D. RAD52 Facilitates Mitotic DNA Synthesis Following Replication Stress. *Mol Cell* **2016**, *64* (6), 1117–1126.

<https://doi.org/10.1016/j.molcel.2016.10.037>.

(12) Sotiriou, S. K.; Kamileri, I.; Lugli, N.; Evangelou, K.; Da-Ré, C.; Huber, F.; Padayachy, L.; Tardy, S.; Nicati, N. L.; Barriot, S.; Ochs, F.; Lukas, C.; Lukas, J.; Gorgoulis, V. G.; Scapozza, L.; Halazonetis, T. D. Mammalian RAD52 Functions in Break-Induced Replication Repair of Collapsed DNA Replication Forks. *Mol Cell* **2016**, *64* (6), 1127–1134.

<https://doi.org/10.1016/j.molcel.2016.10.038>.

(13) Higgs, M. R.; Reynolds, J. J.; Winczura, A.; Blackford, A. N.; Borel, V.; Miller, E. S.; Zlatanou, A.; Nieminuszczy, J.; Ryan, E. L.; Davies, N. J.; Stankovic, T.; Boulton, S. J.;

Niedzwiedz, W.; Stewart, G. S. BOD1L Is Required to Suppress Deleterious Resection of Stressed Replication Forks. *Mol Cell* **2015**, *59* (3), 462–477.

<https://doi.org/10.1016/j.molcel.2015.06.007>.

(14) Karanja, K. K.; Lee, E. H.; Hendrickson, E. A.; Campbell, J. L. Preventing Over-Resection by DNA2 Helicase/Nuclease Suppresses Repair Defects in Fanconi Anemia Cells. *Cell Cycle* **2014**, *13* (10), 1540–1550. <https://doi.org/10.4161/cc.28476>.

(15) Higgs, M. R.; Sato, K.; Reynolds, J. J.; Begum, S.; Bayley, R.; Goula, A.; Vernet, A.; Paquin, K. L.; Skalnik, D. G.; Kobayashi, W.; Takata, M.; Howlett, N. G.; Kurumizaka, H.; Kimura, H.; Stewart, G. S. Histone Methylation by SETD1A Protects Nascent DNA through the Nucleosome Chaperone Activity of FANCD2. *Mol Cell* **2018**, *71* (1), 25–41.e6. <https://doi.org/10.1016/j.molcel.2018.05.018>.

(16) Michl, J.; Zimmer, J.; Buffa, F. M.; McDermott, U.; Tarsounas, M. FANCD2 Limits Replication Stress and Genome Instability in Cells Lacking BRCA2. *Nat Struct Mol Biol* **2016**, *23* (8), 755–757. <https://doi.org/10.1038/nsmb.3252>.

(17) Kais, Z.; Rondinelli, B.; Holmes, A.; O’Leary, C.; Kozono, D.; D’Andrea, A. D.; Ceccaldi, R. FANCD2 Maintains Fork Stability in BRCA1/2-Deficient Tumors and Promotes Alternative End-Joining DNA Repair. *Cell Rep* **2016**, *15* (11), 2488–2499. <https://doi.org/10.1016/j.celrep.2016.05.031>.

(18) Leuzzi, G.; Marabitti, V.; Pichierri, P.; Franchitto, A. WRNIP1 Protects Stalled Forks from Degradation and Promotes Fork Restart after Replication Stress. *EMBO J* **2016**, *35* (13), 1437–1451. <https://doi.org/10.15252/embj.201593265>.

(19) Malacaria, E.; Pugliese, G. M.; Honda, M.; Marabitti, V.; Aiello, F. A.; Spies, M.; Franchitto, A.; Pichierri, P. Rad52 Prevents Excessive Replication Fork Reversal and Protects from Nascent Strand Degradation. *Nat Commun* **2019**, *10* (1), 1412. <https://doi.org/10.1038/s41467-019-09196-9>.

- (20) Hu, J.; Sun, L.; Shen, F.; Chen, Y.; Hua, Y.; Liu, Y.; Zhang, M.; Hu, Y.; Wang, Q.; Xu, W.; Sun, F.; Ji, J.; Murray, J. M.; Carr, A. M.; Kong, D. The Intra-S Phase Checkpoint Targets Dna2 to Prevent Stalled Replication Forks from Reversing. *Cell* **2012**, *149* (6), 1221–1232. <https://doi.org/10.1016/j.cell.2012.04.030>.
- (21) Xu, S.; Wu, X.; Wu, L.; Castillo, A.; Liu, J.; Atkinson, E.; Paul, A.; Su, D.; Schlacher, K.; Komatsu, Y.; You, M. J.; Wang, B. Abro1 Maintains Genome Stability and Limits Replication Stress by Protecting Replication Fork Stability. *Genes Dev* **2017**, *31* (14), 1469–1482. <https://doi.org/10.1101/gad.299172.117>.
- (22) Thakar, T.; Leung, W.; Nicolae, C. M.; Clements, K. E.; Shen, B.; Bielinsky, A.-K.; Moldovan, G.-L. Ubiquitinated-PCNA Protects Replication Forks from DNA2-Mediated Degradation by Regulating Okazaki Fragment Maturation and Chromatin Assembly. *Nat Commun* **2020**, *11* (1), 2147. <https://doi.org/10.1038/s41467-020-16096-w>.
- (23) Kubota, T.; Katou, Y.; Nakato, R.; Shirahige, K.; Donaldson, A. D. Replication-Coupled PCNA Unloading by the Elg1 Complex Occurs Genome-Wide and Requires Okazaki Fragment Ligation. *Cell Rep* **2015**, *12* (5), 774–787. <https://doi.org/10.1016/j.celrep.2015.06.066>.
- (24) Janke, R.; King, G. A.; Kupiec, M.; Rine, J. Pivotal Roles of PCNA Loading and Unloading in Heterochromatin Function. *Proc Natl Acad Sci U S A* **2018**, *115* (9), E2030–E2039. <https://doi.org/10.1073/pnas.1721573115>.
- (25) Gali, V. K.; Dickerson, D.; Katou, Y.; Fujiki, K.; Shirahige, K.; Owen-Hughes, T.; Kubota, T.; Donaldson, A. D. Identification of Elg1 Interaction Partners and Effects on Post-Replication Chromatin Re-Formation. *PLoS Genet* **2018**, *14* (11), e1007783. <https://doi.org/10.1371/journal.pgen.1007783>.
- (26) Rageul, J.; Park, J. J.; Zeng, P. P.; Lee, E.-A.; Yang, J.; Hwang, S.; Lo, N.; Weinheimer, A. S.; Schärer, O. D.; Yeo, J.-E.; Kim, H. SDE2 Integrates into the TIMELESS-

TIPIN Complex to Protect Stalled Replication Forks. *Nat Commun* **2020**, *11* (1), 5495.

<https://doi.org/10.1038/s41467-020-19162-5>.

(27) Rageul, J.; Park, J. J.; Jo, U.; Weinheimer, A. S.; Vu, T. T. M.; Kim, H.

Conditional Degradation of SDE2 by the Arg/N-End Rule Pathway Regulates Stress Response at Replication Forks. *Nucleic Acids Res* **2019**, *47* (8), 3996–4010.

<https://doi.org/10.1093/nar/gkz054>.

(28) Abe, T.; Kawasumi, R.; Giannattasio, M.; Dusi, S.; Yoshimoto, Y.; Miyata, K.;

Umemura, K.; Hirota, K.; Branzei, D. AND-1 Fork Protection Function Prevents Fork Resection and Is Essential for Proliferation. *Nat Commun* **2018**, *9* (1), 3091. <https://doi.org/10.1038/s41467-018-05586-7>.

(29) Tonzi, P.; Yin, Y.; Lee, C. W. T.; Rothenberg, E.; Huang, T. T. Translesion

Polymerase Kappa-Dependent DNA Synthesis Underlies Replication Fork Recovery. *Elife* **2018**, *7*, e41426. <https://doi.org/10.7554/eLife.41426>.

(30) Kannouche, P. L.; Wing, J.; Lehmann, A. R. Interaction of Human DNA

Polymerase Eta with Monoubiquitinated PCNA: A Possible Mechanism for the Polymerase Switch in Response to DNA Damage. *Mol Cell* **2004**, *14* (4), 491–500.

[https://doi.org/10.1016/s1097-2765\(04\)00259-x](https://doi.org/10.1016/s1097-2765(04)00259-x).

(31) Bienko, M.; Green, C. M.; Crosetto, N.; Rudolf, F.; Zapart, G.; Coull, B.;

Kannouche, P.; Wider, G.; Peter, M.; Lehmann, A. R.; Hofmann, K.; Dikic, I. Ubiquitin-Binding Domains in Y-Family Polymerases Regulate Translesion Synthesis. *Science* **2005**, *310* (5755), 1821–1824. <https://doi.org/10.1126/science.1120615>.

(32) Wang, R.; Lenoir, W. F.; Wang, C.; Su, D.; McLaughlin, M.; Hu, Q.; Shen, X.;

Tian, Y.; Klages-Mundt, N.; Lynn, E.; Wood, R. D.; Chen, J.; Hart, T.; Li, L. DNA Polymerase τ Compensates for Fanconi Anemia Pathway Deficiency by Countering DNA Replication Stress.

Proc Natl Acad Sci U S A **2020**, *117* (52), 33436–33445.

<https://doi.org/10.1073/pnas.2008821117>.

(33) Williams, H. L.; Gottesman, M. E.; Gautier, J. Replication-Independent Repair of DNA Interstrand Crosslinks. *Mol Cell* **2012**, *47* (1), 140–147.

<https://doi.org/10.1016/j.molcel.2012.05.001>.

(34) Moldovan, G.-L.; Madhavan, M. V.; Mirchandani, K. D.; McCaffrey, R. M.; Vinciguerra, P.; D'Andrea, A. D. DNA Polymerase POLN Participates in Cross-Link Repair and Homologous Recombination. *Mol Cell Biol* **2010**, *30* (4), 1088–1096.

<https://doi.org/10.1128/MCB.01124-09>.

(35) Garzón, J.; Ursich, S.; Lopes, M.; Hiraga, S.-I.; Donaldson, A. D. Human RIF1-Protein Phosphatase 1 Prevents Degradation and Breakage of Nascent DNA on Replication Stalling. *Cell Rep* **2019**, *27* (9), 2558-2566.e4. <https://doi.org/10.1016/j.celrep.2019.05.002>.

(36) Mukherjee, C.; Tripathi, V.; Manolika, E. M.; Heijink, A. M.; Ricci, G.; Merzouk, S.; de Boer, H. R.; Demmers, J.; van Vugt, M. A. T. M.; Ray Chaudhuri, A. RIF1 Promotes Replication Fork Protection and Efficient Restart to Maintain Genome Stability. *Nat Commun* **2019**, *10* (1), 3287. <https://doi.org/10.1038/s41467-019-11246-1>.

(37) Bouwman, P.; Aly, A.; Escandell, J. M.; Pieterse, M.; Bartkova, J.; van der Gulden, H.; Hiddingh, S.; Thanasoula, M.; Kulkarni, A.; Yang, Q.; Haffty, B. G.; Tommiska, J.; Blomqvist, C.; Drapkin, R.; Adams, D. J.; Nevanlinna, H.; Bartek, J.; Tarsounas, M.; Ganesan, S.; Jonkers, J. 53BP1 Loss Rescues BRCA1 Deficiency and Is Associated with Triple-Negative and BRCA-Mutated Breast Cancers. *Nat Struct Mol Biol* **2010**, *17* (6), 688–695.

<https://doi.org/10.1038/nsmb.1831>.

(38) Ray Chaudhuri, A.; Callen, E.; Ding, X.; Gogola, E.; Duarte, A. A.; Lee, J.-E.; Wong, N.; Lafarga, V.; Calvo, J. A.; Panzarino, N. J.; John, S.; Day, A.; Crespo, A. V.; Shen, B.; Starnes, L. M.; de Rooter, J. R.; Daniel, J. A.; Konstantinopoulos, P. A.; Cortez, D.; Cantor, S. B.;

Fernandez-Capetillo, O.; Ge, K.; Jonkers, J.; Rottenberg, S.; Sharan, S. K.; Nussenzweig, A. Replication Fork Stability Confers Chemoresistance in BRCA-Deficient Cells. *Nature* **2016**, *535* (7612), 382–387. <https://doi.org/10.1038/nature18325>.

(39) Byrum, A. K.; Carvajal-Maldonado, D.; Mudge, M. C.; Valle-Garcia, D.; Majid, M. C.; Patel, R.; Sowa, M. E.; Gygi, S. P.; Harper, J. W.; Shi, Y.; Vindigni, A.; Mosammaparast, N. Mitotic Regulators TPX2 and Aurora A Protect DNA Forks during Replication Stress by Counteracting 53BP1 Function. *J Cell Biol* **2019**, *218* (2), 422–432. <https://doi.org/10.1083/jcb.201803003>.

(40) Liu, W.; Krishnamoorthy, A.; Zhao, R.; Cortez, D. Two Replication Fork Remodeling Pathways Generate Nuclease Substrates for Distinct Fork Protection Factors. *Sci Adv* **2020**, *6* (46), eabc3598. <https://doi.org/10.1126/sciadv.abc3598>.

(41) Teixeira-Silva, A.; Ait Saada, A.; Hardy, J.; Iraqui, I.; Nocente, M. C.; Fréon, K.; Lambert, S. A. E. The End-Joining Factor Ku Acts in the End-Resection of Double Strand Break-Free Arrested Replication Forks. *Nat Commun* **2017**, *8* (1), 1982. <https://doi.org/10.1038/s41467-017-02144-5>.

(42) Anand, R.; Ranjha, L.; Cannavo, E.; Cejka, P. Phosphorylated CtIP Functions as a Co-Factor of the MRE11-RAD50-NBS1 Endonuclease in DNA End Resection. *Mol Cell* **2016**, *64* (5), 940–950. <https://doi.org/10.1016/j.molcel.2016.10.017>.

(43) Cannavo, E.; Cejka, P. Sae2 Promotes DsDNA Endonuclease Activity within Mre11-Rad50-Xrs2 to Resect DNA Breaks. *Nature* **2014**, *514* (7520), 122–125. <https://doi.org/10.1038/nature13771>.

(44) Przetocka, S.; Porro, A.; Bolck, H. A.; Walker, C.; Lezaja, A.; Trenner, A.; von Aesch, C.; Himmels, S.-F.; D'Andrea, A. D.; Ceccaldi, R.; Altmeyer, M.; Sartori, A. A. CtIP-Mediated Fork Protection Synergizes with BRCA1 to Suppress Genomic Instability upon DNA

Replication Stress. *Mol Cell* **2018**, *72* (3), 568-582.e6.

<https://doi.org/10.1016/j.molcel.2018.09.014>.

(45) Zarrizi, R.; Higgs, M. R.; Voßgröne, K.; Rossing, M.; Bertelsen, B.; Bose, M.; Kousholt, A. N.; Rösner, H.; Network, T. C.; Ejlersen, B.; Stewart, G. S.; Nielsen, F. C.; Sørensen, C. S. Germline RBBP8 Variants Associated with Early-Onset Breast Cancer Compromise Replication Fork Stability. *J Clin Invest* **2020**, *130* (8), 4069–4080.

<https://doi.org/10.1172/JCI127521>.

(46) Nieminuszczy, J.; Broderick, R.; Bellani, M. A.; Smethurst, E.; Schwab, R. A.; Cherdyntseva, V.; Evmorfopoulou, T.; Lin, Y.-L.; Minczuk, M.; Pasero, P.; Gagos, S.; Seidman, M. M.; Niedzwiedz, W. EXD2 Protects Stressed Replication Forks and Is Required for Cell Viability in the Absence of BRCA1/2. *Mol Cell* **2019**, *75* (3), 605-619.e6.

<https://doi.org/10.1016/j.molcel.2019.05.026>.

(47) Berti, M.; Teloni, F.; Mijic, S.; Ursich, S.; Fuchs, J.; Palumbieri, M. D.; Krietsch, J.; Schmid, J. A.; Garcin, E. B.; Gon, S.; Modesti, M.; Altmeyer, M.; Lopes, M. Sequential Role of RAD51 Paralog Complexes in Replication Fork Remodeling and Restart. *Nat Commun* **2020**, *11* (1), 3531. <https://doi.org/10.1038/s41467-020-17324-z>.

(48) Poole, L. A.; Cortez, D. Functions of SMARCAL1, ZRANB3, and HLTF in Maintaining Genome Stability. *Crit Rev Biochem Mol Biol* **2017**, *52* (6), 696–714.

<https://doi.org/10.1080/10409238.2017.1380597>.

(49) Bétous, R.; Couch, F. B.; Mason, A. C.; Eichman, B. F.; Manosas, M.; Cortez, D. Substrate-Selective Repair and Restart of Replication Forks by DNA Translocases. *Cell Rep* **2013**, *3* (6), 1958–1969. <https://doi.org/10.1016/j.celrep.2013.05.002>.

(50) Ciccia, A.; Nimonkar, A. V.; Hu, Y.; Hajdu, I.; Achar, Y. J.; Izhar, L.; Petit, S. A.; Adamson, B.; Yoon, J. C.; Kowalczykowski, S. C.; Livingston, D. M.; Haracska, L.; Elledge, S. J. Polyubiquitinated PCNA Recruits the ZRANB3 Translocase to Maintain Genomic Integrity

after Replication Stress. *Mol Cell* **2012**, *47* (3), 396–409.

<https://doi.org/10.1016/j.molcel.2012.05.024>.

(51) Vujanovic, M.; Krietsch, J.; Raso, M. C.; Terraneo, N.; Zellweger, R.; Schmid, J. A.; Taglialatela, A.; Huang, J.-W.; Holland, C. L.; Zwicky, K.; Herrador, R.; Jacobs, H.; Cortez, D.; Ciccina, A.; Penengo, L.; Lopes, M. Replication Fork Slowing and Reversal upon DNA Damage Require PCNA Polyubiquitination and ZRANB3 DNA Translocase Activity. *Mol Cell* **2017**, *67* (5), 882–890.e5. <https://doi.org/10.1016/j.molcel.2017.08.010>.

(52) Unk, I.; Hajdú, I.; Fátyol, K.; Hurwitz, J.; Yoon, J.-H.; Prakash, L.; Prakash, S.; Haracska, L. Human HLTF Functions as a Ubiquitin Ligase for Proliferating Cell Nuclear Antigen Polyubiquitination. *Proc Natl Acad Sci U S A* **2008**, *105* (10), 3768–3773. <https://doi.org/10.1073/pnas.0800563105>.

(53) Motegi, A.; Liaw, H.-J.; Lee, K.-Y.; Roest, H. P.; Maas, A.; Wu, X.; Moinova, H.; Markowitz, S. D.; Ding, H.; Hoeijmakers, J. H. J.; Myung, K. Polyubiquitination of Proliferating Cell Nuclear Antigen by HLTF and SHPRH Prevents Genomic Instability from Stalled Replication Forks. *Proc Natl Acad Sci U S A* **2008**, *105* (34), 12411–12416. <https://doi.org/10.1073/pnas.0805685105>.

(54) Blastyák, A.; Hajdú, I.; Unk, I.; Haracska, L. Role of Double-Stranded DNA Translocase Activity of Human HLTF in Replication of Damaged DNA. *Mol Cell Biol* **2010**, *30* (3), 684–693. <https://doi.org/10.1128/MCB.00863-09>.

(55) Achar, Y. J.; Balogh, D.; Haracska, L. Coordinated Protein and DNA Remodeling by Human HLTF on Stalled Replication Fork. *Proc Natl Acad Sci U S A* **2011**, *108* (34), 14073–14078. <https://doi.org/10.1073/pnas.1101951108>.

(56) Kile, A. C.; Chavez, D. A.; Bacal, J.; Eldirany, S.; Korzhnev, D. M.; Bezsonova, I.; Eichman, B. F.; Cimprich, K. A. HLTF's Ancient HIRAN Domain Binds 3' DNA Ends to

Drive Replication Fork Reversal. *Mol Cell* **2015**, *58* (6), 1090–1100.

<https://doi.org/10.1016/j.molcel.2015.05.013>.

(57) Hishiki, A.; Hara, K.; Ikegaya, Y.; Yokoyama, H.; Shimizu, T.; Sato, M.; Hashimoto, H. Structure of a Novel DNA-Binding Domain of Helicase-like Transcription Factor (HLTF) and Its Functional Implication in DNA Damage Tolerance. *J Biol Chem* **2015**, *290* (21), 13215–13223. <https://doi.org/10.1074/jbc.M115.643643>.

(58) Garcia, V.; Phelps, S. E. L.; Gray, S.; Neale, M. J. Bidirectional Resection of DNA Double-Strand Breaks by Mre11 and Exo1. *Nature* **2011**, *479* (7372), 241–244. <https://doi.org/10.1038/nature10515>.

(59) Paull, T. T.; Gellert, M. The 3' to 5' Exonuclease Activity of Mre 11 Facilitates Repair of DNA Double-Strand Breaks. *Mol Cell* **1998**, *1* (7), 969–979. [https://doi.org/10.1016/s1097-2765\(00\)80097-0](https://doi.org/10.1016/s1097-2765(00)80097-0).

(60) Ayyagari, R.; Gomes, X. V.; Gordenin, D. A.; Burgers, P. M. J. Okazaki Fragment Maturation in Yeast. I. Distribution of Functions between FEN1 AND DNA2. *J Biol Chem* **2003**, *278* (3), 1618–1625. <https://doi.org/10.1074/jbc.M209801200>.

(61) Fortini, B. K.; Pokharel, S.; Polaczek, P.; Balakrishnan, L.; Bambara, R. A.; Campbell, J. L. Characterization of the Endonuclease and ATP-Dependent Flap Endo/Exonuclease of Dna2. *J Biol Chem* **2011**, *286* (27), 23763–23770. <https://doi.org/10.1074/jbc.M111.243071>.

(62) Rossi, S. E.; Foiani, M.; Giannattasio, M. Dna2 Processes behind the Fork Long SsDNA Flaps Generated by Pif1 and Replication-Dependent Strand Displacement. *Nat Commun* **2018**, *9* (1), 4830. <https://doi.org/10.1038/s41467-018-07378-5>.

(63) Fugger, K.; Mistrik, M.; Neelsen, K. J.; Yao, Q.; Zellweger, R.; Kousholt, A. N.; Haahr, P.; Chu, W. K.; Bartek, J.; Lopes, M.; Hickson, I. D.; Sørensen, C. S. FBH1 Catalyzes

Regression of Stalled Replication Forks. *Cell Rep* **2015**, *10* (10), 1749–1757.

<https://doi.org/10.1016/j.celrep.2015.02.028>.

(64) Panzarino, N. J.; Kraiss, J. J.; Cong, K.; Peng, M.; Mosqueda, M.; Nayak, S. U.; Bond, S. M.; Calvo, J. A.; Doshi, M. B.; Bere, M.; Ou, J.; Deng, B.; Zhu, L. J.; Johnson, N.; Cantor, S. B. Replication Gaps Underlie BRCA Deficiency and Therapy Response. *Cancer Res* **2021**, *81* (5), 1388–1397. <https://doi.org/10.1158/0008-5472.CAN-20-1602>.

(65) Somyajit, K.; Spies, J.; Coscia, F.; Kirik, U.; Rask, M.-B.; Lee, J.-H.; Neelsen, K. J.; Mund, A.; Jensen, L. J.; Paull, T. T.; Mann, M.; Lukas, J. Homology-Directed Repair Protects the Replicating Genome from Metabolic Assaults. *Dev Cell* **2021**, *56* (4), 461–477.e7. <https://doi.org/10.1016/j.devcel.2021.01.011>.

(66) Chen, H.; Symington, L. S. Overcoming the Chromatin Barrier to End Resection. *Cell Res* **2013**, *23* (3), 317–319. <https://doi.org/10.1038/cr.2012.148>.

(67) Price, B. D.; D'Andrea, A. D. Chromatin Remodeling at DNA Double-Strand Breaks. *Cell* **2013**, *152* (6), 1344–1354. <https://doi.org/10.1016/j.cell.2013.02.011>.

(68) Adkins, N. L.; Niu, H.; Sung, P.; Peterson, C. L. Nucleosome Dynamics Regulates DNA Processing. *Nat Struct Mol Biol* **2013**, *20* (7), 836–842. <https://doi.org/10.1038/nsmb.2585>.

(69) Smith, D. J.; Whitehouse, I. Intrinsic Coupling of Lagging-Strand Synthesis to Chromatin Assembly. *Nature* **2012**, *483* (7390), 434–438. <https://doi.org/10.1038/nature10895>.

(70) Yadav, T.; Whitehouse, I. Replication-Coupled Nucleosome Assembly and Positioning by ATP-Dependent Chromatin-Remodeling Enzymes. *Cell Rep* **2016**, *15* (4), 715–723. <https://doi.org/10.1016/j.celrep.2016.03.059>.

(71) Schmid, J. A.; Berti, M.; Walser, F.; Raso, M. C.; Schmid, F.; Krietsch, J.; Stoy, H.; Zwicky, K.; Ursich, S.; Freire, R.; Lopes, M.; Penengo, L. Histone Ubiquitination by the

DNA Damage Response Is Required for Efficient DNA Replication in Unperturbed S Phase. *Mol Cell* **2018**, *71* (6), 897-910.e8. <https://doi.org/10.1016/j.molcel.2018.07.011>.

(72) Delamarre, A.; Barthe, A.; de la Roche Saint-André, C.; Luciano, P.; Forey, R.; Padioleau, I.; Skrzypczak, M.; Ginalski, K.; Géli, V.; Pasero, P.; Lengronne, A. MRX Increases Chromatin Accessibility at Stalled Replication Forks to Promote Nascent DNA Resection and Cohesin Loading. *Mol Cell* **2020**, *77* (2), 395-410.e3. <https://doi.org/10.1016/j.molcel.2019.10.029>.

(73) Kim, J. J.; Lee, S. Y.; Choi, J.-H.; Woo, H. G.; Xhemalce, B.; Miller, K. M. PCAF-Mediated Histone Acetylation Promotes Replication Fork Degradation by MRE11 and EXO1 in BRCA-Deficient Cells. *Mol Cell* **2020**, *80* (2), 327-344.e8. <https://doi.org/10.1016/j.molcel.2020.08.018>.

(74) Agudelo Garcia, P. A.; Lovejoy, C. M.; Nagarajan, P.; Park, D.; Popova, L. V.; Freitas, M. A.; Parthun, M. R. Histone Acetyltransferase 1 Is Required for DNA Replication Fork Function and Stability. *J Biol Chem* **2020**, *295* (25), 8363–8373. <https://doi.org/10.1074/jbc.RA120.013496>.

(75) Schwab, R. A.; Nieminuszczy, J.; Shin-ya, K.; Niedzwiedz, W. FANCI Couples Replication Past Natural Fork Barriers with Maintenance of Chromatin Structure. *J Cell Biol* **2013**, *201* (1), 33–48. <https://doi.org/10.1083/jcb.201208009>.

(76) Peng, M.; Cong, K.; Panzarino, N. J.; Nayak, S.; Calvo, J.; Deng, B.; Zhu, L. J.; Morocz, M.; Hegedus, L.; Haracska, L.; Cantor, S. B. Opposing Roles of FANCI and HLF1 Protect Forks and Restrain Replication during Stress. *Cell Rep* **2018**, *24* (12), 3251–3261. <https://doi.org/10.1016/j.celrep.2018.08.065>.

(77) Feng, G.; Yuan, Y.; Li, Z.; Wang, L.; Zhang, B.; Luo, J.; Ji, J.; Kong, D. Replication Fork Stalling Elicits Chromatin Compaction for the Stability of Stalling Replication

Forks. *Proc Natl Acad Sci U S A* **2019**, *116* (29), 14563–14572.

<https://doi.org/10.1073/pnas.1821475116>.

(78) Guillemette, S.; Serra, R. W.; Peng, M.; Hayes, J. A.; Konstantinopoulos, P. A.; Green, M. R.; Cantor, S. B. Resistance to Therapy in BRCA2 Mutant Cells Due to Loss of the Nucleosome Remodeling Factor CHD4. *Genes Dev* **2015**, *29* (5), 489–494.

<https://doi.org/10.1101/gad.256214.114>.

(79) Dungrawala, H.; Bhat, K. P.; Le Meur, R.; Chazin, W. J.; Ding, X.; Sharan, S. K.; Wessel, S. R.; Sathe, A. A.; Zhao, R.; Cortez, D. RADX Promotes Genome Stability and Modulates Chemosensitivity by Regulating RAD51 at Replication Forks. *Mol Cell* **2017**, *67* (3), 374–386.e5. <https://doi.org/10.1016/j.molcel.2017.06.023>.

(80) Clements, K. E.; Thakar, T.; Nicolae, C. M.; Liang, X.; Wang, H.-G.; Moldovan, G.-L. Loss of E2F7 Confers Resistance to Poly-ADP-Ribose Polymerase (PARP) Inhibitors in BRCA2-Deficient Cells. *Nucleic Acids Res* **2018**, *46* (17), 8898–8907.

<https://doi.org/10.1093/nar/gky657>.

(81) Tang, J.; Cho, N. W.; Cui, G.; Manion, E. M.; Shanbhag, N. M.; Botuyan, M. V.; Mer, G.; Greenberg, R. A. Acetylation Limits 53BP1 Association with Damaged Chromatin to Promote Homologous Recombination. *Nat Struct Mol Biol* **2013**, *20* (3), 317–325.

<https://doi.org/10.1038/nsmb.2499>.

(82) Li, M. L.; Jiang, Q.; Bhanu, N. V.; Wu, J.; Li, W.; Garcia, B. A.; Greenberg, R. A. Phosphorylation of TIP60 Suppresses 53BP1 Localization at DNA Damage Sites. *Mol Cell Biol* **2019**, *39* (1), e00209-18. <https://doi.org/10.1128/MCB.00209-18>.

(83) Clements, K. E.; Schleicher, E. M.; Thakar, T.; Hale, A.; Dhoonmoon, A.; Tolman, N. J.; Sharma, A.; Liang, X.; Imamura Kawasawa, Y.; Nicolae, C. M.; Wang, H.-G.; De, S.; Moldovan, G.-L. Identification of Regulators of Poly-ADP-Ribose Polymerase Inhibitor

Response through Complementary CRISPR Knockout and Activation Screens. *Nat Commun* **2020**, *11* (1), 6118. <https://doi.org/10.1038/s41467-020-19961-w>.

(84) Daza-Martin, M.; Starowicz, K.; Jamshad, M.; Tye, S.; Ronson, G. E.; MacKay, H. L.; Chauhan, A. S.; Walker, A. K.; Stone, H. R.; Beesley, J. F. J.; Coles, J. L.; Garvin, A. J.; Stewart, G. S.; McCorvie, T. J.; Zhang, X.; Densham, R. M.; Morris, J. R. Isomerization of BRCA1-BARD1 Promotes Replication Fork Protection. *Nature* **2019**, *571* (7766), 521–527. <https://doi.org/10.1038/s41586-019-1363-4>.

(85) Billing, D.; Horiguchi, M.; Wu-Baer, F.; Tagliatela, A.; Leuzzi, G.; Nanez, S. A.; Jiang, W.; Zha, S.; Szabolcs, M.; Lin, C.-S.; Ciccia, A.; Baer, R. The BRCT Domains of the BRCA1 and BARD1 Tumor Suppressors Differentially Regulate Homology-Directed Repair and Stalled Fork Protection. *Mol Cell* **2018**, *72* (1), 127-139.e8. <https://doi.org/10.1016/j.molcel.2018.08.016>.

(86) Quinet, A.; Tirman, S.; Jackson, J.; Šviković, S.; Lemaçon, D.; Carvajal-Maldonado, D.; González-Acosta, D.; Vessoni, A. T.; Cybulla, E.; Wood, M.; Tavis, S.; Batista, L. F. Z.; Méndez, J.; Sale, J. E.; Vindigni, A. PRIMPOL-Mediated Adaptive Response Suppresses Replication Fork Reversal in BRCA-Deficient Cells. *Mol Cell* **2020**, *77* (3), 461-474.e9. <https://doi.org/10.1016/j.molcel.2019.10.008>.

(87) Lossaint, G.; Larroque, M.; Ribeyre, C.; Bec, N.; Larroque, C.; Décaillet, C.; Gari, K.; Constantinou, A. FANCD2 Binds MCM Proteins and Controls Replisome Function upon Activation of s Phase Checkpoint Signaling. *Mol Cell* **2013**, *51* (5), 678–690. <https://doi.org/10.1016/j.molcel.2013.07.023>.

(88) Wang, A. T.; Kim, T.; Wagner, J. E.; Conti, B. A.; Lach, F. P.; Huang, A. L.; Molina, H.; Sanborn, E. M.; Zierhut, H.; Cornes, B. K.; Abhyankar, A.; Sougnez, C.; Gabriel, S. B.; Auerbach, A. D.; Kowalczykowski, S. C.; Smogorzewska, A. A Dominant Mutation in Human RAD51 Reveals Its Function in DNA Interstrand Crosslink Repair Independent of

Homologous Recombination. *Mol Cell* **2015**, *59* (3), 478–490.

<https://doi.org/10.1016/j.molcel.2015.07.009>.

(89) Rickman, K. A.; Noonan, R. J.; Lach, F. P.; Sridhar, S.; Wang, A. T.; Abhyankar, A.; Huang, A.; Kelly, M.; Auerbach, A. D.; Smogorzewska, A. Distinct Roles of BRCA2 in Replication Fork Protection in Response to Hydroxyurea and DNA Interstrand Cross-Links. *Genes Dev* **2020**, *34* (11–12), 832–846. <https://doi.org/10.1101/gad.336446.120>.

(90) Ding, X.; Ray Chaudhuri, A.; Callen, E.; Pang, Y.; Biswas, K.; Klarmann, K. D.; Martin, B. K.; Burkett, S.; Cleveland, L.; Stauffer, S.; Sullivan, T.; Dewan, A.; Marks, H.; Tubbs, A. T.; Wong, N.; Buehler, E.; Akagi, K.; Martin, S. E.; Keller, J. R.; Nussenzweig, A.; Sharan, S. K. Synthetic Viability by BRCA2 and PARP1/ARTD1 Deficiencies. *Nat Commun* **2016**, *7*, 12425. <https://doi.org/10.1038/ncomms12425>.

(91) Ceccaldi, R.; Liu, J. C.; Amunugama, R.; Hajdu, I.; Primack, B.; Petalcorin, M. I. R.; O'Connor, K. W.; Konstantinopoulos, P. A.; Elledge, S. J.; Boulton, S. J.; Yusufzai, T.; D'Andrea, A. D. Homologous-Recombination-Deficient Tumours Are Dependent on Pol θ -Mediated Repair. *Nature* **2015**, *518* (7538), 258–262. <https://doi.org/10.1038/nature14184>.

(92) Mateos-Gomez, P. A.; Gong, F.; Nair, N.; Miller, K. M.; Lazzerini-Denchi, E.; Sfeir, A. Mammalian Polymerase θ Promotes Alternative NHEJ and Suppresses Recombination. *Nature* **2015**, *518* (7538), 254–257. <https://doi.org/10.1038/nature14157>.

(93) Lim, K. S.; Li, H.; Roberts, E. A.; Gaudiano, E. F.; Clairmont, C.; Sambel, L. A.; Ponnienselvan, K.; Liu, J. C.; Yang, C.; Kozono, D.; Parmar, K.; Yusufzai, T.; Zheng, N.; D'Andrea, A. D. USP1 Is Required for Replication Fork Protection in BRCA1-Deficient Tumors. *Mol Cell* **2018**, *72* (6), 925–941.e4. <https://doi.org/10.1016/j.molcel.2018.10.045>.

(94) Ying, S.; Hamdy, F. C.; Helleday, T. Mre11-Dependent Degradation of Stalled DNA Replication Forks Is Prevented by BRCA2 and PARP1. *Cancer Res* **2012**, *72* (11), 2814–2821. <https://doi.org/10.1158/0008-5472.CAN-11-3417>.

- (95) Coquel, F.; Silva, M.-J.; Técher, H.; Zadorozhny, K.; Sharma, S.; Nieminuszczy, J.; Mettling, C.; Dardillac, E.; Barthe, A.; Schmitz, A.-L.; Promonet, A.; Cribier, A.; Sarrazin, A.; Niedzwiedz, W.; Lopez, B.; Costanzo, V.; Krejci, L.; Chabes, A.; Benkirane, M.; Lin, Y.-L.; Pasero, P. SAMHD1 Acts at Stalled Replication Forks to Prevent Interferon Induction. *Nature* **2018**, *557* (7703), 57–61. <https://doi.org/10.1038/s41586-018-0050-1>.
- (96) Reisländer, T.; Lombardi, E. P.; Groelly, F. J.; Miar, A.; Porru, M.; Di Vito, S.; Wright, B.; Lockstone, H.; Biroccio, A.; Harris, A.; Londoño-Vallejo, A.; Tarsounas, M. BRCA2 Abrogation Triggers Innate Immune Responses Potentiated by Treatment with PARP Inhibitors. *Nat Commun* **2019**, *10* (1), 3143. <https://doi.org/10.1038/s41467-019-11048-5>.
- (97) Ding, L.; Kim, H.-J.; Wang, Q.; Kearns, M.; Jiang, T.; Ohlson, C. E.; Li, B. B.; Xie, S.; Liu, J. F.; Stover, E. H.; Howitt, B. E.; Bronson, R. T.; Lazo, S.; Roberts, T. M.; Freeman, G. J.; Konstantinopoulos, P. A.; Matulonis, U. A.; Zhao, J. J. PARP Inhibition Elicits STING-Dependent Antitumor Immunity in Brca1-Deficient Ovarian Cancer. *Cell Rep* **2018**, *25* (11), 2972-2980.e5. <https://doi.org/10.1016/j.celrep.2018.11.054>.
- (98) Bunting, S. F.; Callén, E.; Wong, N.; Chen, H.-T.; Polato, F.; Gunn, A.; Bothmer, A.; Feldhahn, N.; Fernandez-Capetillo, O.; Cao, L.; Xu, X.; Deng, C.-X.; Finkel, T.; Nussenzweig, M.; Stark, J. M.; Nussenzweig, A. 53BP1 Inhibits Homologous Recombination in Brca1-Deficient Cells by Blocking Resection of DNA Breaks. *Cell* **2010**, *141* (2), 243–254. <https://doi.org/10.1016/j.cell.2010.03.012>.
- (99) Xu, G.; Chapman, J. R.; Brandsma, I.; Yuan, J.; Mistrik, M.; Bouwman, P.; Bartkova, J.; Gogola, E.; Warmerdam, D.; Barazas, M.; Jaspers, J. E.; Watanabe, K.; Pieterse, M.; Kersbergen, A.; Sol, W.; Celie, P. H. N.; Schouten, P. C.; van den Broek, B.; Salman, A.; Nieuwland, M.; de Rink, I.; de Ronde, J.; Jalink, K.; Boulton, S. J.; Chen, J.; van Gent, D. C.; Bartek, J.; Jonkers, J.; Borst, P.; Rottenberg, S. REV7 Counteracts DNA Double-Strand Break

Resection and Affects PARP Inhibition. *Nature* **2015**, *521* (7553), 541–544.

<https://doi.org/10.1038/nature14328>.

(100) Noordermeer, S. M.; Adam, S.; Setiাপutra, D.; Barazas, M.; Pettitt, S. J.; Ling, A. K.; Olivieri, M.; Álvarez-Quilón, A.; Moatti, N.; Zimmermann, M.; Annunziato, S.; Krastev, D. B.; Song, F.; Brandsma, I.; Frankum, J.; Brough, R.; Sherker, A.; Landry, S.; Szilard, R. K.; Munro, M. M.; McEwan, A.; Gouillet de Rugy, T.; Lin, Z.-Y.; Hart, T.; Moffat, J.; Gingras, A.-C.; Martin, A.; van Attikum, H.; Jonkers, J.; Lord, C. J.; Rottenberg, S.; Durocher, D. The Shieldin Complex Mediates 53BP1-Dependent DNA Repair. *Nature* **2018**, *560* (7716), 117–121.

<https://doi.org/10.1038/s41586-018-0340-7>.

(101) Ghezraoui, H.; Oliveira, C.; Becker, J. R.; Bilham, K.; Moralli, D.; Anzilotti, C.; Fischer, R.; Deobagkar-Lele, M.; Sanchiz-Calvo, M.; Fueyo-Marcos, E.; Bonham, S.; Kessler, B. M.; Rottenberg, S.; Cornall, R. J.; Green, C. M.; Chapman, J. R. 53BP1 Cooperation with the REV7-Shieldin Complex Underpins DNA Structure-Specific NHEJ. *Nature* **2018**, *560* (7716), 122–127. <https://doi.org/10.1038/s41586-018-0362-1>.

(102) Mirman, Z.; Lottersberger, F.; Takai, H.; Kibe, T.; Gong, Y.; Takai, K.; Bianchi, A.; Zimmermann, M.; Durocher, D.; de Lange, T. 53BP1-RIF1-Shieldin Counteracts DSB Resection through CST- and Pol α -Dependent Fill-In. *Nature* **2018**, *560* (7716), 112–116. <https://doi.org/10.1038/s41586-018-0324-7>.

(103) Dev, H.; Chiang, T.-W. W.; Lescale, C.; de Krijger, I.; Martin, A. G.; Pilger, D.; Coates, J.; Sczaniecka-Clift, M.; Wei, W.; Ostermaier, M.; Herzog, M.; Lam, J.; Shea, A.; Demir, M.; Wu, Q.; Yang, F.; Fu, B.; Lai, Z.; Balmus, G.; Belotserkovskaya, R.; Serra, V.; O'Connor, M. J.; Bruna, A.; Beli, P.; Pellegrini, L.; Caldas, C.; Deriano, L.; Jacobs, J. J. L.; Galanty, Y.; Jackson, S. P. Shieldin Complex Promotes DNA End-Joining and Counters Homologous Recombination in BRCA1-Null Cells. *Nat Cell Biol* **2018**, *20* (8), 954–965.

<https://doi.org/10.1038/s41556-018-0140-1>.

(104) Gupta, R.; Somyajit, K.; Narita, T.; Maskey, E.; Stanlie, A.; Kremer, M.; Typas, D.; Lammers, M.; Mailand, N.; Nussenzweig, A.; Lukas, J.; Choudhary, C. DNA Repair Network Analysis Reveals Shieldin as a Key Regulator of NHEJ and PARP Inhibitor Sensitivity. *Cell* **2018**, *173* (4), 972-988.e23. <https://doi.org/10.1016/j.cell.2018.03.050>.

(105) Murai, J.; Huang, S. N.; Das, B. B.; Renaud, A.; Zhang, Y.; Doroshov, J. H.; Ji, J.; Takeda, S.; Pommier, Y. Differential Trapping of PARP1 and PARP2 by Clinical PARP Inhibitors. *Cancer Res* **2012**, *72* (21), 5588–5599. <https://doi.org/10.1158/0008-5472.CAN-12-2753>.

(106) Blessing, C.; Mandemaker, I. K.; Gonzalez-Leal, C.; Preisser, J.; Schomburg, A.; Ladurner, A. G. The Oncogenic Helicase ALC1 Regulates PARP Inhibitor Potency by Trapping PARP2 at DNA Breaks. *Mol Cell* **2020**, *80* (5), 862-875.e6. <https://doi.org/10.1016/j.molcel.2020.10.009>.

(107) Juhász, S.; Smith, R.; Schauer, T.; Spekhardt, D.; Mamar, H.; Zentout, S.; Chapuis, C.; Huet, S.; Timinszky, G. The Chromatin Remodeler ALC1 Underlies Resistance to PARP Inhibitor Treatment. *Sci Adv* **2020**, *6* (51), eabb8626. <https://doi.org/10.1126/sciadv.abb8626>.

(108) Verma, P.; Zhou, Y.; Cao, Z.; Deraska, P. V.; Deb, M.; Arai, E.; Li, W.; Shao, Y.; Puentes, L.; Li, Y.; Patankar, S.; Mach, R. H.; Faryabi, R. B.; Shi, J.; Greenberg, R. A. ALC1 Links Chromatin Accessibility to PARP Inhibitor Response in Homologous Recombination-Deficient Cells. *Nat Cell Biol* **2021**, *23* (2), 160–171. <https://doi.org/10.1038/s41556-020-00624-3>.

(109) Zimmermann, M.; Murina, O.; Reijns, M. A. M.; Agathangelou, A.; Challis, R.; Tarnauskaitė, Ž.; Muir, M.; Fluteau, A.; Aregger, M.; McEwan, A.; Yuan, W.; Clarke, M.; Lambros, M. B.; Paneesha, S.; Moss, P.; Chandrashekhar, M.; Angers, S.; Moffat, J.; Brunton, V. G.; Hart, T.; de Bono, J.; Stankovic, T.; Jackson, A. P.; Durocher, D. CRISPR Screens Identify

Genomic Ribonucleotides as a Source of PARP-Trapping Lesions. *Nature* **2018**, *559* (7713), 285–289. <https://doi.org/10.1038/s41586-018-0291-z>.

(110) Maya-Mendoza, A.; Moudry, P.; Merchut-Maya, J. M.; Lee, M.; Strauss, R.; Bartek, J. High Speed of Fork Progression Induces DNA Replication Stress and Genomic Instability. *Nature* **2018**, *559* (7713), 279–284. <https://doi.org/10.1038/s41586-018-0261-5>.

(111) Cong, K.; Peng, M.; Kousholt, A. N.; Lee, W. T. C.; Lee, S.; Nayak, S.; Kraiss, J.; VanderVere-Carozza, P. S.; Pawelczak, K. S.; Calvo, J.; Panzarino, N. J.; Turchi, J. J.; Johnson, N.; Jonkers, J.; Rothenberg, E.; Cantor, S. B. Replication Gaps Are a Key Determinant of PARP Inhibitor Synthetic Lethality with BRCA Deficiency. *Mol Cell* **2021**, *81* (15), 3128-3144.e7. <https://doi.org/10.1016/j.molcel.2021.06.011>.

(112) Piberger, A. L.; Bowry, A.; Kelly, R. D. W.; Walker, A. K.; González-Acosta, D.; Bailey, L. J.; Doherty, A. J.; Méndez, J.; Morris, J. R.; Bryant, H. E.; Petermann, E. PrimPol-Dependent Single-Stranded Gap Formation Mediates Homologous Recombination at Bulky DNA Adducts. *Nat Commun* **2020**, *11* (1), 5863. <https://doi.org/10.1038/s41467-020-19570-7>.

(113) Benureau, Y.; Pouvelle, C.; Tavares, E. M.; Dupaigne, P.; Despras, E.; Cam, E. L.; Kannouche, P. Replication Intermediate Architecture Reveals the Chronology of DNA Damage Tolerance Pathways at UV-Stalled Replication Forks in Human Cells. *bioRxiv* October 12, 2020, p 2020.10.12.336107. <https://doi.org/10.1101/2020.10.12.336107>.

(114) Berti, M.; Ray Chaudhuri, A.; Thangavel, S.; Gomathinayagam, S.; Kenig, S.; Vujanovic, M.; Odreman, F.; Glatter, T.; Graziano, S.; Mendoza-Maldonado, R.; Marino, F.; Lucic, B.; Biasin, V.; Gstaiger, M.; Aebersold, R.; Sidorova, J. M.; Monnat, R. J.; Lopes, M.; Vindigni, A. Human RECQ1 Promotes Restart of Replication Forks Reversed by DNA Topoisomerase I Inhibition. *Nat Struct Mol Biol* **2013**, *20* (3), 347–354. <https://doi.org/10.1038/nsmb.2501>.

- (115) Hanzlikova, H.; Kalasova, I.; Demin, A. A.; Pennicott, L. E.; Cihlarova, Z.; Caldecott, K. W. The Importance of Poly(ADP-Ribose) Polymerase as a Sensor of Unligated Okazaki Fragments during DNA Replication. *Mol Cell* **2018**, *71* (2), 319–331.e3. <https://doi.org/10.1016/j.molcel.2018.06.004>.
- (116) Guilliam, T. A.; Yeeles, J. T. P. Reconstitution of Translesion Synthesis Reveals a Mechanism of Eukaryotic DNA Replication Restart. *Nat Struct Mol Biol* **2020**, *27* (5), 450–460. <https://doi.org/10.1038/s41594-020-0418-4>.
- (117) Taylor, M. R. G.; Yeeles, J. T. P. The Initial Response of a Eukaryotic Replisome to DNA Damage. *Mol Cell* **2018**, *70* (6), 1067–1080.e12. <https://doi.org/10.1016/j.molcel.2018.04.022>.
- (118) Lee, K.; Fu, H.; Aladjem, M. I.; Myung, K. ATAD5 Regulates the Lifespan of DNA Replication Factories by Modulating PCNA Level on the Chromatin. *J Cell Biol* **2013**, *200* (1), 31–44. <https://doi.org/10.1083/jcb.201206084>.
- (119) Choe, K. N.; Moldovan, G.-L. Forging Ahead through Darkness: PCNA, Still the Principal Conductor at the Replication Fork. *Mol Cell* **2017**, *65* (3), 380–392. <https://doi.org/10.1016/j.molcel.2016.12.020>.
- (120) Leung, W.; Baxley, R. M.; Moldovan, G.-L.; Bielinsky, A.-K. Mechanisms of DNA Damage Tolerance: Post-Translational Regulation of PCNA. *Genes (Basel)* **2018**, *10* (1), E10. <https://doi.org/10.3390/genes10010010>.
- (121) Zheng, L.; Shen, B. Okazaki Fragment Maturation: Nucleases Take Centre Stage. *J Mol Cell Biol* **2011**, *3* (1), 23–30. <https://doi.org/10.1093/jmcb/mjq048>.
- (122) Alabert, C.; Jasencakova, Z.; Groth, A. Chromatin Replication and Histone Dynamics. *Adv Exp Med Biol* **2017**, *1042*, 311–333. https://doi.org/10.1007/978-981-10-6955-0_15.

- (123) Sauer, P. V.; Gu, Y.; Liu, W. H.; Mattioli, F.; Panne, D.; Luger, K.; Churchill, M. E. Mechanistic Insights into Histone Deposition and Nucleosome Assembly by the Chromatin Assembly Factor-1. *Nucleic Acids Res* **2018**, *46* (19), 9907–9917.
<https://doi.org/10.1093/nar/gky823>.
- (124) Mailand, N.; Gibbs-Seymour, I.; Bekker-Jensen, S. Regulation of PCNA-Protein Interactions for Genome Stability. *Nat Rev Mol Cell Biol* **2013**, *14* (5), 269–282.
<https://doi.org/10.1038/nrm3562>.
- (125) Técher, H.; Koundrioukoff, S.; Nicolas, A.; Debatisse, M. The Impact of Replication Stress on Replication Dynamics and DNA Damage in Vertebrate Cells. *Nat Rev Genet* **2017**, *18* (9), 535–550. <https://doi.org/10.1038/nrg.2017.46>.
- (126) Zeman, M. K.; Cimprich, K. A. Causes and Consequences of Replication Stress. *Nat Cell Biol* **2014**, *16* (1), 2–9. <https://doi.org/10.1038/ncb2897>.
- (127) Hoegge, C.; Pfander, B.; Moldovan, G.-L.; Pyrowolakis, G.; Jentsch, S. RAD6-Dependent DNA Repair Is Linked to Modification of PCNA by Ubiquitin and SUMO. *Nature* **2002**, *419* (6903), 135–141. <https://doi.org/10.1038/nature00991>.
- (128) Stelter, P.; Ulrich, H. D. Control of Spontaneous and Damage-Induced Mutagenesis by SUMO and Ubiquitin Conjugation. *Nature* **2003**, *425* (6954), 188–191.
<https://doi.org/10.1038/nature01965>.
- (129) Yang, W.; Gao, Y. Translesion and Repair DNA Polymerases: Diverse Structure and Mechanism. *Annu Rev Biochem* **2018**, *87*, 239–261. <https://doi.org/10.1146/annurev-biochem-062917-012405>.
- (130) Vaisman, A.; Woodgate, R. Translesion DNA Polymerases in Eukaryotes: What Makes Them Tick? *Crit Rev Biochem Mol Biol* **2017**, *52* (3), 274–303.
<https://doi.org/10.1080/10409238.2017.1291576>.

- (131) Arakawa, H.; Moldovan, G.-L.; Saribasak, H.; Saribasak, N. N.; Jentsch, S.; Buerstedde, J.-M. A Role for PCNA Ubiquitination in Immunoglobulin Hypermutation. *PLoS Biol* **2006**, *4* (11), e366. <https://doi.org/10.1371/journal.pbio.0040366>.
- (132) Genome dynamics of the human embryonic kidney 293 lineage in response to cell biology manipulations - PubMed <https://pubmed.ncbi.nlm.nih.gov/25182477/> (accessed 2022-03-14).
- (133) Mardin, B. R.; Drainas, A. P.; Waszak, S. M.; Weischenfeldt, J.; Isokane, M.; Stütz, A. M.; Raeder, B.; Efthymiopoulos, T.; Buccitelli, C.; Segura-Wang, M.; Northcott, P.; Pfister, S. M.; Lichter, P.; Ellenberg, J.; Korbel, J. O. A Cell-Based Model System Links Chromothripsis with Hyperploidy. *Mol Syst Biol* **2015**, *11* (9), 828. <https://doi.org/10.15252/msb.20156505>.
- (134) Wang, G.; Levy, D. D.; Seidman, M. M.; Glazer, P. M. Targeted Mutagenesis in Mammalian Cells Mediated by Intracellular Triple Helix Formation. *Mol Cell Biol* **1995**, *15* (3), 1759–1768. <https://doi.org/10.1128/MCB.15.3.1759>.
- (135) Daigh, L. H.; Liu, C.; Chung, M.; Cimprich, K. A.; Meyer, T. Stochastic Endogenous Replication Stress Causes ATR-Triggered Fluctuations in CDK2 Activity That Dynamically Adjust Global DNA Synthesis Rates. *Cell Syst* **2018**, *7* (1), 17-27.e3. <https://doi.org/10.1016/j.cels.2018.05.011>.
- (136) Rondinelli, B.; Gogola, E.; Yücel, H.; Duarte, A. A.; van de Ven, M.; van der Sluijs, R.; Konstantinopoulos, P. A.; Jonkers, J.; Ceccaldi, R.; Rottenberg, S.; D'Andrea, A. D. EZH2 Promotes Degradation of Stalled Replication Forks by Recruiting MUS81 through Histone H3 Trimethylation. *Nat Cell Biol* **2017**, *19* (11), 1371–1378. <https://doi.org/10.1038/ncb3626>.
- (137) Li, M.; Xu, X.; Chang, C.-W.; Zheng, L.; Shen, B.; Liu, Y. SUMO2 Conjugation of PCNA Facilitates Chromatin Remodeling to Resolve Transcription-Replication Conflicts. *Nat Commun* **2018**, *9* (1), 2706. <https://doi.org/10.1038/s41467-018-05236-y>.

- (138) Moldovan, G.-L.; Dejsuphong, D.; Petalcorin, M. I. R.; Hofmann, K.; Takeda, S.; Boulton, S. J.; D'Andrea, A. D. Inhibition of Homologous Recombination by the PCNA-Interacting Protein PARI. *Mol Cell* **2012**, *45* (1), 75–86.
<https://doi.org/10.1016/j.molcel.2011.11.010>.
- (139) Quinet, A.; Lemaçon, D.; Vindigni, A. Replication Fork Reversal: Players and Guardians. *Mol Cell* **2017**, *68* (5), 830–833. <https://doi.org/10.1016/j.molcel.2017.11.022>.
- (140) Cortez, D. Replication-Coupled DNA Repair. *Mol Cell* **2019**, *74* (5), 866–876.
<https://doi.org/10.1016/j.molcel.2019.04.027>.
- (141) Duxin, J. P.; Moore, H. R.; Sidorova, J.; Karanja, K.; Honaker, Y.; Dao, B.; Piwnicka-Worms, H.; Campbell, J. L.; Monnat, R. J.; Stewart, S. A. Okazaki Fragment Processing-Independent Role for Human Dna2 Enzyme during DNA Replication. *J Biol Chem* **2012**, *287* (26), 21980–21991. <https://doi.org/10.1074/jbc.M112.359018>.
- (142) Becker, J. R.; Pons, C.; Nguyen, H. D.; Costanzo, M.; Boone, C.; Myers, C. L.; Bielinsky, A.-K. Genetic Interactions Implicating Postreplicative Repair in Okazaki Fragment Processing. *PLoS Genet* **2015**, *11* (11), e1005659. <https://doi.org/10.1371/journal.pgen.1005659>.
- (143) Ogi, T.; Lehmann, A. R. The Y-Family DNA Polymerase Kappa (Pol Kappa) Functions in Mammalian Nucleotide-Excision Repair. *Nat Cell Biol* **2006**, *8* (6), 640–642.
<https://doi.org/10.1038/ncb1417>.
- (144) Karras, G. I.; Jentsch, S. The RAD6 DNA Damage Tolerance Pathway Operates Uncoupled from the Replication Fork and Is Functional beyond S Phase. *Cell* **2010**, *141* (2), 255–267. <https://doi.org/10.1016/j.cell.2010.02.028>.
- (145) Lopes, M.; Foiani, M.; Sogo, J. M. Multiple Mechanisms Control Chromosome Integrity after Replication Fork Uncoupling and Restart at Irreparable UV Lesions. *Mol Cell* **2006**, *21* (1), 15–27. <https://doi.org/10.1016/j.molcel.2005.11.015>.

(146) Kang, Z.; Fu, P.; Alcivar, A. L.; Fu, H.; Redon, C.; Foo, T. K.; Zuo, Y.; Ye, C.; Baxley, R.; Madireddy, A.; Buisson, R.; Bielinsky, A.-K.; Zou, L.; Shen, Z.; Aladjem, M. I.; Xia, B. BRCA2 Associates with MCM10 to Suppress PRIMPOL-Mediated Repriming and Single-Stranded Gap Formation after DNA Damage. *Nat Commun* **2021**, *12* (1), 5966.

<https://doi.org/10.1038/s41467-021-26227-6>.

(147) Simoneau, A.; Xiong, R.; Zou, L. The Trans Cell Cycle Effects of PARP Inhibitors Underlie Their Selectivity toward BRCA1/2-Deficient Cells. *Genes Dev* **2021**, *35* (17–18), 1271–1289. <https://doi.org/10.1101/gad.348479.121>.

(148) Taglialatela, A.; Leuzzi, G.; Sannino, V.; Cuella-Martin, R.; Huang, J.-W.; Wu-Baer, F.; Baer, R.; Costanzo, V.; Ciccio, A. REV1-Pol ζ Maintains the Viability of Homologous Recombination-Deficient Cancer Cells through Mutagenic Repair of PRIMPOL-Dependent SsDNA Gaps. *Mol Cell* **2021**, *81* (19), 4008-4025.e7.

<https://doi.org/10.1016/j.molcel.2021.08.016>.

(149) Tirman, S.; Quinet, A.; Wood, M.; Meroni, A.; Cybulla, E.; Jackson, J.; Pegoraro, S.; Simoneau, A.; Zou, L.; Vindigni, A. Temporally Distinct Post-Replicative Repair Mechanisms Fill PRIMPOL-Dependent SsDNA Gaps in Human Cells. *Mol Cell* **2021**, *81* (19), 4026-4040.e8. <https://doi.org/10.1016/j.molcel.2021.09.013>.

(150) Paes Dias, M.; Tripathi, V.; van der Heijden, I.; Cong, K.; Manolika, E.-M.; Bhin, J.; Gogola, E.; Galanos, P.; Annunziato, S.; Lieftink, C.; Andújar-Sánchez, M.; Chakrabarty, S.; Smith, G. C. M.; van de Ven, M.; Beijersbergen, R. L.; Bartkova, J.; Rottenberg, S.; Cantor, S.; Bartek, J.; Ray Chaudhuri, A.; Jonkers, J. Loss of Nuclear DNA Ligase III Reverts PARP Inhibitor Resistance in BRCA1/53BP1 Double-Deficient Cells by Exposing SsDNA Gaps. *Mol Cell* **2021**, S1097-2765(21)00739-5. <https://doi.org/10.1016/j.molcel.2021.09.005>.

- (151) Roy, S.; Luzwick, J. W.; Schlacher, K. SIRF: Quantitative in Situ Analysis of Protein Interactions at DNA Replication Forks. *J Cell Biol* **2018**, *217* (4), 1521–1536. <https://doi.org/10.1083/jcb.201709121>.
- (152) Fromental-Ramain, C.; Ramain, P.; Hamiche, A. The Drosophila DAXX-Like Protein (DLP) Cooperates with ASF1 for H3.3 Deposition and Heterochromatin Formation. *Mol Cell Biol* **2017**, *37* (12), e00597-16. <https://doi.org/10.1128/MCB.00597-16>.
- (153) Ransom, M.; Dennehey, B. K.; Tyler, J. K. Chaperoning Histones during DNA Replication and Repair. *Cell* **2010**, *140* (2), 183–195. <https://doi.org/10.1016/j.cell.2010.01.004>.
- (154) Schulz, L. L.; Tyler, J. K. The Histone Chaperone ASF1 Localizes to Active DNA Replication Forks to Mediate Efficient DNA Replication. *FASEB J* **2006**, *20* (3), 488–490. <https://doi.org/10.1096/fj.05-5020fje>.
- (155) Tagami, H.; Ray-Gallet, D.; Almouzni, G.; Nakatani, Y. Histone H3.1 and H3.3 Complexes Mediate Nucleosome Assembly Pathways Dependent or Independent of DNA Synthesis. *Cell* **2004**, *116* (1), 51–61. [https://doi.org/10.1016/s0092-8674\(03\)01064-x](https://doi.org/10.1016/s0092-8674(03)01064-x).
- (156) Ray-Gallet, D.; Woolfe, A.; Vassias, I.; Pellentz, C.; Lacoste, N.; Puri, A.; Schultz, D. C.; Pchelintsev, N. A.; Adams, P. D.; Jansen, L. E. T.; Almouzni, G. Dynamics of Histone H3 Deposition in Vivo Reveal a Nucleosome Gap-Filling Mechanism for H3.3 to Maintain Chromatin Integrity. *Mol Cell* **2011**, *44* (6), 928–941. <https://doi.org/10.1016/j.molcel.2011.12.006>.
- (157) Cantor, S. B.; Calvo, J. A. Fork Protection and Therapy Resistance in Hereditary Breast Cancer. *Cold Spring Harb Symp Quant Biol* **2017**, *82*, 339–348. <https://doi.org/10.1101/sqb.2017.82.034413>.
- (158) Yu, C.; Gan, H.; Han, J.; Zhou, Z.-X.; Jia, S.; Chabes, A.; Farrugia, G.; Ordog, T.; Zhang, Z. Strand-Specific Analysis Shows Protein Binding at Replication Forks and PCNA

Unloading from Lagging Strands When Forks Stall. *Mol Cell* **2014**, *56* (4), 551–563.

<https://doi.org/10.1016/j.molcel.2014.09.017>.

(159) Mórocz, M.; Gali, H.; Raskó, I.; Downes, C. S.; Haracska, L. Single Cell Analysis of Human RAD18-Dependent DNA Post-Replication Repair by Alkaline Bromodeoxyuridine Comet Assay. *PLoS One* **2013**, *8* (8), e70391.

<https://doi.org/10.1371/journal.pone.0070391>.

(160) Guillian, T. A.; Doherty, A. J. PrimPol—Prime Time to Reprime. *Genes (Basel)* **2017**, *8* (1), 20. <https://doi.org/10.3390/genes8010020>.

(161) Ercilla, A.; Benada, J.; Amitash, S.; Zonderland, G.; Baldi, G.; Somyajit, K.; Ochs, F.; Costanzo, V.; Lukas, J.; Toledo, L. Physiological Tolerance to SsDNA Enables Strand Uncoupling during DNA Replication. *Cell Rep* **2020**, *30* (7), 2416–2429.e7.

<https://doi.org/10.1016/j.celrep.2020.01.067>.

(162) Zhang, H.; Gan, H.; Wang, Z.; Lee, J.-H.; Zhou, H.; Ordog, T.; Wold, M. S.; Ljungman, M.; Zhang, Z. RPA Interacts with HIRA and Regulates H3.3 Deposition at Gene Regulatory Elements in Mammalian Cells. *Mol Cell* **2017**, *65* (2), 272–284.

<https://doi.org/10.1016/j.molcel.2016.11.030>.

(163) Kang, M.-S.; Ryu, E.; Lee, S.-W.; Park, J.; Ha, N. Y.; Ra, J. S.; Kim, Y. J.; Kim, J.; Abdel-Rahman, M.; Park, S. H.; Lee, K.-Y.; Kim, H.; Kang, S.; Myung, K. Regulation of PCNA Cycling on Replicating DNA by RFC and RFC-like Complexes. *Nat Commun* **2019**, *10* (1), 2420. <https://doi.org/10.1038/s41467-019-10376-w>.

(164) Wessel, S. R.; Mohni, K. N.; Luzwick, J. W.; Dugrawala, H.; Cortez, D. Functional Analysis of the Replication Fork Proteome Identifies BET Proteins as PCNA Regulators. *Cell Rep* **2019**, *28* (13), 3497–3509.e4. <https://doi.org/10.1016/j.celrep.2019.08.051>.

- (165) Dieckman, L. M.; Boehm, E. M.; Hingorani, M. M.; Washington, M. T. Distinct Structural Alterations in Proliferating Cell Nuclear Antigen Block DNA Mismatch Repair. *Biochemistry* **2013**, *52* (33), 5611–5619. <https://doi.org/10.1021/bi400378e>.
- (166) Goellner, E. M.; Smith, C. E.; Campbell, C. S.; Hombauer, H.; Desai, A.; Putnam, C. D.; Kolodner, R. D. PCNA and Msh2-Msh6 Activate an Mlh1-Pms1 Endonuclease Pathway Required for Exo1-Independent Mismatch Repair. *Mol Cell* **2014**, *55* (2), 291–304. <https://doi.org/10.1016/j.molcel.2014.04.034>.
- (167) Lau, P. J.; Flores-Rozas, H.; Kolodner, R. D. Isolation and Characterization of New Proliferating Cell Nuclear Antigen (POL30) Mutator Mutants That Are Defective in DNA Mismatch Repair. *Mol Cell Biol* **2002**, *22* (19), 6669–6680. <https://doi.org/10.1128/MCB.22.19.6669-6680.2002>.
- (168) Shibahara, K.; Stillman, B. Replication-Dependent Marking of DNA by PCNA Facilitates CAF-1-Coupled Inheritance of Chromatin. *Cell* **1999**, *96* (4), 575–585. [https://doi.org/10.1016/s0092-8674\(00\)80661-3](https://doi.org/10.1016/s0092-8674(00)80661-3).
- (169) Zhang, Z.; Shibahara, K.; Stillman, B. PCNA Connects DNA Replication to Epigenetic Inheritance in Yeast. *Nature* **2000**, *408* (6809), 221–225. <https://doi.org/10.1038/35041601>.
- (170) Liu, W. H.; Roemer, S. C.; Port, A. M.; Churchill, M. E. A. CAF-1-Induced Oligomerization of Histones H3/H4 and Mutually Exclusive Interactions with Asf1 Guide H3/H4 Transitions among Histone Chaperones and DNA. *Nucleic Acids Res* **2012**, *40* (22), 11229–11239. <https://doi.org/10.1093/nar/gks906>.
- (171) Mattioli, F.; Gu, Y.; Yadav, T.; Balsbaugh, J. L.; Harris, M. R.; Findlay, E. S.; Liu, Y.; Radebaugh, C. A.; Stargell, L. A.; Ahn, N. G.; Whitehouse, I.; Luger, K. DNA-Mediated Association of Two Histone-Bound Complexes of Yeast Chromatin Assembly Factor-1 (CAF-1)

Drives Tetrasome Assembly in the Wake of DNA Replication. *Elife* **2017**, *6*, e22799.

<https://doi.org/10.7554/eLife.22799>.

(172) Sauer, P. V.; Timm, J.; Liu, D.; Sitbon, D.; Boeri-Erba, E.; Velours, C.; Mücke, N.; Langowski, J.; Ochsenbein, F.; Almouzni, G.; Panne, D. Insights into the Molecular Architecture and Histone H3-H4 Deposition Mechanism of Yeast Chromatin Assembly Factor 1. *Elife* **2017**, *6*, e23474. <https://doi.org/10.7554/eLife.23474>.

(173) Donham, D. C.; Scorgie, J. K.; Churchill, M. E. A. The Activity of the Histone Chaperone Yeast Asf1 in the Assembly and Disassembly of Histone H3/H4-DNA Complexes. *Nucleic Acids Res* **2011**, *39* (13), 5449–5458. <https://doi.org/10.1093/nar/gkr097>.

(174) Loppin, B.; Bonnefoy, E.; Anselme, C.; Laurençon, A.; Karr, T. L.; Couble, P. The Histone H3.3 Chaperone HIRA Is Essential for Chromatin Assembly in the Male Pronucleus. *Nature* **2005**, *437* (7063), 1386–1390. <https://doi.org/10.1038/nature04059>.

(175) Mello, J. A.; Silljé, H. H. W.; Roche, D. M. J.; Kirschner, D. B.; Nigg, E. A.; Almouzni, G. Human Asf1 and CAF-1 Interact and Synergize in a Repair-Coupled Nucleosome Assembly Pathway. *EMBO Rep* **2002**, *3* (4), 329–334. <https://doi.org/10.1093/embo-reports/kvf068>.

(176) Tyler, J. K.; Collins, K. A.; Prasad-Sinha, J.; Amriott, E.; Bulger, M.; Harte, P. J.; Kobayashi, R.; Kadonaga, J. T. Interaction between the Drosophila CAF-1 and ASF1 Chromatin Assembly Factors. *Mol Cell Biol* **2001**, *21* (19), 6574–6584. <https://doi.org/10.1128/MCB.21.19.6574-6584.2001>.

(177) Huang, T.-H.; Fowler, F.; Chen, C.-C.; Shen, Z.-J.; Sleckman, B.; Tyler, J. K. The Histone Chaperones ASF1 and CAF-1 Promote MMS22L-TONSL-Mediated Rad51 Loading onto SsDNA during Homologous Recombination in Human Cells. *Mol Cell* **2018**, *69* (5), 879–892.e5. <https://doi.org/10.1016/j.molcel.2018.01.031>.

- (178) Groth, A.; Ray-Gallet, D.; Quivy, J.-P.; Lukas, J.; Bartek, J.; Almouzni, G. Human Asf1 Regulates the Flow of S Phase Histones during Replication Stress. *Mol Cell* **2005**, *17* (2), 301–311. <https://doi.org/10.1016/j.molcel.2004.12.018>.
- (179) Vaitiankova, A.; Burdova, K.; Sobol, M.; Gautam, A.; Benada, O.; Hanzlikova, H.; Caldecott, K. W. PARP Inhibition Impedes the Maturation of Nascent DNA Strands during DNA Replication. *Nat Struct Mol Biol* **2022**. <https://doi.org/10.1038/s41594-022-00747-1>.
- (180) Bai, G.; Kermi, C.; Stoy, H.; Schiltz, C. J.; Bacal, J.; Zaino, A. M.; Hadden, M. K.; Eichman, B. F.; Lopes, M.; Cimprich, K. A. HLTf Promotes Fork Reversal, Limiting Replication Stress Resistance and Preventing Multiple Mechanisms of Unrestrained DNA Synthesis. *Mol Cell* **2020**, *78* (6), 1237-1251.e7. <https://doi.org/10.1016/j.molcel.2020.04.031>.
- (181) Quinet, A.; Carvajal-Maldonado, D.; Lemacon, D.; Vindigni, A. DNA Fiber Analysis: Mind the Gap! *Methods Enzymol* **2017**, *591*, 55–82. <https://doi.org/10.1016/bs.mie.2017.03.019>.
- (182) Park, S. H.; Kang, N.; Song, E.; Wie, M.; Lee, E. A.; Hwang, S.; Lee, D.; Ra, J. S.; Park, I. B.; Park, J.; Kang, S.; Park, J. H.; Hohng, S.; Lee, K.-Y.; Myung, K. ATAD5 Promotes Replication Restart by Regulating RAD51 and PCNA in Response to Replication Stress. *Nat Commun* **2019**, *10* (1), 5718. <https://doi.org/10.1038/s41467-019-13667-4>.
- (183) Liu, W.; Roubal, I.; Polaczek, P.; Meng, Y.; Choe, W.; Caron, M.-C.; Sedgeman, C. A.; Xi, Y.; Liu, C.; Wu, Q.; Zheng, L.; Masson, J.-Y.; Shen, B.; Campbell, J. L. FANCD2 Directly Inhibits DNA2 Nuclease at Stalled Replication Forks and Acts as a RAD51 Mediator in Strand Exchange. *bioRxiv* July 9, 2021, p 2021.07.08.450798. <https://doi.org/10.1101/2021.07.08.450798>.
- (184) Wysocka, J.; Reilly, P. T.; Herr, W. Loss of HCF-1-Chromatin Association Precedes Temperature-Induced Growth Arrest of TsBN67 Cells. *Mol Cell Biol* **2001**, *21* (11), 3820–3829. <https://doi.org/10.1128/MCB.21.11.3820-3829.2001>.

- (185) Liu, W.; Zhou, M.; Li, Z.; Li, H.; Polaczek, P.; Dai, H.; Wu, Q.; Liu, C.; Karanja, K. K.; Popuri, V.; Shan, S.-O.; Schlacher, K.; Zheng, L.; Campbell, J. L.; Shen, B. A Selective Small Molecule DNA2 Inhibitor for Sensitization of Human Cancer Cells to Chemotherapy. *EBioMedicine* **2016**, *6*, 73–86. <https://doi.org/10.1016/j.ebiom.2016.02.043>.
- (186) Dempster, J. M.; Rossen, J.; Kazachkova, M.; Pan, J.; Kugener, G.; Root, D. E.; Tsherniak, A. *Extracting Biological Insights from the Project Achilles Genome-Scale CRISPR Screens in Cancer Cell Lines*; 2019; p 720243. <https://doi.org/10.1101/720243>.
- (187) Pacini, C.; Dempster, J. M.; Boyle, I.; Gonçalves, E.; Najgebauer, H.; Karakoc, E.; van der Meer, D.; Barthorpe, A.; Lightfoot, H.; Jaaks, P.; McFarland, J. M.; Garnett, M. J.; Tsherniak, A.; Iorio, F. Integrated Cross-Study Datasets of Genetic Dependencies in Cancer. *Nat Commun* **2021**, *12* (1), 1661. <https://doi.org/10.1038/s41467-021-21898-7>.
- (188) Meyers, R. M.; Bryan, J. G.; McFarland, J. M.; Weir, B. A.; Sizemore, A. E.; Xu, H.; Dharia, N. V.; Montgomery, P. G.; Cowley, G. S.; Pantel, S.; Goodale, A.; Lee, Y.; Ali, L. D.; Jiang, G.; Lubonja, R.; Harrington, W. F.; Strickland, M.; Wu, T.; Hawes, D. C.; Zhivich, V. A.; Wyatt, M. R.; Kalani, Z.; Chang, J. J.; Okamoto, M.; Stegmaier, K.; Golub, T. R.; Boehm, J. S.; Vazquez, F.; Root, D. E.; Hahn, W. C.; Tsherniak, A. Computational Correction of Copy Number Effect Improves Specificity of CRISPR-Cas9 Essentiality Screens in Cancer Cells. *Nat Genet* **2017**, *49* (12), 1779–1784. <https://doi.org/10.1038/ng.3984>.
- (189) Gao, J.; Aksoy, B. A.; Dogrusoz, U.; Dresdner, G.; Gross, B.; Sumer, S. O.; Sun, Y.; Jacobsen, A.; Sinha, R.; Larsson, E.; Cerami, E.; Sander, C.; Schultz, N. Integrative Analysis of Complex Cancer Genomics and Clinical Profiles Using the CBioPortal. *Sci Signal* **2013**, *6* (269), p11. <https://doi.org/10.1126/scisignal.2004088>.

Vita

Tanay Thakar

EDUCATION

Northwestern University, Evanston IL
MS, Biotechnology

June 2015

University of Pune, Pune, India
BTech, Biotechnology

June 2013

PUBLICATIONS

1) **T.Thakar**, J. Straka, C.M. Nicolae, G.L. Moldovan. Lagging strand gap suppression connects BRCA-mediated fork protection to nucleosome assembly by ensuring PCNA-dependent CAF-1 recycling. *Under Revision at Nature Communications*.
(<https://www.biorxiv.org/content/10.1101/2021.11.08.467732v1.full>)

2) **T. Thakar**, W. Leung, C.M. Nicolae, K.E. Clements, B. Shen, A.K. Bielinsky, G.L. Moldovan. Ubiquitinated-PCNA protects stalled replication forks from DNA2-mediated degradation by regulating Okazaki fragment maturation and chromatin assembly. *Nature Communications*. 2020;11(1):2147. Published 2020 May 1. doi:10.1038/s41467-020-16096-w.

3) **T.Thakar**, G.L. Moldovan. The emerging determinants of replication fork integrity (Review). *Nucleic Acids Research*. 2021;gkab344. doi: 10.1093/nar/gkab344. Epub ahead of print.

4) A. Datta, K. Biswas, J.A. Sommers, H. Thompson, S. Awate, C.M. Nicolae, **T. Thakar**, G.L. Moldovan, R.H. Shoemaker, S.K. Sharan, R.M. Brosh Jr. WRN helicase safeguards deprotected replication forks in BRCA2-mutated cancer cells. *Nature Communications*. 2021;doi: 10.1038/s41467-021-26811-w.

5) M.J. O'Connor, **T.Thakar**, C.M. Nicolae, G.L. Moldovan. PARP14 regulates cyclin D1 expression to promote cell-cycle progression. *Oncogene*. 2021;doi: 10.1038/s41388-021-01881-8.

6) K.E. Clements, E.M. Schleicher, **T. Thakar**, A. Hale, A. Dhoonmoon, N.J. Tolman, C.M. Nicolae, A. Sharma, X. Liang, H.G. Wang, G.L. Moldovan. Identification of regulators of poly-ADP-ribose polymerase (PARP) inhibitor resistance in BRCA2-deficient cells through dual CRISPR knockout and activation screens. *Nature Communications*. 2020;11(1):6118. doi: 10.1038/s41467-020-19961-w.

7) T.M Yamamoto, A. McMellen, Z.L. Watson, J. Aguilera, M.J. Sikora, R. Ferguson, E. Nurmammedov, **T. Thakar**, G.L. Moldovan, H. Kim, D.M. Cittelley, H. Wilson, K. Behbakht, and B.G. Bitler. Activation of Wnt signaling promotes olaparib resistant ovarian cancer. *Molecular Carcinogenesis*. 2019;58(10):1770-1782. doi:10.1002/mc.23064.

8) K.E. Clements, **T. Thakar**, C.M. Nicolae, X. Liang, H.G. Wang, and G.L. Moldovan. Loss of E2F7 confers resistance to poly-ADP-ribose polymerase (PARP) inhibitors in BRCA2-deficient cells. *Nucleic Acids Research*. 2018;46(17):8898-8907. doi:10.1093/nar/gky657.

9) W. Leung, R. M. Baxley, **T. Thakar**, J. P. Buytendorp, L. Wang, C. B. Rogers, A. Tella, G.L. Moldovan, N. Shima, and A.K. Bielinsky. PCNA-K164 ubiquitination facilitates origin licensing and mitotic DNA synthesis. *Submitted*.
(<https://www.biorxiv.org/content/10.1101/2020.06.25.172361v1.full>)